NASA-CR-191332

SBIR-09.20-7640
Release Date 6/16/93

Report 94044
March 8, 1991

LOW COST ATTITUDE CONTROL SYSTEM
REACTION WHEEL DEVELOPMENT
FINAL REPORT

(NASA-CR-191332) LOW COST ATTITUDE CONTROL SYSTEM REACTION WHEEL DEVELOPMENT Final Report (Ithaco) 100 p

N94-13140

Unclas

G3/18 0186508

Prepared for

National Aeronautics and Space Administration
Goddard Space Flight Center
Greenbelt, MD 20771

Prepared by:

ITHACO, Inc.
735 W. Clinton St.
P.O. Box 6437
Ithaca, NY 14851-6437

TECHNICAL REPORT STANDARD TITLE PAGE

1. Report No.	2. Government Accession. No.	3. Recipient's Catalog No.
4. Title and Subtitle Low Cost Attitude Control System Reaction Wheel Development Final Report		5. Report Date 6. Performing Organization Code
7. Author(s) William Bialke		8. Performing Organization Report No. #94044
9. Performing Organization Name and Address ITHACO, Inc. 735 W. Clinton St. P.O Box 6437 Ithaca, NY 14851-6437		10. Work Unit No. 11. Contract or Grant No. NAS5-30307
12. Sponsoring Agency Name and Address Mr. Seymour Kant NASA/Goddard Space Flight Center Greenbelt, MD 20771		13. Type of Report and Period Covered Final Report 14. Sponsoring Agency Code
15. Supplementary Notes		

16. Abstract

In order to satisfy a growing demand for low cost attitude control systems for small spacecraft, development of a low power and low cost Reaction Wheel Assembly was initiated. This report addresses the details of the versatile design resulting from this effort. Tradeoff analyses for each of the major components are included, as well as test data from an engineering prototype of the hardware.

17. Key Words (Selected by Author(s)) Attitude Control System Reaction Wheel Momentum Wheel Earth Sensor	18. Distribution Statement

19. Security Classif. (of this report)	20. Security Classif. (of this page)	21. No. of Pages	22. Price

TABLE OF CONTENTS

1.0 PREFACE 1

1.1 Objective 1
1.2 Scope of Work 1
1.3 Conclusions 1

2.0 PHASE I SUMMARY 2

3.0 PHASE II GOALS 4

4.0 HARDWARE DESIGN APPROACH 6

4.1 Design Specifications 7

5.0 HARDWARE DESIGN TRADEOFFS 8

5.1 Structure 8
5.1.1 Housing 8
5.1.1.1 Housing Form 8
5.1.1.2 Housing Material 12
5.1.1.3 Structural Dynamics 12
5.1.1.4 Sealing 17
5.1.2 Rotor Construction 17
5.1.3 Bearing Mounts 19
5.2 Bearings 20
5.2.1 Ball Bearing Tradeoffs 20
5.2.1.1 Bearing Type 20
5.2.1.2 Bearing Preload 22
5.2.1.3 Bearing Material 22
5.2.1.4 Bearing Load Ratings 23
5.2.1.5 Bearing Tolerances 23
5.2.1.6 Bearing Selection 24
5.3 Lubrication 25
5.3.1 Lubricant Wear Testing 27
5.3.2 Lubricant Performance 27
5.3.3 Lubricant Life 31
5.3.4 Lubricant Optical Transmission 36
5.3.5 Lubricant Selection 36
5.4 Motor 38
5.4.1 Motor Type 38
5.4.2 Motor Selection 39
5.5 Tachometer 41
5.5.1 Tachometer Selection 41

TABLE OF CONTENTS (CONT'D)

5.6 Motor Driver 42
5.6.1 Motor Driver Design Goals 42
5.6.2 Motor Characteristics 42
5.6.3 Driver Topology 43
5.6.3.1 Power Bridge 43
5.6.3.2 Commutation 43
5.6.3.3 Pulse Width Modulation 43
5.6.3.4 Supplementary Features 45
5.6.4 Motor Driver Packaging 46

6.0 FINAL DESIGN DESCRIPTION 47

6.1 Ball Bearing Suspension System 47
6.2 Lubrication System 47
6.3 Motor 50

7.0 BREADBOARD UNIT MANUFACTURE 51

7.1 Rotor Assembly Manufacture 51
7.2 Stator Manufacture 51
7.3 Breadboard Unit Configuration 52

8.0 BREADBOARD UNIT TEST DATA 53

8.1 Modal Survey 53
8.2 Drag Torque Data 53
8.3 Bearing EHD Film Testing 58
8.4 External Magnetic Field Measurements 58
8.5 Power Consumption Measurements 64
8.6 Acceptance Test Plan 64
8.6.1 Functional Test 64
8.6.2 Performance Test 64
8.6.3 Burn-In 66
8.6.4 Random Vibration 66

9.0 PHASE III STATUS 67

10.0 CONCLUSION 67

11.0 REFERENCES 67

APPENDIX A - ITHACO REPORT 93945, REV. A

1.0 PREFACE

1.1 Objective

This report documents and summarizes the development work performed under Small Business Innovation Research Contract NAS5-30307.

1.2 Scope of Work

In order to make a low cost attitude control system viable for small, inexpensive satellites, development of a low cost, low power consumption reaction wheel was completed. The development effort performed included all of the detail design and engineering testing of a reaction wheel and motor driver capable of being integrated into a combination reaction wheel and earth scanner, or SCANWHEEL®.

1.3 Conclusions

The development effort did not encounter any insurmountable obstacles which would preclude the low-cost manufacture of a low-power consumption Reaction Wheel Assembly. Simplistic and reliable techniques were employed to result in a rugged, yet efficient, design. Processes are in place to manufacture the reaction wheel in large or small quantities, and with options for various levels of traceability and documentation.

2.0 PHASE I SUMMARY

The objective of the Phase I effort was to develop a source for a low cost spaceflight worthy reaction wheel, in order to make an attitude control system feasible for small, low cost satellites. Three vendors were solicited for cost proposals, and a make/buy decision was made to design and produce the low cost RWA at ITHACO.

The three vendors which were contacted in the Phase I effort were Honeywell, Bendix, and Schaeffer Magnetics. Honeywell and Bendix have been in the business of supplying space flight reaction wheels for many years. Schaeffer Magnetics was in the process of initiating a reaction wheel design and was a viable alternative. Both Honeywell and Bendix quoted non-recurring costs for the reaction wheel on the order of $600K - $800K, and recurring costs on the order of $60-100 K per reaction wheel. Even with relaxed specifications and deletion of requirements for traceability and process documentation, the major reaction wheel suppliers were unable to reduce the costs of a reaction wheel to the level required for low cost missions, thus they were eliminated from procurement competition due to price. The remaining potential source at Schaeffer Magnetics was found to be comparable to ITHACO in regard to design and manufacturing capability but did not submit a bid. In order to maintain more flexibility in the control during the design and manufacture, and to minimize overall costs, it was decided to design and manufacture the low cost reaction wheel at ITHACO.

Additional results of the Phase I effort included a baseline design of the ITHACO reaction wheel. This baseline design is shown in Figure 2-1. The key features to this design were spun aluminum parts, no hermetic seal, and a compliant bearing mount. The bearings are mounted in a compliant Viton housing, which minimizes the required alignment of the bearings during assembly, in an attempt to reduce manufacturing costs. The compliant support also reduces bearing loads during random vibration and shock loading. The evolution of the design in the Phase II effort resulted in a substantially different design than this baseline.

The final report of the Phase I effort is contained in ITHACO Report 93558.

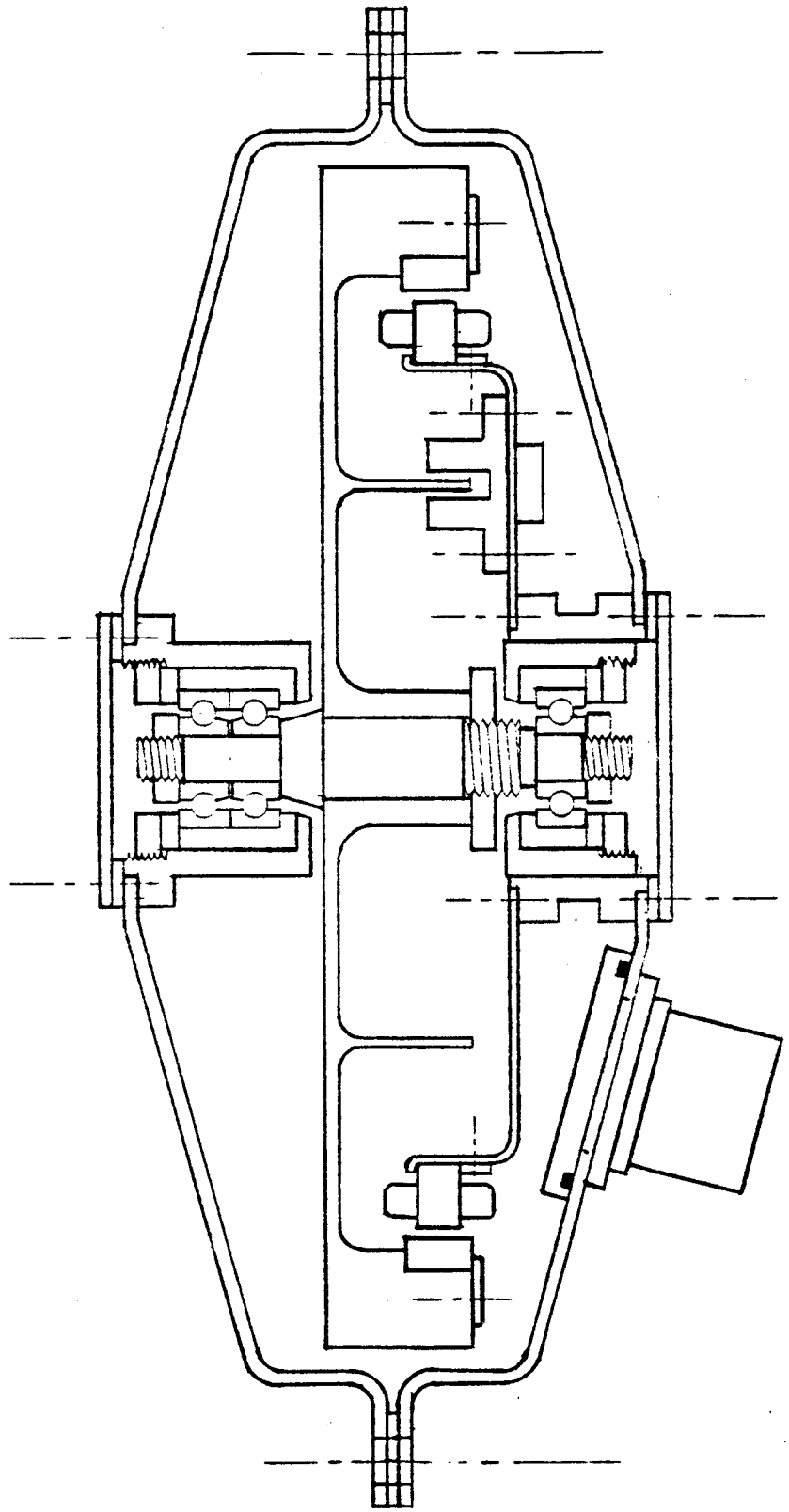

Figure 2-1: The evolution of the design in the Phase II effort resulted in a substantially different design than this Phase I baseline.

3.0 PHASE II GOALS

In order to satisfy a growing need for low cost attitude control systems for small spacecraft with minimal power resources, the Phase II objectives were to develop and manufacture a low cost reaction wheel with minimum power consumption. A major obstacle in the production of a low cost attitude control system was the availability of a low cost reaction wheel. Magnetic torquers and control electronics can be built inexpensively, but no source had yet existed for low cost reaction wheels. In addition, typical reaction wheels on the market consume too much power for the stringent power budgets of small spacecraft. A second obstacle in the production of a low cost attitude control system was the expense and power consumption of a horizon sensor. Development of a combined reaction wheel and horizon scanner provides solutions to the cost and power consumption concerns of conventional hardware for a low cost attitude control system. A combined reaction wheel and horizon scanner, or SCANWHEEL, requires only one set of bearings and one motor, which reduces the power consumption, weight, and cost over two separate pieces of hardware, while improving the system reliability.

One potential spacecraft application for a low cost/low power consumption attitude control system is the NASA Standard GAS CAN Satellite. This 150 pound satellite currently known as XSAT (Exceptional Satellite) was designed to be ejected from a Get Away Special (GAS) Cannister on the Space Shuttle. An attitude control system is intended to be added to XSAT on a mission peculiar basis in order to accommodate the requirements of each specific payload. In order to take advantage of this potential low cost satellite bus, a primary goal for the Phase II SBIR was to ensure that the SCANWHEEL design was compatible with XSAT.

The funding for this SBIR was only sufficient to support the development of the reaction/momentum wheel portion of the SCANWHEEL. A separate SBIR contract (NAS-30088) for an earth scanner was directed to develop the earth scanner portion of the SCANWHEEL. A goal in this SBIR, then, was to design the reaction/momentum wheel to be compatible with the addition of an horizon sensor module to form a SCANWHEEL. The development performed per contract NAS-30088 is documented in Final Report 94047.

A photograph of the hardware developed in the Phase II effort is shown in Figure 3-1.

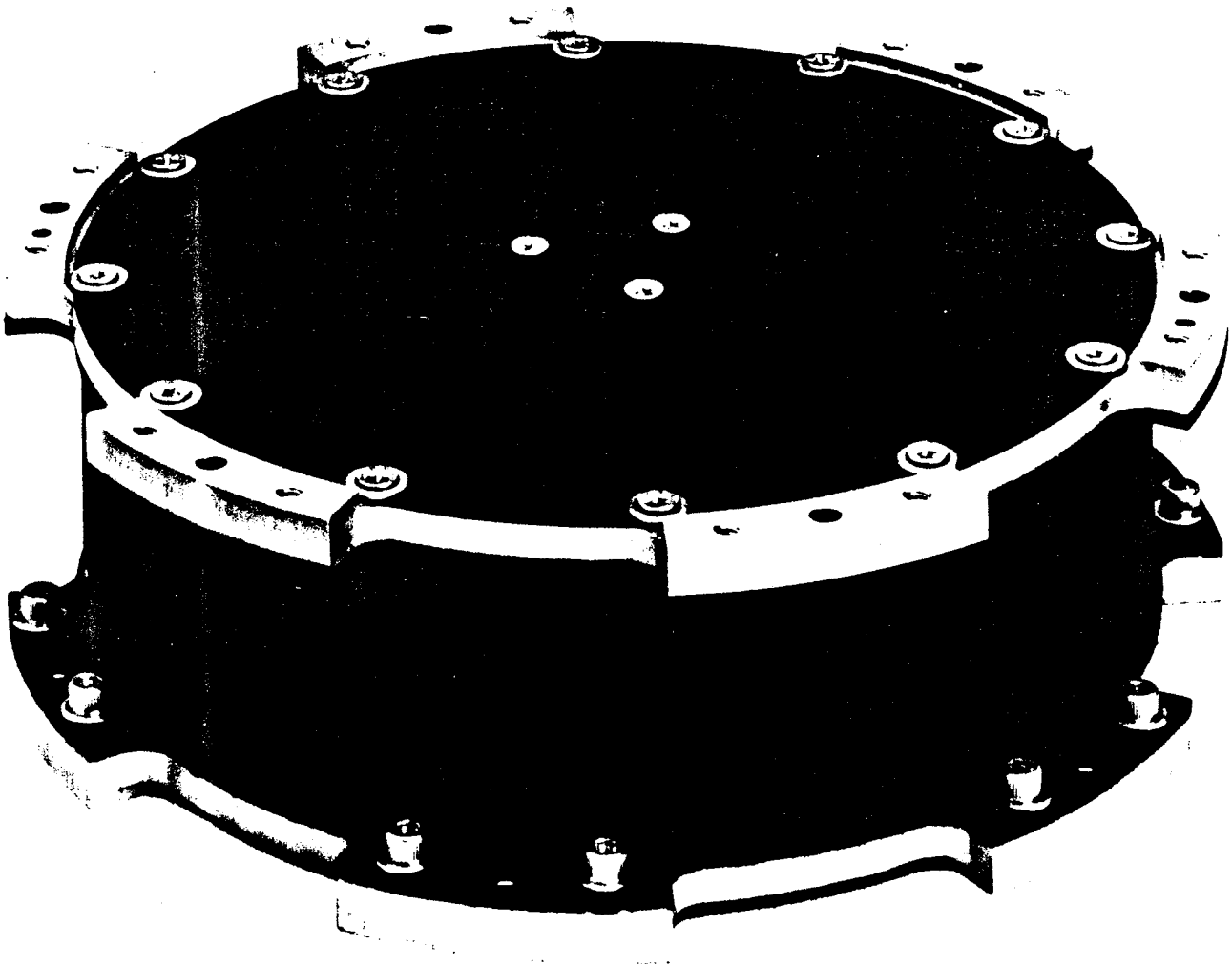

Figure 3-1: The Reaction Wheel Outline Provides Dual Mounting Surfaces To Expand Mounting Options on the Spacecraft

4.0 HARDWARE DESIGN APPROACH

A set of ground rules was established early in the design phase of the wheel, in order to ensure that the design tradeoff decisions made during the hardware development were compatible with the ultimate program goals. The basic approach to achieve low cost was to maintain simplicity by taking advantage of standard components and common materials. At the same time, a rigid ground rule was established to maintain the ability to upgrade any feature in the design to Class S spacecraft hardware. Modularity in the design was also stressed as a ground rule, to take advantage of quantity buys of components and batch processing of subassemblies, and to minimize manufacturing costs. In order to accommodate a variety of users with the same hardware, versatility in the design was a prominent goal. This was to be accomplished by allowing for the addition of various options to the hardware without impact to the basic components. Being able to satisfy the specific requirements of a variety of users is directly in line with the pursuit of low cost hardware.

A ranking of the critical tradeoff parameters was established to be used in the tradeoff analyses during the design process. These basic parameters are power consumption, cost, reliability, and weight.

The highest ranked tradeoff parameter was deemed to be power consumption. Small spacecraft typically have a minimum amount of surface area for solar cells, thus power is at a premium. As an example, the XSAT satellite has a total power generation capability of 7.8 Watts. The power consumption of the bus is 2.5 Watts average, so the power consumption of the attitude control system must be restricted to less than 3 watts total to leave just over 2 Watts for the experiment. The low power consumption was therefore imperative to enable the wheel to be practical, given this type of power budget.

The second ranked tradeoff parameter was cost. It was reasoned low cost production of hardware was essential to allow an attitude control system to be within the reach of the budgets of small satellites. If the costs were too high, the small satellite experimenters would inevitably sacrifice the attitude control system. In addition, the market already has sources for expensive reaction wheels, with little room for unproven competition. The only way to break into this market was with unique, low cost hardware.

The third ranked tradeoff parameter was reliability. The long term reliability and lifetime are less important in the low cost/high value spacecraft for which the hardware was targeted. While maintaining the ground rule of upgradeability, the approach was to design the hardware for a one year mission as a minimum, with a goal of three years. Typical spaceflight hardware is designed with 5 to 10 year missions in mind. The design approach to fulfill the one year mission was to keep each component as simple as possible, while leaving room for the 'bells and whistles' in case the hardware is commissioned to be used on a longer term mission.

4.0 HARDWARE DESIGN APPROACH (CONT'D)

The lowest ranked tradeoff parameter was weight. In small satellites such as XSAT, weight is not as critical as power, cost, and reliability. In some cases, hardware designs are taken to great extremes in order to minimize weight. The heroic efforts taken during this process can significantly increase the costs by increasing the complexity and decreasing the dimensional tolerances of the mechanical parts, and can lower the reliability by reducing clearances and safety margins. However, good engineering practices of mechanical design were to be used to result in the lowest practical weight. There is typically a see-saw tradeoff between weight and power in electromagnetic devices, so the high emphasis on low power automatically results in a de-emphasis on weight. In order to minimize material costs, the use of exotic material was discouraged. Beryllium, magnesium, titanium and composites are frequently used in spaceflight hardware to minimize structural weight, but in keeping with low cost and simplicity, these materials were not to be used in the design.

4.1 Design Specifications

The design specifications for the reaction wheel were established in the Phase I SBIR, and documented in ITHACO Report 93387. A summary of the relevant specifications is presented in Table 4-1. The size was established as that expected for a small satellite on the order of XSAT. The 6 volt bus was chosen for the same reason, as that is the bus voltage of the XSAT bus. The typical bus voltage for spacecraft is 28 volts, but smaller spacecraft have fewer solar cells to string together in series, so the bus voltage is usually lower. A goal of the design was to make it useable with either a 28 volt bus or a 6 volt bus.

Table 4-1

Parameter	Minimum Requirement	Goal
Nominal Operating Speed	1000 rpm	±6000 rpm
Operating Life	1 year	3 years
Storage Life	5 years	5 years
Torque Capability	>0.02 N-m (2.8 oz-in)	increasable
Torque Ripple	none	<0.002 N-m (<10%)
Angular Momentum @ 1000 rpm	0.67 N-m-s (0.5 ft-lbf-sec)	increasable
Power Consumption @ 1000 rpm	<1.0 W	<0.5 W
Weight	<2.5 Kg (5.5 lbm)	
Temperature Range	0°C to 50°C	-34°C to 71°C
Bus Voltage	6 V	6 V, 15 V or 28 V

5.0 HARDWARE DESIGN TRADEOFFS

The following sections address the specific tradeoff analyses performed in the design and selection of the major components of the reaction wheel. The resulting mechanical configuration of the reaction wheel is depicted in Figure 5-1.

5.1 Structure

The basis for the structural design is primarily dictated by the random vibration and thermal environments encountered by spacecraft hardware. Random vibration responses of a heavy flywheel suspended by ball bearings can result in significant force loads on the bearings and support structure, and therefore must be carefully assessed. High thermal impedances in the design can result in high operating temperatures for bearings which will reduce the operating lifetime.

5.1.1 Housing

The housing must perform several functions simultaneously. In addition to sealing the bearings for cleanliness, the housing must provide structural support of the rotor, a conductive heatsink for low impedance heat rejection from the motor and bearings, and provide a means for mounting the assembly to the spacecraft.

5.1.1.1 Housing Form

Four basic configurations for a flywheel suspension are shown in Figure 5-2. The most basic configuration is a simple housing which features a combined support structure and enclosure. This can accommodate either a clamshell housing arrangement as shown in Figure 5.2-a, or a pill-box approach shown in Figure 5.2-b. The clamshell approach provides a high rocking stiffness due to the large bearing separation, and reduces stresses in the case of an evacuated design due to the high strength of the conical sections. The pill-box configuration results in a lower rocking stiffness, but is easier to mount to the spacecraft. Either of the cantilever shaft options shown in Figure 5.2-c and Figure 5.2-d require bearings with a large diameter in order to achieve the required shaft strength and stiffness, resulting in higher drag torque and thus higher power consumption than alternate designs.

In order to make the hardware truly modular, an approach was conceived which allowed two units to be coupled in tandem, or stacked, in order to increase the momentum storage capacity. It was reasoned that if a significant number of units were being manufactured, it would be more cost effective to build two standard units, rather than one larger custom unit. This could also be used to provide redundancy. The pill-box housing fulfilled this objective. Mounting surfaces on both sides of the housing also provides a platform on which to attach an optics package for the SCANWHEEL option. By establishing the mounting surface on the outside perimeter of the unit, the span between mounting pads is maximized, which minimizes alignment errors due to machining tolerances. This is especially important as a mounting surface for the SCANWHEEL optics package. Figure 5-3 shows the versatility of the pill box housing configuration. In addition to the modularity, this approach provides more mounting options on the spacecraft.

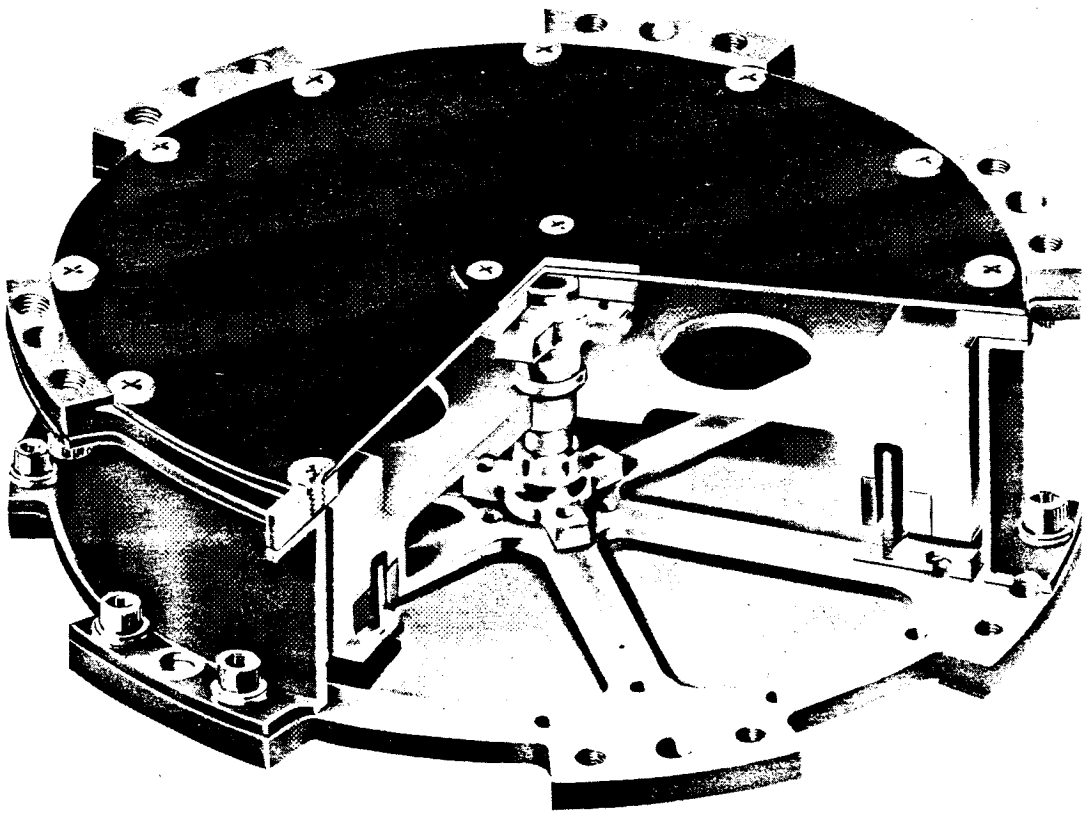

Figure 5-1: Simplistic and reliable techniques were employed in the mechanical development of the reaction wheel to result in a rugged, yet efficient design

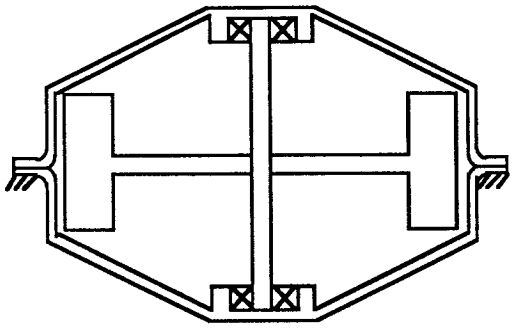

(a)
Clamshell Housing - Inner Race Roatation

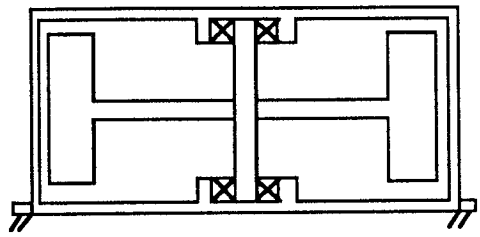

(b)
Pill Box Housing - Inner Race Rotation

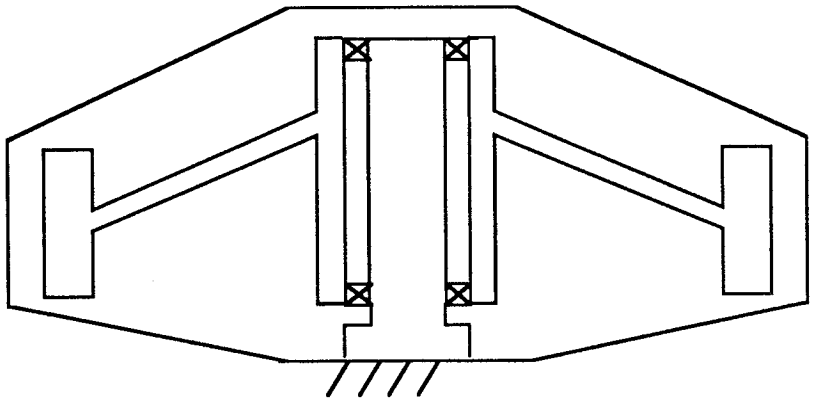

(c)
Cantilever Shaft - Outer Race Rotation

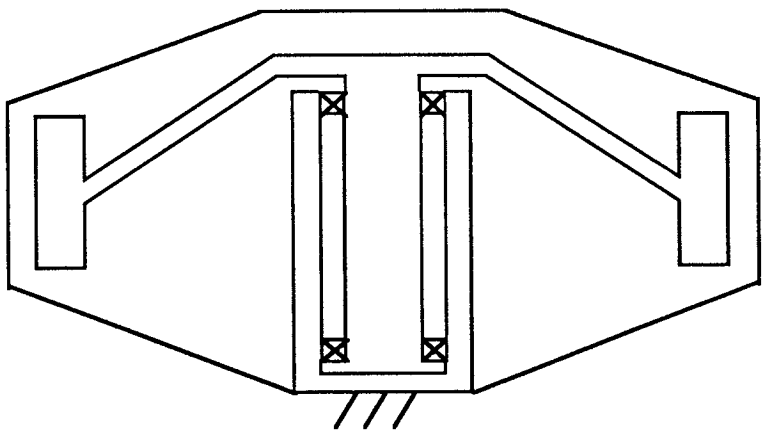

(d)
Cantilever Shaft - Inner Race Rotation

Figure 5-2: Candidate Structural Configuration For An Enclosed Flywheel

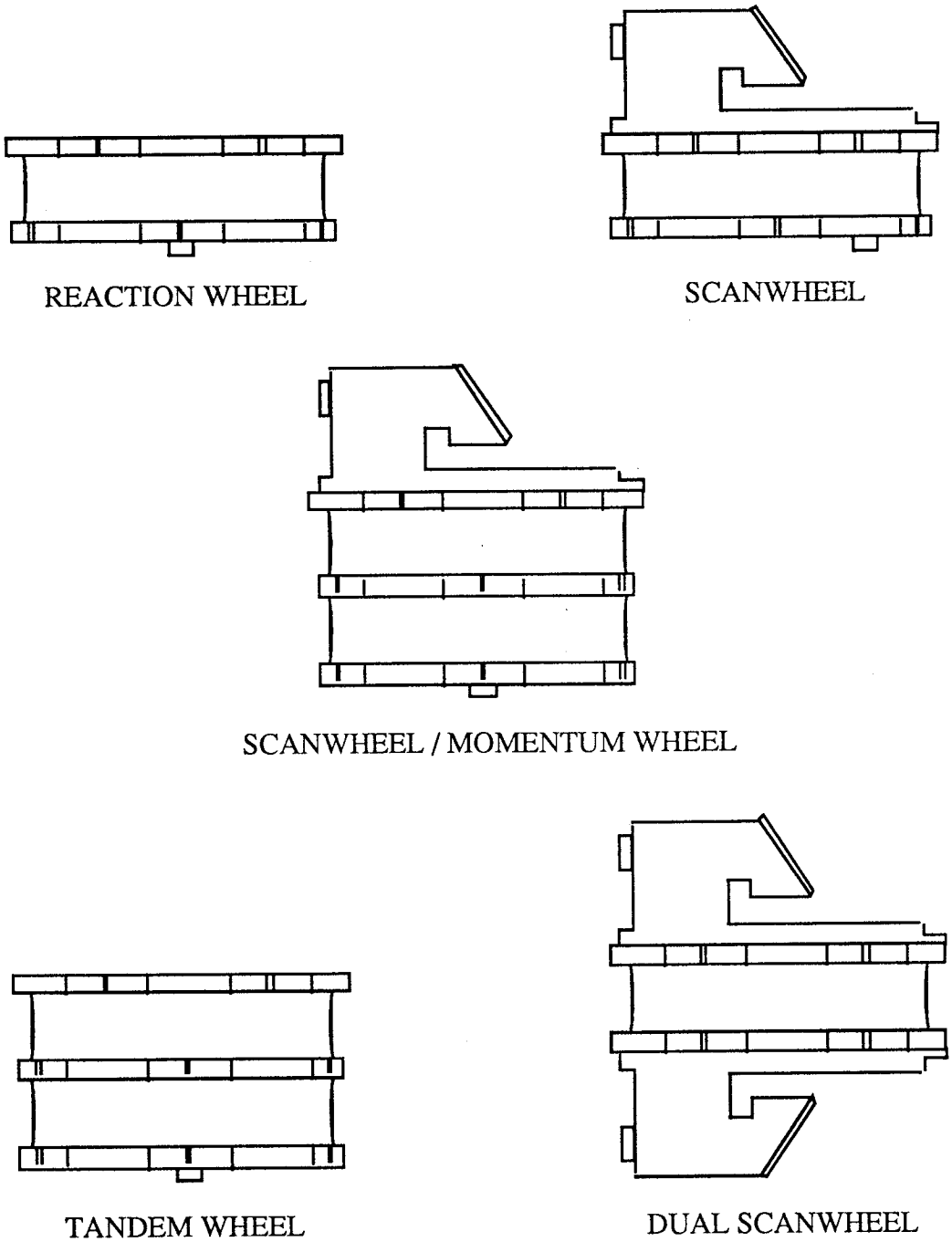

Figure 5-3: The cylindrical pill box reaction wheel configuration results in a variety of integration possibilities

5.1.1.2 Housing Material

The baseline design utilized spun aluminum components to construct the housing and support the motor. This approach was discarded due to the low strength of the spun aluminum thicknesses, and due to the potential dimensional instability of the formed material. The optical system and the ball bearing suspension requires stable alignment of surfaces which may be compromised with spun parts. Spun parts or hydroformed parts require critical heat treating procedures to regain the dimensional stability of the material, which complicates the fabrication and increases the chances for error.

Magnesium is used in many reaction wheel housing designs due to its low density and high structural damping, but the raw material expense and safety concerns during machining are not compatible with the low cost objectives of the design. In addition, the poor thermal conductivity and high susceptibility of magnesium to galvanic corrosion further discourage its use where weight is not a primary concern.

The potential high volume of production suggested that castings be considered for fabrication of the housing components. The recurring cost of the parts is significantly less than for a machined part, but for a high reliability application, X-ray and dye penetrant inspection on every piece brings the cost of each part close to the procurement cost for machined parts produced in relatively large lots on numerically controlled equipment. In addition, the aluminum alloys used for casting are relatively low strength, resulting in lower safety margins and higher weight. The non-recurring costs also makes the casting option less flexible for design changes or modifications to the mechanical design.

Aluminum was selected as the primary structural material due to its relative low cost, high thermal conductivity, and low stiffness. A variety of aluminum alloys are categorized as highly resistant to stress corrosion cracking in Table 1 of MSFC-SPEC-522A, which allows their use in structural applications on Space Shuttle payloads without a Material Usage Agreement. In order to eliminate all these potential waivers, it was decided to limit material selection to materials in Table 1 of MSFC-SPEC-522A, and dissimilar metal combinations were required to comply with MIL-STD-889.

5.1.1.3 Structural Dynamics

The stiffness of the housing is the most critical parameter in the structural design, since the structural dynamics of the system is a function of the stiffness characteristics and the rotor mass. If the natural frequency resulting from these parameters is too high, the resulting random vibration response accelerations will cause excessive loads to be transmitted through the bearings. If the resonant frequency is too low, it may fall within the range of the rotation frequency of the rotor during operation, which will amplify the induced vibration to the spacecraft due to rotor imbalance. The maximum expected operating frequency of the rotor in any application is 6000 rpm, which corresponds to a minimum resonant frequency of 100 Hz. In order to determine an upper limit to the resonant frequency, a random vibration response analysis is required.

The dynamic model, represented in Figure 5-4, is assumed to be essentially a single degree of freedom system in the axial direction, and a two-degree of freedom system in the radial direction. This will result in three dominant vibration modes, which are referred to as the axial mode, the radial translation mode, and the radial rocking mode. In the radial translation mode, the deflections of the k_2 springs are in phase, and in the radial rocking mode they are 180° out of phase. These modes are represented in Figure 5-5.

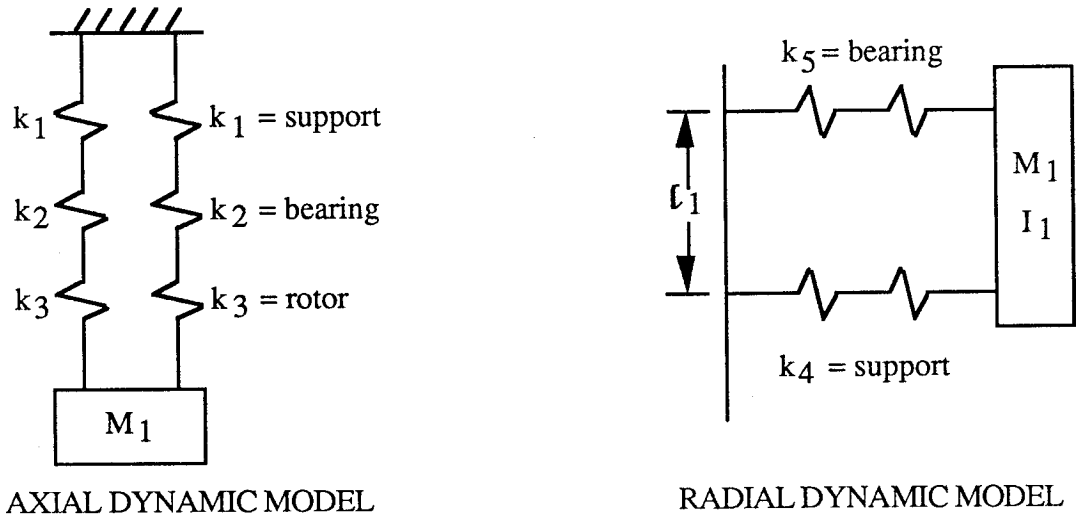

Figure 5-4: Due to high concentrated mass of the flywheel, a lumped mass dynamic model is a very realistic approximation for the reaction wheel

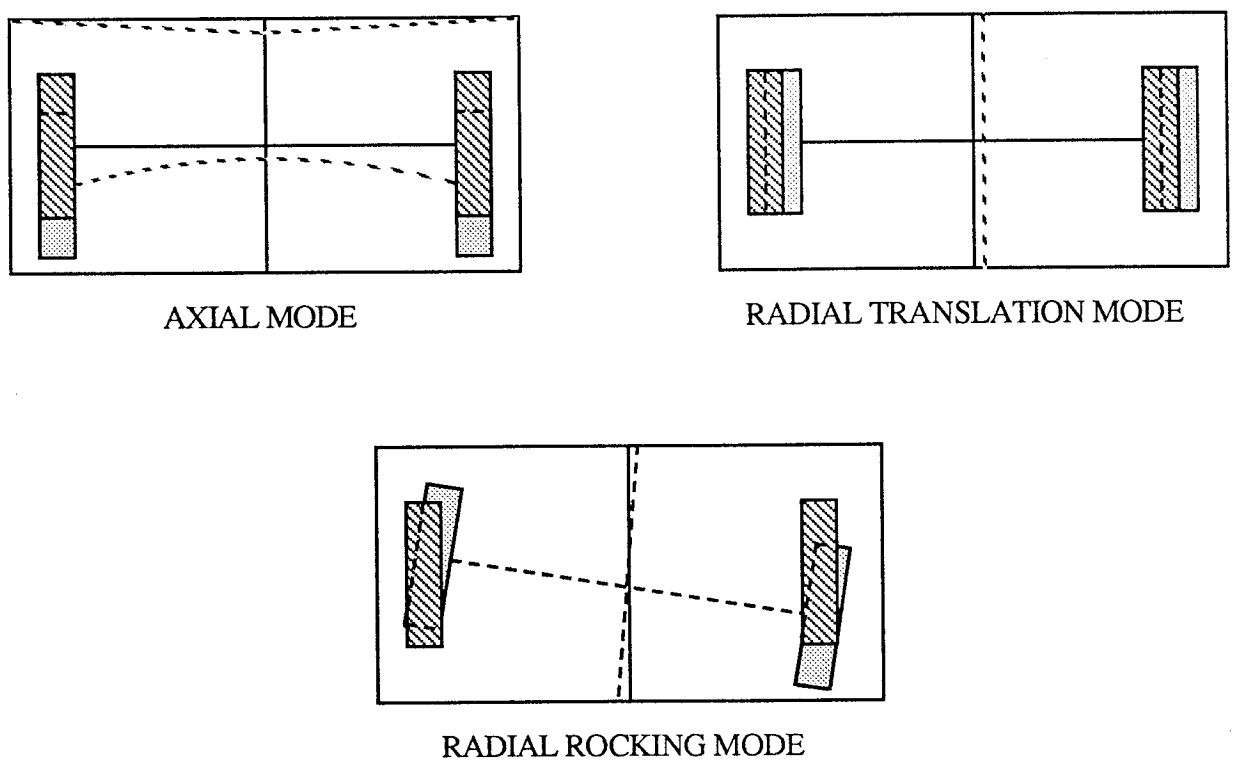

Figure 5-5: The three primary vibration modes of the reaction wheel play a large part in predicting bearing loads during random vibration exposure

5.1.1.3 Structural Dynamics (Cont'd)

The response of a single degree of freedom system to a specified random vibration environment can be predicted by using Mile's equation, which correlates a power spectral density input into an equivalent 3σ probable sinusoidal response as follows:

$$a = 3\sqrt{\frac{\pi}{2} f_n \text{ PSD } Q}$$

where a = acceleration
f_n = resonant frequency
PSD = power spectral density at f_n
Q = transmissibility

Mile's equation demonstrates the dependency of the statistical response acceleration from random vibration input on the resonant frequency and the input power spectral density. When the two severe spectrums shown in Figure 5-6 are combined, they demonstrate a break point at approximately 350 Hz. Higher frequencies than 350 Hz increase the statistical response accelerations due the larger frequency component, and lower frequencies than 350 Hz result in higher response accelerations due to the increasing power spectral density of spectrum 1. In order to optimize the design to accommodate both spectrums, it was decided to tune the stiffness of the structure to attain a radial resonant frequency of 350 Hz.

In the selected pill-box housing configuration, the dominant mode with the highest frequency will be the radial translation mode. The low membrane stiffness of the housing in the axial direction will yield a significantly lower frequency mode for the axial mode, and the bearing span can selected to do the same for the rocking mode. The relatively small diameter of the housing, however, results in a high radial stiffness due to the full compliment of material about each bearing mount. The stiffness of this type of housing suspending a three pound rotor results in primary resonant frequencies on the order 1 KHz. A primary structural resonance in the 600 to 800 Hz range, given a typical spaceflight random vibration input spectrum, results in 3σ response accelerations on the order of 240 g's. If the resonant frequency is reduced to 350 Hz, the 3σ response accelerations are approximately reduced in half. Tuning of the structural stiffness in order to attain the desired 350 Hz requires the use of a flexure support. A spoked 'spider web' flexure was found to be the most practical support. By axially offsetting the bearing centerline from the plane of the flexure, a moment is produced during radial loading which capitalizes on the bending compliance of the flexure spokes. Figure 5-7 shows the free body model of the flexure and the resulting stiffness model equation used to tune the radial translation resonance. The corresponding axial and rocking stiffness models and equations are shown in Figures 5-8 and 5-9.

A pair of spoked flexures separated by a cylindrical ring has several other advantages from a packaging standpoint. The spokes allow visual and mechanical access to the flywheel when it is completely assembled into the housing. This eliminates the undesirable blind assembly characteristic of some reaction wheel designs which combine the enclosure and support structure into a single part. With open flexures on both sides of the housing, inspection can be performed prior to close-up for presence of contamination, sufficient motor gap clearances and correct direction of rotation polarity. During troubleshooting, visual examination of the rotor and bearings can be performed without disturbing the critical existing conditions in the assembly. The axial symmetry of the housing allows the same flexure to be used on both sides of the housing, which improves manufacturability.

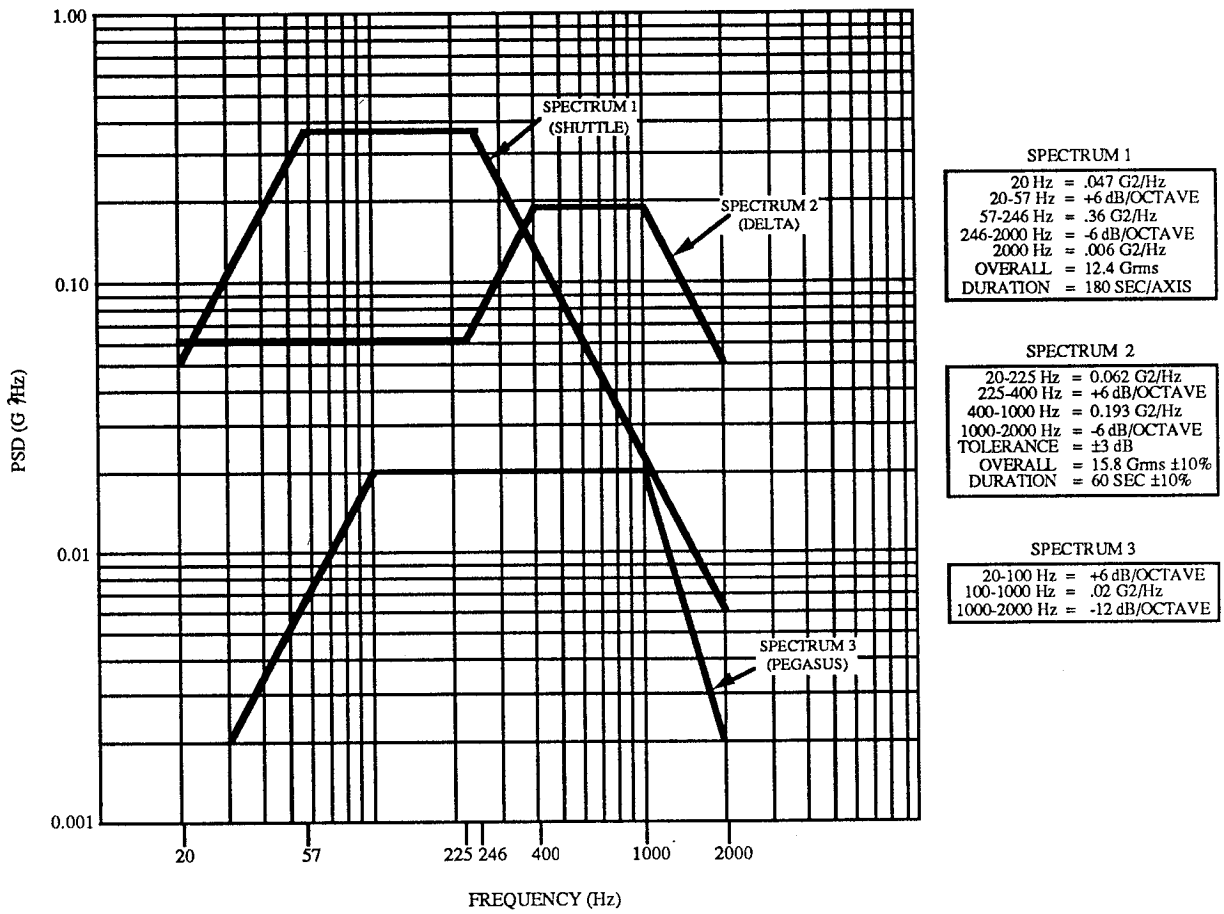

Figure 5-6: The reaction wheel is designed to be compatible with a variety of random vibration environments

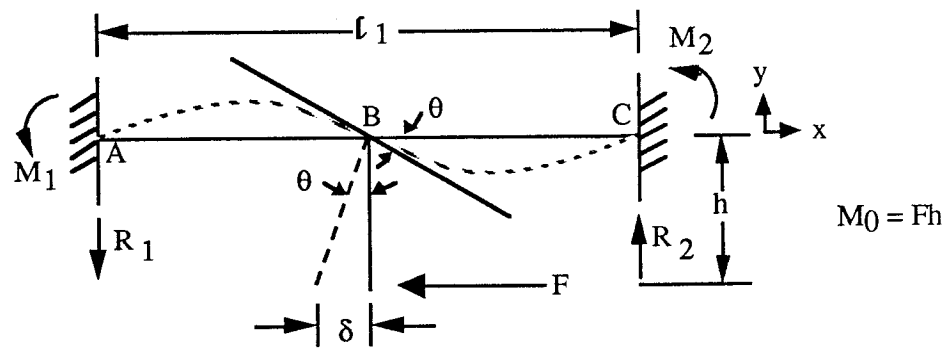

$$k_r = \frac{F}{\delta} = \frac{F}{h\theta} = \frac{16\ EI}{h^2 \ell_1}$$

Figure 5-7: A radial stiffness model of the supporting flexure was used to tune the radial resonance of the rotor to 350 Hz

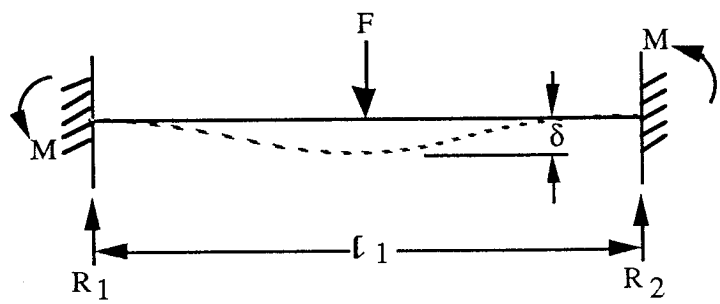

$$k = \frac{F}{y} = \frac{192\ EI}{\ell_1^3} \qquad k_a = \frac{576\ EI}{\ell_1^3} \text{ for 6 spokes}$$

Figure 5-8: Axial Stiffness Model

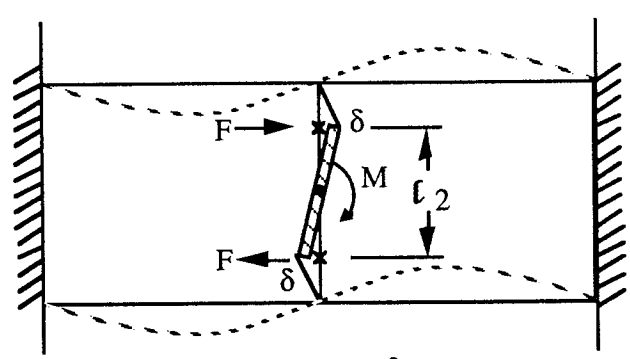

$$k_T = \frac{8\ EI\ \ell_2^2}{h^2 \ell 1}$$

Figure 5-9: Angular Stiffness Model

5.1.1.4 Sealing

Many reaction wheel designs are hermetically sealed, for a variety of reasons. One reason is to maintain the same level of performance in ground testing as in orbit. This is achieved by either evacuating the interior to a hard vacuum and sealing for life, or temporarily evacuating and sealing the interior for all ground testing and venting the interior prior to launch so it will be exposed to space vacuum. An alternate method backfills the interior with one half atmosphere of inert gas and seals the housing for life, in order to minimize the evacuation stresses on the housing and maintain an operating pressure compatible with the vapor pressure of natural hydrocarbon oils. The backfilled approach also improves the heat transfer within the mechanism by utilizing forced convection from the rotor, at the cost of additional power consumption due to rotor windage.

The potential use of the reaction wheel in combination with a scanning mirror prohibits sealing of the unit without a large, complex and expensive infrared window. In order to eliminate the costs associated with both hermetically sealing the housing and incorporating this impractical window, it was decided to develop a vented design. The major penalty resulting from this decision is that the performance data taken in air will be skewed by the windage torque, requiring a bell jar or thermal vacuum test set-up to acquire actual performance data. However, the windage torque can be easily characterized and removed from the data by a computer data acquisition system. Vented designs have been successfully flown in many momentum wheel and scanner applications, so heritage is not a significant issue.

A quasi-sealed environment was attained by using thin (0.020") aluminum sheet stock to fabricate covers which are placed over the spoked support structure. These are referred to as dust covers, or access panels. The weight of these covers is very small, because of the minimum thickness used. The faying surfaces of the covers are sufficiently smooth to prevent large contaminants from entering the unit interior, in order to maintain bearing cleanliness. Venting is achieved by a check valve effect of the cover edges. When a significant positive pressure differential exists between the interior of the housing and the outside, the cover edges deflect slightly due to the pressure loading. This allows quick venting of the interior during ambient depressurization. During ambient repressurization, the edges of the cover are clamped by the application of external pressure, and filter the air which slowly backfills the housing interior.

5.1.2 Rotor Construction

A typical solution to optimize the inertia to weight ratio of a flywheel is to couple a high inertia rim to a central shaft with a thin web. The objective is to concentrate the mass at the largest possible radius. A common technique is to use bi-metal construction, with a steel shaft to match the thermal expansion coefficient of the bearing material, an aluminum or beryllium web to minimize the weight of this non-inertia contributing component, and a high density rim such as tungsten, steel, or inconel to maximize the inertia contribution. The method of assembling these components is typically an interference fit. An interference fit on the rim, however, leaves significant residual hoop stresses in this area, and creates a situation for additional thermal stresses due to the dissimilar CTE's of the materials during exposure to temperature extremes. These hoop stresses are superimposed on top of operating stresses in the rotor due to centripidel forces, reducing the margins of safety in the rotor design.

5.1.2 Rotor Construction (Cont'd)

A configuration was chosen which utilized a 15-5 PH stainless steel shaft in order to match the CTE of the bearing material as closely as practical. The rim material is desired to be non-magnetic, to minimize the potential field disturbances, and to avoid eddy current losses between the rotor and the aluminum housing, should the rotor become slightly magnetized. A stainless steel rim was a potential candidate, but the strength of non-magnetic stainless steel in the 300 or 400 series is very low, resulting in low safety margins for high speed operation. Simple calculations revealed only a minor weight penalty for using a low density rim material. A benefit to using a low density material is a sharp increase in rotor strength due to the increased cross section. In order to reduce costs by minimizing the number of parts in the rotor assembly, an aluminum part combining the rim and web was selected. Aluminum alloy 6061 has been found to be inexpensive to machine, highly resistant to stress corrosion cracking, very dimensionally stable, and exhibiting an extremely high fracture toughness.

The stainless steel shaft is thermal fitted into the aluminum flywheel and secured additionally with a stainless steel hex nut. The motor selected in a subsequent section consists of high inertia cold rolled steel components bonded into the aluminum rim with structural epoxy. Samarium Cobalt magnets are bonded to the cold rolled steel magnet ring with the same structural epoxy, and aluminum spacers are bonded in the area between the magnets for increased inertia and improved structural strength. The cold rolled steel components are plated with electroless nickel to prevent corrosion. A thermal fit was not used on the motor components to avoid the thermal stresses in the rim and the potential distortions which could occur in the motor gap. The concentration of the mass of the motor on the rim more than compensates for the slight weight penalty accepted in order to use a low density material such as aluminium in the inertia rim. The web can be thinned down to reduce weight at the sacrifice of reduced stiffness. Rather than reducing the web thickness, the unneeded weight was removed by boring lightening holes in the rim. This retains much of the original stiffness, and allows visual and mechanical access through the rotor. This improves the inspectibility of the assembled unit, improving the reliability by more complete screening of workmanship defects.

In order to minimize the imbalance of the rotor due to the tolerances on the parts and the inevitable asymmetry of the structural epoxy used to bond the magnets and motor iron into the flywheel, a balancing process is required. The equipment and expertise required to perform precision balancing are extensive, so it was decided to subcontract the balancing. Schenck-Trebel has an operation nearby on Long Island, which does large and small volume, coarse and precision balancing of rotors. Schenck's equipment is known worldwide as the best balancing equipment available. Subcontracting was set up with Schenck to ship our completed rotor to them with tooling bearings mounted on the shaft, and they fabricated tooling to suspend the rotor on their balancing equipment. When left to the professionals, experience has shown that the precision balancing can be a very simple and reliable process. The balancing operation is performed by removing material from the edge of the aluminum rim on a grinder. The low density aluminum alloy rim is ideal for balancing operations, for it improves the resolution obtainable in a typical balance cut.

5.1.3 Bearing Mounts

The baseline design used a compliant bearing mounting scheme, to avoid the potential bearing stresses due to misalignment of the bearings. This was to be achieved by mounting the bearings in a flexible elastomer. This concept has a lot of merit for stressless operation of a set of bearings operating with minimal loads, however, the dimensional stability of such a configuration may not be sufficient for the application. Elastomeric materials tend to cold flow over time, resulting in dimensional changes in the direction of the momentum vector of the flywheel. Low accuracy systems may not require this stability, but the ground rule requiring upgradeability excludes this configuration. In addition, the application where a scanning mirror is coupled to the shaft requires even more dimensional stability of the rotation axis. As a result, a rigid bearing mounting scheme is required.

The considerations involved in selecting the bearing mounting scheme include alignment, thermal compatibility, and the prevention of fretting corrosion between similar materials. A 15-5 PH stainless steel bearing mount aligned within the linebored housing with a precision slip fit was selected due to its close CTE match with the bearing material. The sleeve within the mount in which the outer race of the bearing is installed is coated with Titanium Nitride to prevent the fretting corrosion which would be inevitable at the bearing and mount interface due to the relative microscopic movements of the race during operation. The spring preload scheme selected requires one bearing to be fixed, and one bearing to be able to float axially during relative changes in the shaft and housing dimensions due to thermal expansion and transient pressure differentials on the housing. The Titanium Nitride coating ensures that this floating action of the second bearing is preserved.

The preload spring requires some method of snubbing excessive deflections, so that the spring is never fully compressed. This was achieved by specifying flanged bearings. On the fixed end, the flange is used to mount the bearing. On the floating end, the flange limits the excursion of the spring. This configuration also allows the use of identical bearing mounts on both ends. This results in fewer part types for lower cost procurement.

The inner races of the bearings are secured to the shaft with precision spanner nuts. A double nut scheme is employed for the implementation of positive locking techniques. A common method of positively locking hardware is to stake the threads with epoxy. In applications near bearings, use of epoxy is not recommended due to the potential of epoxy migrating to critical bearing surfaces. The use of a double nut allows the first nut to be installed with no staking. The second nut locks the first nut, and can be staked with epoxy since it is sufficiently removed from the critical surfaces. This configuration has another advantage when a scan mirror is coupled to the shaft in a SCANWHEEL application. By eliminating the second nut on the scanner side of the housing, a mirror can be easily added by screwing it directly onto the threaded shaft, thereby becoming the second nut.

5.2 Bearings

Alternatives to ball bearing suspension systems for reaction wheels and other spaceflight systems have been sought for many years. Magnetic bearings have been successfully built and tested in order to increase the lifetime of rotating assemblies, but have rarely won out over conventional ball bearing suspensions in flight hardware fabrication. A weight penalty is encountered when the massive magnetic bearings are compared to compact passive ball bearing suspension systems, and the active control system required to stabilize the magnetically suspended rotor typically lowers the overall reliability to the point that passive ball bearings are a superior choice. The power required for the bearing control system also consumes a large portion of the power gained from the low drag torque advantage of the magnetic bearing. The low cost and minimum lifetime requirements for the SBIR reaction wheel excluded magnetic bearings from contention, resulting in a tradeoff analysis between various configurations of ball bearing systems.

5.2.1 Ball Bearing Tradeoffs

Ball bearing suspension systems have been used successfully in many reaction wheel applications. The variety of configurations are as numerous as the number of reaction wheel vendors. The tradeoffs involved in the selection of the bearing configuration are the bearing type, the preload scheme, the bearing materials and geometry, and the mounting method.

5.2.1.1 Bearing Type

The first tradeoff issue which must be addressed is the bearing type. Because of the precision and size of the bearings which are required for the reaction wheel, the bearings fall in the category of series R instrument bearings. Series R deep groove bearings have full shoulders on both sides of the raceways of the inner and outer rings. They can accept radial loads, thrust loads in either direction, or combinations of loads. In order to allow assembly with the full shoulders, these bearings require a two-piece steel ribbon type retainer. Series R angular contact bearings have one ring shoulder partially or totally removed. They can support thrust loads in one direction or combinations of radial and thrust loads, but not radial loading alone. Load and speed capacities are higher than for deep groove bearings, since the removed shoulder on one race allows a higher ball compliment. The removed shoulder also allows the use of a phenolic retainer commonly referred to as a 'halo cage'. This is desirable for low retainer wear, and the ability to vacuum impregnate the retainer with a small supply of lubricant. Both deep groove and angular contact ball bearings can be combined to form a duplex pair for increased capacity and rigidity. Figure 5-10 shows alternative methods of combining both types of bearings, in duplex pairs and separately. Two axially separated deep groove bearings have the advantage that they could potentially be used without preloading, resulting in low drag torque, but this would result in high non-repetitive runnout. Two duplex pairs have the advantage of high capacity and low runnout, but will be more costly and consume more power due to the higher bearing count and expense of matching the duplex pairs. A set of duplex pairs on one end and a deep groove bearing on the other end has the advantage of high capacity, but requires two types of bearings which will reduce the advantage of quantity buys. A set of two angular contact bearings has all of the advantages of low runnout due to the required preload, low cost and low drag torque due to the low bearing count, and high capacity from the angular contact bearings. The disadvantage of this configuration of being unable to accept bi-directional thrust loading during operation is not an issue in the reaction wheel design, since the application does not require thrust loading during operation. This configuration was therefore selected, requiring a preload scheme.

TYPE		ADVANTAGES
DUAL DEEP GROOVE	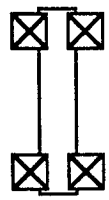	LOW DRAG LOW COST
DUAL DUPLEX PAIRS	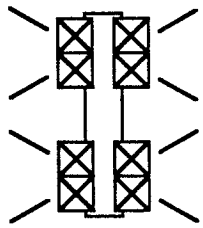	HIGH CAPACITY LOW RUNOUT
DUAL ANGULAR CONTACT	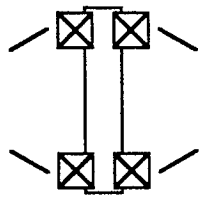	LOW RUNOUT LOW DRAG LOW COST HIGH CAPACITY
DUPLEX PAIR / DEEP GROOVE	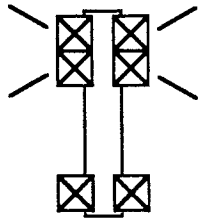	HIGH CAPACITY

Figure 5-10: Bearing Configuration Tradeoff

5.2.1.2 Bearing Preload

Preloading is required for the angular contact ball bearings selected, and is desirable for a precision device such as the reaction wheel in order to remove radial and axial play for more precise shaft positioning. Preloading also has the advantage of increasing the axial and radial stiffness of the suspension system. By maintaining ball-race contact, noise is reduced by preventing ball skidding, and load sharing is improved between bearings. The only disadvantages with preloading is that increased wear and higher drag torque results when compared to a bearing with zero load. However, the precision and stability required for the reaction wheel when it is used in an optical scanning system as a SCANWHEEL dictate that a preloaded scheme be incorporated.

There are basically three methods of preloading; springs, axial adjustment and duplex pairs. Duplex pairs are matched sets of bearings with the inner or outer ring faces selectively relieved a precise amount to result in an interference between the ball and race, which when compressed becomes the preload. The drawbacks of this type of preloading are a susceptibility to gross torque variations due to misalignment, and a sensitivity to differential thermal expansion within the bearing assembly. The primary advantage of the duplex pair is its inherent rigidity, which is not a specific requirement for the reaction wheel. Duplex bearings can also be separated by a distance by using Duplex bearing spacers. However, the rotor construction on the reaction wheel prefers access to the rotating portion of the suspension between the two bearings, which is unattainable with the duplex bearing spacers. Preload can also be applied with axial adjustment to remove the end play. This type of preload is very sensitive to temperature changes, and has large room for error during assembly. The simplest method of preloading is with a spring. This turns out to be the preferred method for the reaction wheel due to this simplicity, and the fact that it easily accommodates differential thermal expansion between the shaft and housing. Spring preloading also accommodates minor misalignment better than alternate methods. A stainless steel wavy washer spring was selected to preload the bearing pair.

5.2.1.3 Bearing Material

The most commonly used materials in spaceflight ball bearing manufacture are 52100 chrome steel and 440C stainless steel. The 52100 chrome steel is typically specified when capacity is critical, due to its superior hardness, however, it is susceptible to corrosion if exposed to moisture. The 440C stainless steel is more resistant to corrosion, but does not attain the hardness of the 52100 chrome steel. The inert environment of space vacuum reduces the risk of corrosion resistance during operation, but corrosion must still be controlled during storage and assembly. The tradeoffs between these materials are not significant in the application.

5.2.1.3 Bearing Material (Cont'd)

Several new materials have been recently introduced in the ball bearing market. Ceramic bearings and hybrid bearings with ceramic balls have been developed which greatly reduce wear, and have the potential of being used without lubricants. The brittle nature of the ceramics, however, is not compatible with the random vibration and pyrotechnic shock associated with spaceflight environments. Another state of the art technology in ball bearing design is incorporating Titanium Carbide (TiC) coated balls. During operation in the sub-EHD speed region, a lubricant is ineffective in providing satisfactory film to prevent contact between the balls and races. When this happens the asperities of the mating components can come together under sufficient pressure to micro-weld. As the ball advances, the weld area breaks, resulting in metal particles in the lubricant. As wear progresses, the lubricant becomes a slurry of degraded lubricant and metal wear particles, which further accelerates the deterioration of the mating components. Using dissimilar materials for the balls and races significantly reduces the wear in this regime. The insolubility of the TiC ball coating with the steel races eliminates the microwelding during sub-EHD operation. In addition, the TiC coating provides an 'emergency lubrication' scheme, providing extended lifetime throughout the entire operating speed range even after the lubricant supply is completely exhausted.

5.2.1.4 Bearing Load Ratings

The required capacity of the selected bearings is dictated by the loading during launch random vibration. In order to avoid permanent deformation of the bearing races (known as brinelling), the maximum contact stress levels in the bearing must be below 580,000 psi. This stress level is the basis for static load ratings established by the bearing manufacturers. The expected load levels are determined by random vibration analysis of the structure. These loads vary significantly depending on the launch vehicle's random vibration spectrum and the dynamics of the reaction wheel structure.

5.2.1.5 Bearing Tolerances

The standard tolerances on bearings are specified by the Anti-Friction Bearing Manufacturers' Association (AFBMA). Tolerance classes are specified in various degrees of precision from ABEC 3 to ABEC 9. The ABEC 7 class or better was selected for the reaction wheel, based on recommendations in DOD-A-83577A, the military specification for moving mechanical assemblies for space vehicles.

5.2.1.6 Bearing Selection

The final bearing selection was based on availability. In order to minimize costs and lead time, it was decided to purchase bearings available off-the-shelf from leading bearing manufacturers. A high capacity R4 bearing was selected from The Barden Corporation. This bearing is a hybrid of a conventional R4 bearing which has a high load rating. Thin section bearing tolerances, larger balls and a low conformity ratio were designed into the bearing to lower the contact stresses and increase the capacity. The negative tradeoff of this configuration is higher drag torque. However, these same parameters increase the lubricant film thickness, resulting is less asperity contact and less wear. The Barden Corporation does not have TiC coated balls available off-the-shelf, but a standard R4 bearing is available from Miniature Precision Bearing Corporation (MPB) with TiC coated balls. A comparison of the parameters of the MPB bearing and the Barden bearing is shown in Table 5-1. The capacity of the Barden bearing allows it to be used with nearly any current launch vehicle random vibration spectrum. The capacity of the TiC coated MPB bearing is compatible with many of the new small launch vehicles, including the Pegasus and the Air Force Small Launch Vehicle. Since there are many potential applications of small satellites which may use the smaller launch vehicles, it was decided to maintain flexibility in the design to allow either bearing to be used. This was simplified by the fact that the outline of both bearings is identical.

Table 5-1
Bearing Selection Comparison

Manufacturer	MPB	Barden
Part Number	CR4FM7LD	SFR4HX1
Material	52100 Steel w/TiC coated balls	440C Stainless Steel
Ball Size	3/32"	9/64"
Ball Compliment	9	8
Contact Angle	10.0°	12.7°
Axial Capacity	140 lbf	407 lbf
Radial Capacity	67 lbf	206 lbf
Dynamic Load Rating	172 lbf	520 lbf
Maximum PSD @ 365 Hz*	0.028 g^2/Hz	0.26 g^2/Hz
Maximum PSD @ 90 Hz**	0.28 g^2/Hz	2.4 g^2/Hz
Maximum Random rms acceleration	14.8 Grms	45.2 Grms
Maximum Steady State acceleration	37.8 g's	116 g's

* 3 sigma loads, Q=10
** 3 sigma loads, Q=6

5.3 Lubrication

Lubrication is required in a ball bearing to provide a separation film between the ball and race surfaces in order to minimize wear usually associated with microwelding of mating asperities on the bearing surfaces. The most common types of lubrication systems are dry films and liquid lubricants such as oil and grease.

Dry film lubricants such as MoS_2 have the advantage of vacuum stability and low viscous drag and are used in some low duty cycle applications, but do not have the endurance for a continuously operating system such as a reaction wheel. There have been non-spaceflight applications where the TiC coated balls have been used without lubrication. This would be extremely attractive for the attributes of low power consumption, no outgassing contamination, and no lifetime dependency on lubricant loss rates. This was considered to be too unproven and risky for a rugged, low cost design.

Liquid lubrication systems using grease and/or oil have been used successfully in many reaction wheel applications. An oil lubrication system was eventually selected over grease in order to avoid the unpredictable drag torque behavior of greases over temperature and life. Since the suspension system is vented to space vacuum, a low vapor pressure oil is required to minimize lubricant depletion due to evaporation. Bray 815Z oil was originally selected, since it has been used successfully on ITHACO's Conical Earth Sensors, and has become routine for space hardware since it meets NASA/NHB outgassing and flammability requirements. Bray 815Z is a synthetic flourocarbon perfluoropolyalkylether (PFPE) oil.

Many experiences with synthetic flourocarbons such as Bray 815Z have shown that they do not perform well under boundary lubrication conditions (Ref.1,2). Typically, performance in the boundary region is enhanced by using antiwear additives. However, the PFPE fluids are unable to dissolve additives, so significant wear can be expected when operating in the boundary region. In addition, the Bray 815Z has demonstrated polymerization when used in high wear applications. It has been demonstrated that under boundary lubrication, metal flourides are formed at the asperity contacts, which then go on to catalytically decompose the remaining fluid.

The TiC balls used in the MPB bearings would indeed reduce the amount of wear during boundary region operation and greatly reduce the chances of polymerization of the Bray oil (Ref 2), but the knowledge of a catastrophic failure mechanism with the chosen lubricant in a required operating mode demanded that alternatives be investigated.

Several candidate lubricants were involved in the initial tradeoff study to select a lubricant for the suspension system. The natural hydrocarbons were rejected due to their high vapor pressures which were incompatible with the required vented design. A newly synthesized hydrocarbon from Pennzoil which has a vapor pressure as low as the Bray 815Z was considered to be unproven. This lubricant, known as Pennzane™ X2000, has since been life tested in a spaceflight mechanism at TRW (Ref. 3) and has been tested in boundary lubrication tests at Aerospace Corp (Ref. 4). The test results have demonstrated successful performance operating in the boundary region under vacuum conditions.

5.3 Lubrication (Cont'd)

The properties of the Bray 815Z and the Pennzane™ X2000 are listed in Table 5-2 for comparison. The relevant properties include the viscosity, the viscosity index, and the vapor pressure. It can be seen from the table that the viscosity of the Bray is higher at room temperature, which will contribute to less wear by promoting a lower EHD liftoff speed. The high viscosity index of the Bray is also desirable to reduce the performance variations over temperature excursions and to sustain EHD liftoff as temperatures are increased. The vapor pressures of the two oils are nearly identical, but the molecular weight of the Pennzane™ is lower, which will result in less lubricant depletion due to evaporation. Drag torque at room temperature should be less with the Pennzane™ than with the Bray 815Z due to the lower viscosity, but low temperature drag torque will increase due to the low viscosity index and higher pour point of the Pennzane™.

Table 5-2
Lubricant Property Comparison

	Bray 815Z	Pennzane™ X2000
Viscosity		
@100°C (ASTM D445)	45 cSt	14.7 cSt
@40°C (ASTM D445)	148 cSt	112.0 cSt
@0°C (ASTM D2602)		1000 cP
@-20°C (ASTM D2602)	1125 cSt	6000 cP
@-40°C	11500 cSt	66500 cP
Viscosity Index (ASTM D2270)	350	135
Flash Point (ASTM D92)	299°C	315°C
Fire Point (ASTM D92)	330°C	326°C
Pour Point (ASTM D97)	-112°C	-57°C
Molecular Weight	7000 gm/mole	910 gm/mole
Density @ 20°C (ASTM D1298)	1.866 gm/ml	0.846 gm/ml
Refractive Index (ASTM D1747)	1.294	1.4691
Total Weight Loss	0.8%	0.160%
Vacuum Condensable Material	0.05%	0.056%
Vapor Pressure 125°C	2×10^{-7} Torr	4×10^{-7} Torr
Vapor Pressure 20°C	8.7×10^{-12}	1×10^{-12} Torr

5.3.1 Lubricant Wear Testing

In order to assess the suitability of Pennzane™ in the T-SCANWHEEL, a sample was procured and tested in the T-SCANWHEEL Engineering model (Ref. 5). The testing performed consisted of measurements of EHD liftoff speeds and drag torque with the Pennzane™ lubricant as a function of temperature. The EHD liftoff speed was measured by monitoring, on a chart recorder, the electrical series resistance through the bearings during the acceleration of the rotor. The speed at which electrical isolation was acquired was recorded, and the testing was repeated while the temperature of the assembly was elevated. The results are compared with similar tests performed using the Bray 815Z. A graph of the EHD liftoff speed versus temperature for the Barden high capacity bearings is shown in Figure 5-11, with the Bray data superimposed on the Pennzane™ data. The data show that the Pennzane™ lubricant may result in more bearing surface wear than the Bray 815Z at a similar temperature. This is due primarily to its lower viscosity and lower viscosity index. From these data it can be seen that the Pennzane™ provides sufficient EHD liftoff capability in the application of a SCANWHEEL operating at a biased speed of 2000 to 3000 rpm, as long as the ambient temperature is below 35°C. Table 5-3 shows the relative EHD liftoff speeds for the two lubricants and the two optional bearings used in the suspension system. The fact that the EHD liftoff speed for the MPB bearings is greater than for the Barden high capacity bearings is compensated for by the TiC coated balls, so both bearings are relatively equal as far as wear is concerned.

The Pennzane™ lubricant alone will result in more wear than the Bray when used at speeds below 2000 rpm as in a bi-directional reaction wheel application. However, the additional wear is not catastrophic like the potential polymerization of the Bray, and can be minimized with an extreme pressure additive such as lead napthanate.

Table 5-3

	Nominal EHD Liftoff Speed @ 23°C	
	Bray 815Z	Pennzane™
Barden SFR4HX1	550 rpm	1000 rpm
MPB CR4FM7 w/TiC coated balls	1200 rpm	2100 rpm

5.3.2 Lubricant Performance

The performance of a lubricant in the reaction wheel application is primarily a function of viscosity. Higher viscosity will cause higher bearing drag torque, which will result in a loss of torque margin, and higher steady state power consumption. The viscosity versus temperature relationship for the Pennzane™ and the Bray 815Z is presented in Figure 5-12. The lower viscosity index of the Pennzane™ is apparent, and will be a source of more varied performance over temperature. In order to quantify the performance changes, testing was performed on the engineering model reaction wheel at room temperature and at -30°C. Steady state power consumption at 2500 rpm was compared, and drag torque measurements were made from 2500 rpm to 100 rpm. The drag torque data for the high capacity 440C stainless steel Barden bearing (SFR4HX1) is shown in Figure 5-13. All of the drag torque data were taken in air, and windage was removed mathematically to result in a measurement of bearing drag torque. The comparison is made using 10 ml of free oil in identical bearings. As expected, it can be seen that the room temperature drag torque is lower with the Pennzane™ due to its lower viscosity, but the low viscosity index results in significant increases in drag torque at low temperature. With the high capacity Barden bearings, the drag torque with the Pennzane™ at cold temperature will increase by approximately one oz-in over the Bray 815Z. This will increase the steady state power consumption at 2500 rpm by approximately 2 Watts at cold temperatures.

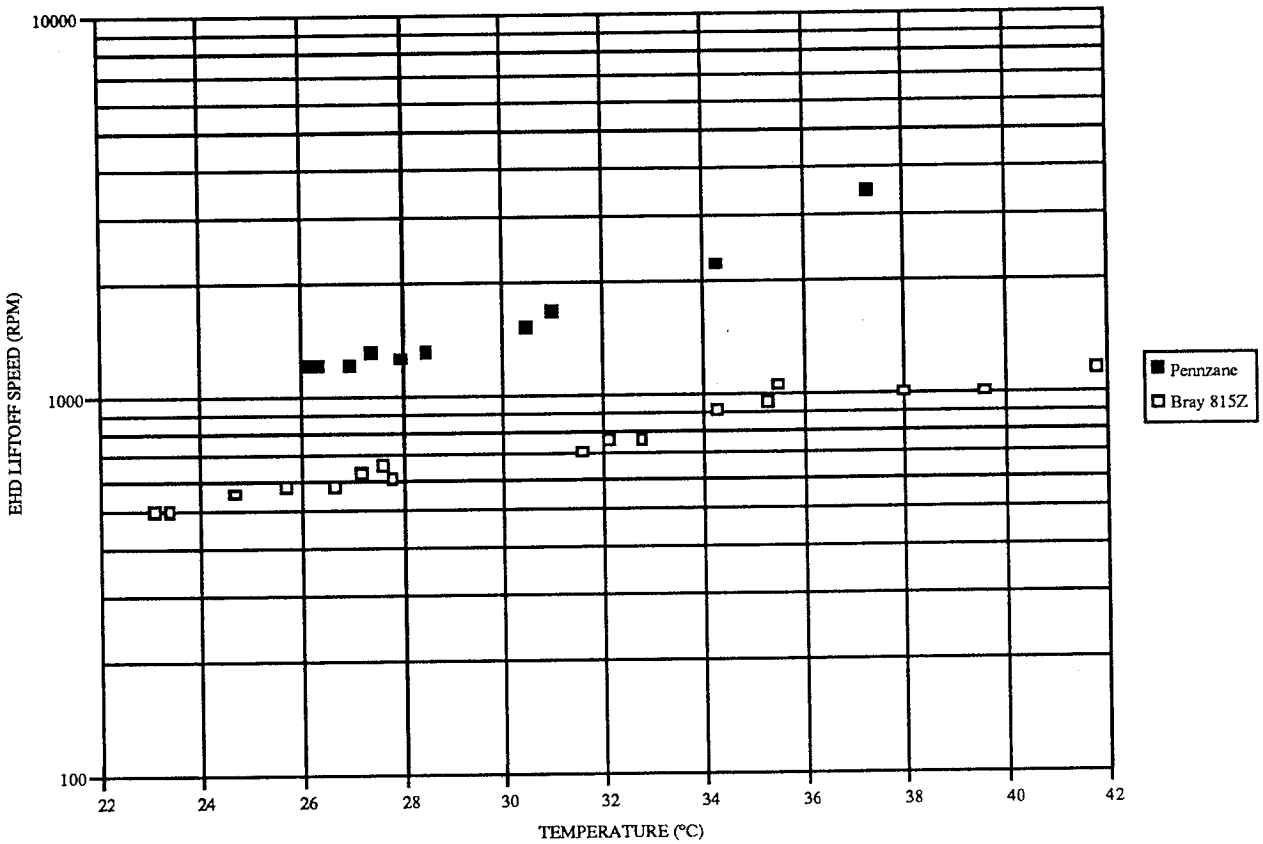

Figure 5-11: EHD Liftoff Vs. Temperature (SFR4HX1 Bearings)

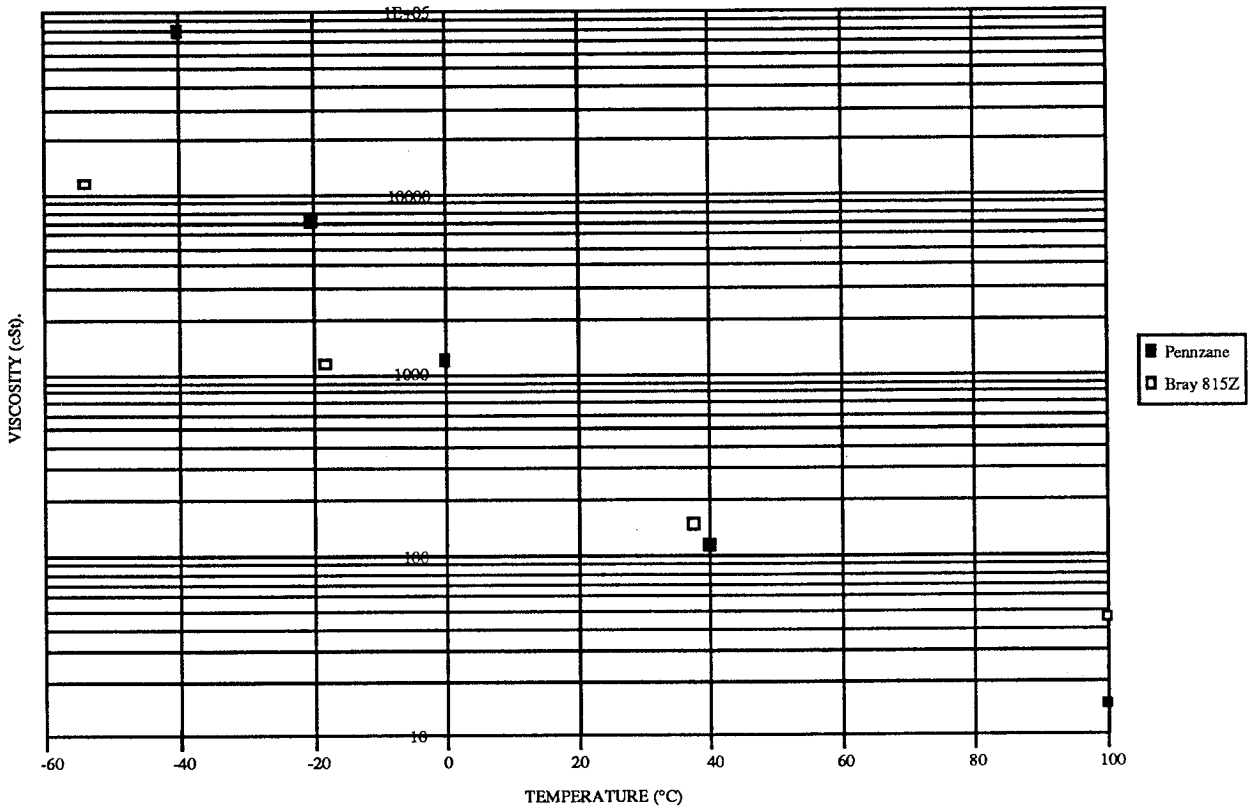

Figure 5-12: Lubricant Viscosity Vs. Temperature

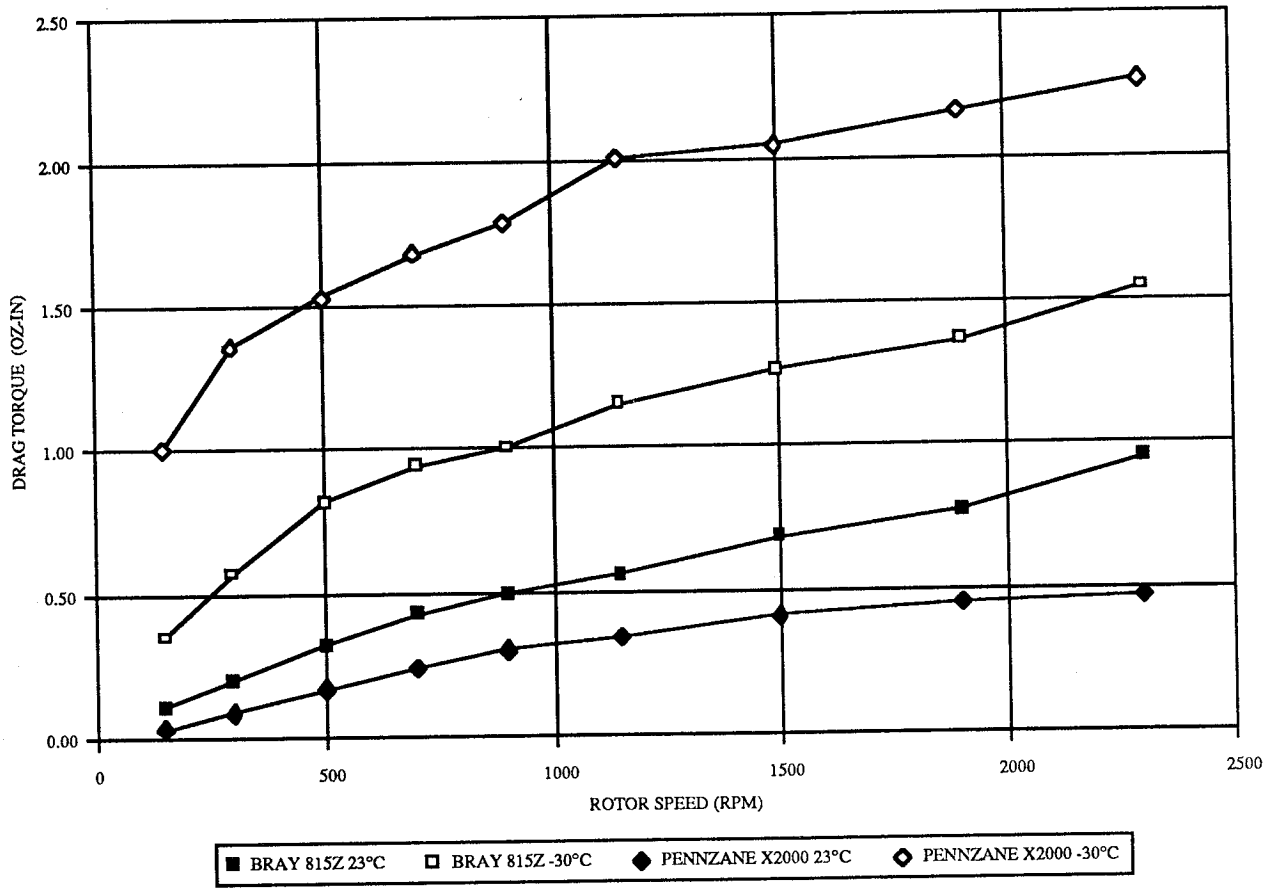

Figure 5-13: Bearing Drag Torque (Barden SFR4HX1)

5.3.2 Lubricant Performance (Cont'd)

The Barden bearings utilize a very close race conformity in order to optimize the load carrying capacity, which results in high drag torque friction levels. The close conformity also increases the dependency of drag torque on lubricant viscosity. The alternative standard R4 bearing from MPB with TiC coated balls is also used interchangeability in the reaction wheel design, which exhibits lower drag torque friction. This bearing contains smaller balls and a higher conformity ratio to minimize the drag torque losses. However, the static load capacities of this bearing are only compatible with launch vehicles with low random vibration levels such as the Pegasus. These bearings were also tested with the Pennzane™ lubricant at low temperatures. Figure 5-14 shows that the steady state drag torque at temperatures down to 0°C is relatively unaffected. However, below 0°C, the drag torque becomes somewhat unpredictable. Figure 5-15 shows the drag torque at -10°C, where some unpredictability in the drag torque is seen below 1800 rpm. Figure 5-16 shows the drag torque behavior at -20°C. A severe reduction is observed in the drag torque at this temperature above 1500 rpm. Below 1500 rpm the drag torque increases and becomes unpredictable. It is surmised that this effect is due to temporary channeling of the high viscosity oil at high steady state speeds, and subsequent collapsing of the channels as the ball velocity is reduced to a point where the thick lubricant can flow back into the ball track before the next ball advances. This condition may prevent the lubricant from wetting the bearing surfaces and forming an EHD film, so higher wear could result at temperatures below 0°C. Figure 5-17 shows the bearing drag at -30°C. At this severe temperature, the drag torque becomes extremely unpredictable. The conclusions of this testing with the MPB bearings suggest that the lubrication mechanisms are not 100% effective at temperatures below 0°C, resulting in increased bearing wear and unpredictable torque behavior. For this reason, long term operation with the Pennzane™ lubricant should be avoided at this temperature extreme.

The temperature testing also included measurements of the breakaway torque required to cold start the motor. In all cases, the cold start was achieved with less than 0.3 Volts of torque command, which corresponds to less than 0.2 oz-in. This did not seem significantly affected by temperature with either of the two alternate bearings.

5.3.3 Lubricant Life

When determining the design lifetime of a pair of lightly loaded instrument bearings such as those used in the reaction wheel design, the classical ball bearing failure mode of fatigue is not a serious consideration. Rather, failure is typically initiated by lubrication system inadequacy, which in the reaction wheel design would most likely result from lubricant depletion due to evaporation and surface migration. The oil supply within the bearing is retained between the balls and the raceways within the limits of surface tension. A meniscus of oil is formed at the ball/race contact which is circulated beneath the balls to form the EHD separation film.

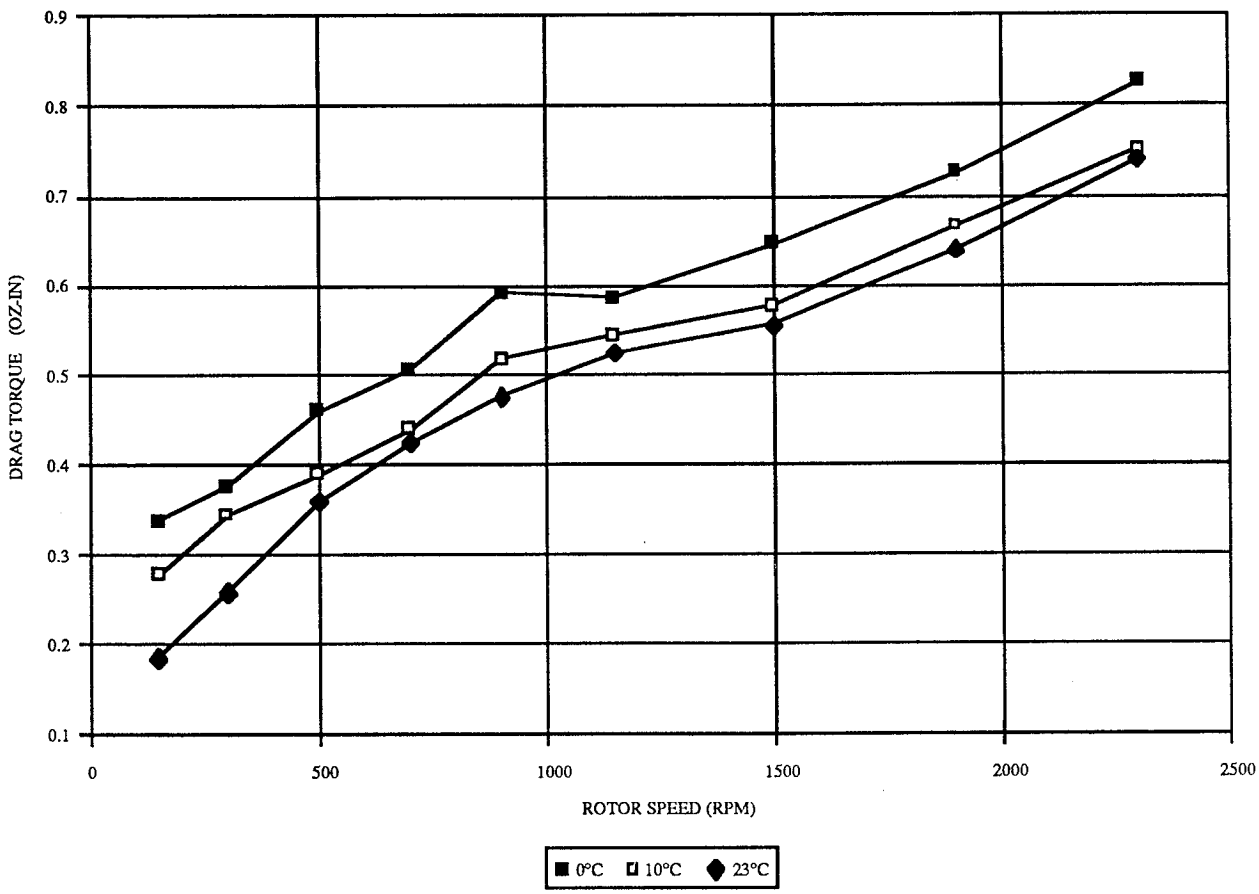

Figure 5-14: Drag Torque Vs. Speed and Temperature (MPB CR4FM7 with TiC Coated Balls and Pennzane™ Lubricant)

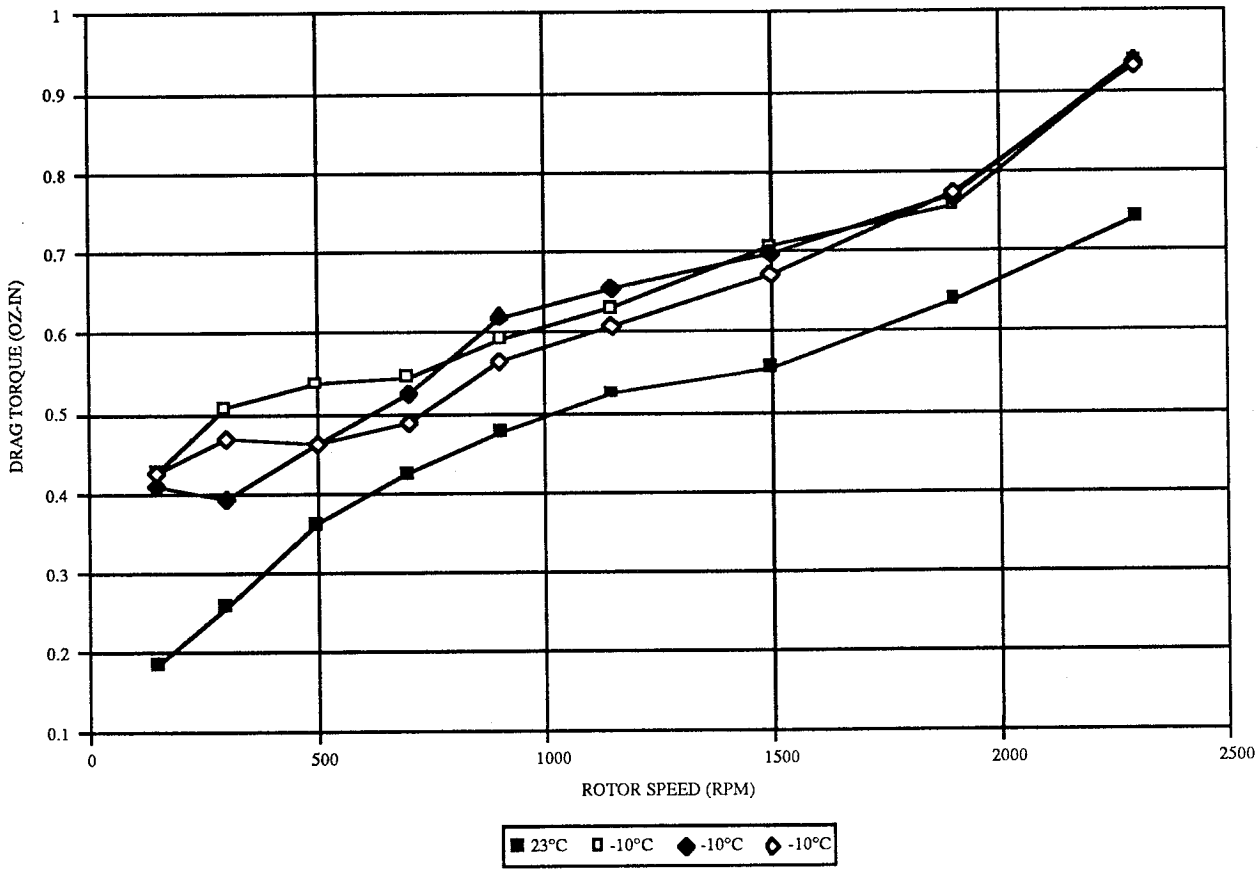

Figure 5-15: Drag Torque Vs. Rotor Speed at -10°C (MPB CR4FM7 with TiC Coated Balls and Pennzane™ Lubricant)

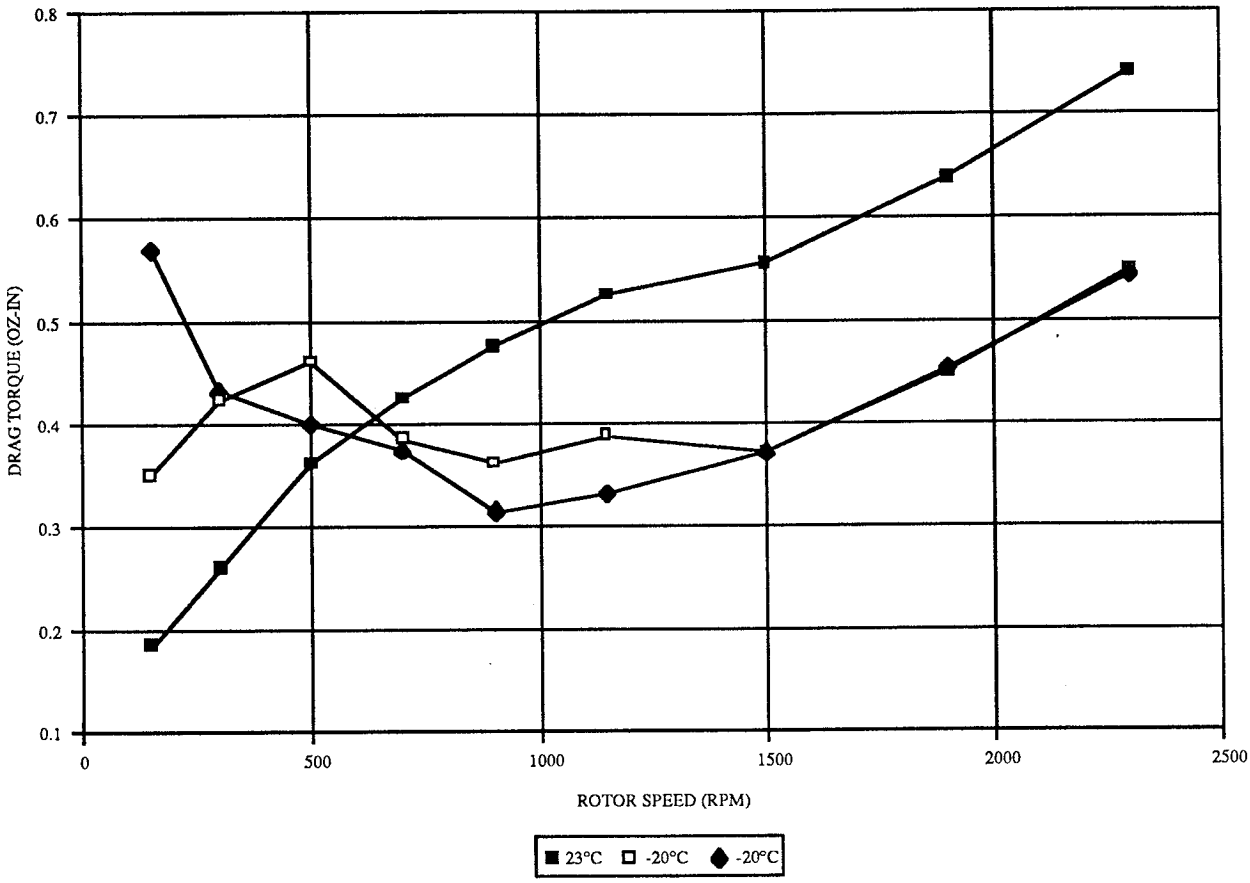

Figure 5-16: Drag Torque Vs. Speed at -20°C (MPB CR4FM7 with TiC Coated Balls and Pennzane™ Lubricant)

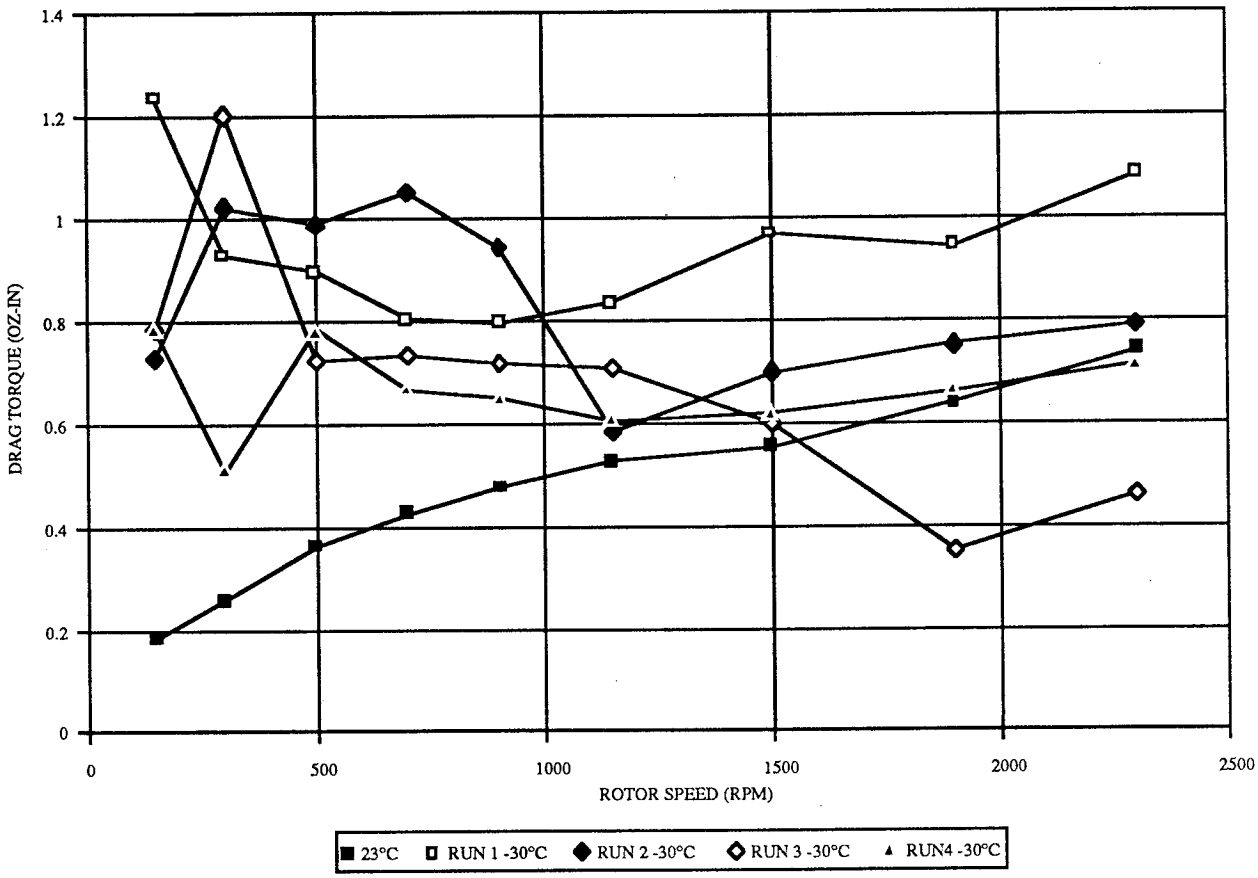

Figure 5-17: Drag Torque Vs. Rotor Speed at -30°C (MPB CR4FM7 with TiC Coated Balls and Pennzane™ Lubricant)

5.3.3 Lubricant Life (Cont'd)

The evaporation loss rate can be calculated by:

$$G = \sqrt{\frac{M}{T}} \frac{P}{17.14}$$

where G=evaporation rate, g/cm^2 s; M=molecular weight; T=absolute temperature, K; and P = vapor pressure, torr at temperature T (Ref. 6). This equation neglects the benefit of the labyrinth seals, thus providing a conservative estimate. The two important lubricant properties which affect the evaporation rate are thus the molecular weight and the vapor pressure. From Table 5-2, both of these parameters are lower for Pennzane™ than for the Bray 815Z, which will result in a lower evaporative loss rate for the Pennzane™. If the density of each lubricant is considered by assuming that the same volume of each lubricant is used, the lubricant properties result in evaporation rate of the Pennzane™ to be 10% of the evaporation rate of the Bray 815Z at 20°C. In addition, losses due to surface migration will be less with the Pennzane™ than with the Bray 815Z due to the higher surface free energy of the Pennzane™.

5.3.4 Lubricant Optical Transmission

The lubricant in the reaction wheel may be used in the vicinity of a rotating scan mirror which reflects infrared radiation into a narrow bandpass optical system to detect the earth's horizon. After long term exposure in space vacuum, there is a possibility that some of the lubricant may condense on the mirror surface and reduce the effective transmission of the optical system. Infrared absorption scans for the two lubricants are shown in Figure 5-18 and Figure 5-19. Comparison of the scans of both lubricants reveals that the Pennzane™ is much clearer in the region of the horizon sensor's infrared bandpass from 14.2 to 15.6 microns. An absorption spike occurs at 13.8 microns (wavenumber 721 cm^{-1}) in the Pennzane™, but it is very narrowband and not in the horizon sensor's optical passband. The Bray 815Z demonstrates some broadband absorbance at 14.5 microns (wavenumber 690 cm^{-1}) which is in the optical passband, so the Pennzane™ has preferable optical properties. Both lubricants are virtually transparent in the visible portion of the spectrum.

5.3.5 Lubricant Selection

With the exception of its low viscosity index, the Pennzane™ X2000 appears to be superior to the Bray 815Z for the reaction wheel applications. When used as a momentum wheel application operating at a biased speed of 2000 rpm or more, the bearing surface wear should be the same regardless of which lubricant is used since both are operating in the EHD regime. Low temperature performance in a biased speed application appears to be only slightly affected by the low viscosity index of the Pennzane™. In applications required to operate throughout the entire speed range, the Pennzane™ does exhibit a power consumption penalty at low temperatures and potentially unpredictable drag torque while varying speeds below 0° C, but the alternative of using the Bray which may polymerize in such a boundary lubrication application is unacceptable. Therefore, the Pennzane™ X2000 was selected to be used in the reaction wheel in all applications. Long term operation at temperatures above 35° C and below 0°C should be avoided in order to minimize wear and prolong life.

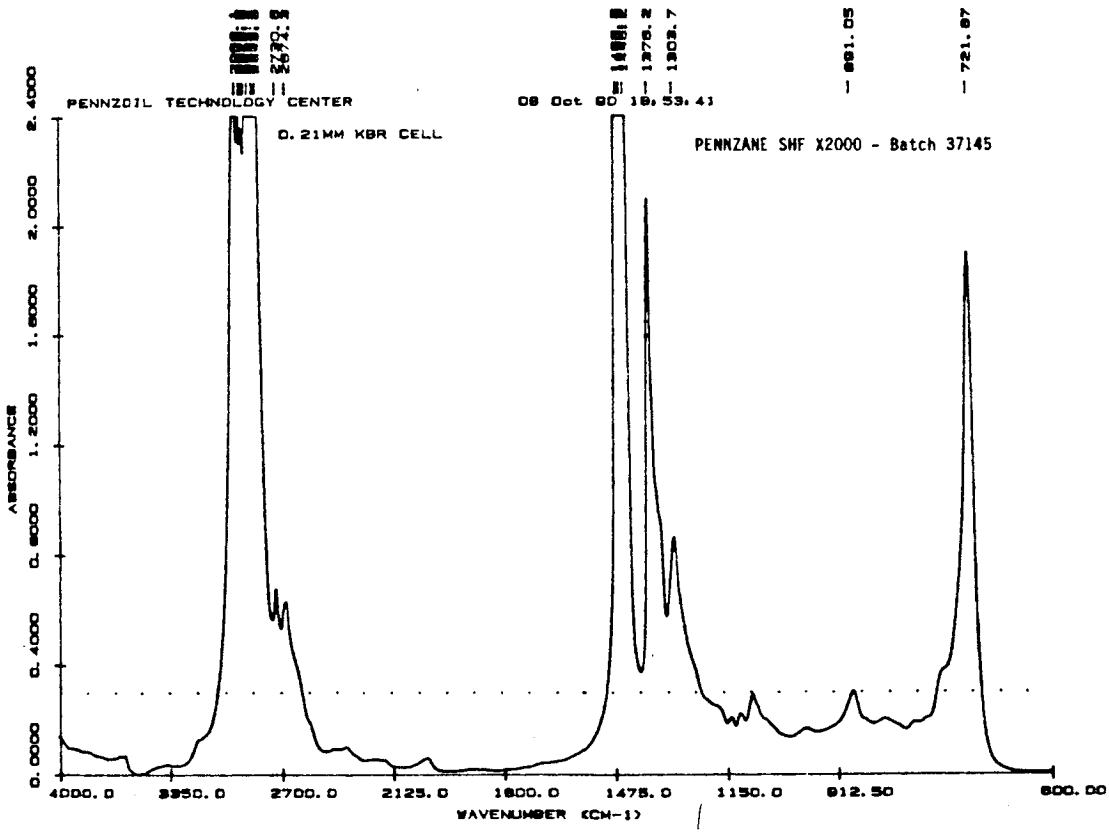

Figure 5-18: Pennzane™ X2000 Absorbance Spectrum

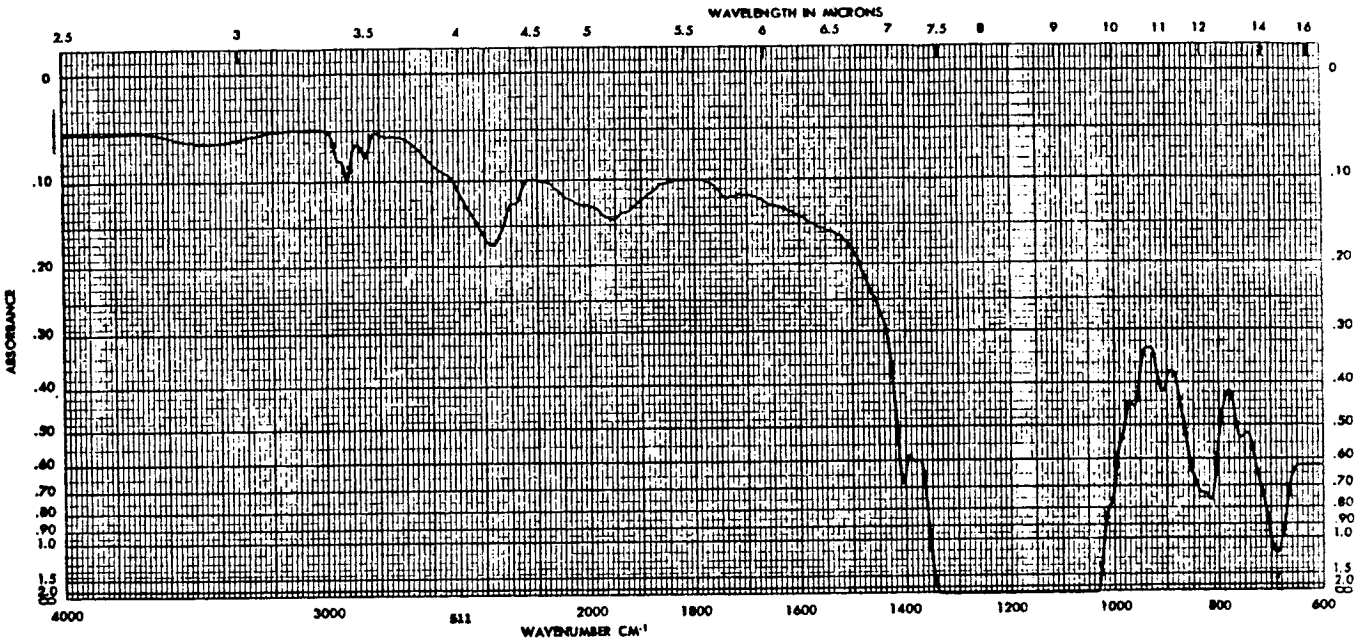

Figure 5-19: Bray 815Z Absorbance Spectrum

5.4 Motor

An integral direct drive motor is required in the reaction wheel to spin up the flywheel, maintain speed, and provide instantaneous reaction torque to the spacecraft.

5.4.1 Motor Type

The two candidate motor types which do not require contacting brushes are AC induction motors and brushless DC motors.

The AC induction motor has the advantage that it involves no permanent magnets, and therefore has no drag torque from eddy current losses, and no cogging. The induction motor is driven open loop by a simple circuit consisting of two square wave current sources 90° out of phase. There is no low frequency torque ripple, and the speed is conveniently limited by the synchronous frequency of the driver. This type of motor has been used successfully in many reaction wheel applications. The disadvantages of the induction motor are that the torque is not linear with respect to rotation speed, and the efficiency is extremely low. The linearity is desirable, but not necessarily critical, since it has been successfully dealt with in numerous attitude control systems. However, the high priority placed on power consumption in the tradeoff considerations deals the induction motor a severe blow.

Most of the more recent reaction wheel designs employ a brushless DC motor due to its higher efficiency and linear torque. Hall sensors are typically employed for discrete commutation, which serve a second function of providing a tachometer signal. This type of motor is more power efficient than the induction motor, resulting also in a lower stator mass required to conduct waste heat away from the windings. One disadvantage is a slightly more complex motor driver requiring rotor position feedback information for commutation. This can be accomplished with the use of hall sensors, optical switches or eddy current probes. The fact that this type of information is required for tachometer feedback from the wheel for the attitude control system turns this into an advantage. The brushless DC motor does have significant torque ripple, at a frequency corresponding to the commutation rate, which is the number of poles multiplied by the number of phases and the rotation rate. For a two phase, six pole motor operating at 500 rpm, this corresponds to a torque ripple frequency of 100 Hz, which could be low enough to cause undesirable torque disturbances on some spacecraft. The presence of rotating permanent magnets in the brushless DC motor design also produces cogging and eddy current drag torque.

During the development of magnetic bearings for spaceflight applications, an ironless armature brushless DC motor was developed by Phil Studer at NASA GSFC and Henry MacLanski of MacBar mechanisms. The ironless armature motor was required for the magnetic bearings for its characteristic of no radial forces, which can be a significant destabilizing force in the active magnetic bearing control system. In a reaction wheel application, the ironless armature motor is ideal, since it minimizes the overall system weight by placing all of the motor iron on the flywheel.

5.4.1 Motor Type (Cont')

A cross section of an ironless armature motor is shown in Figure 5-20. It consists of a thin armature which supports the windings, with a set of magnets on one side and a flux return path on the other side. The result is a motor which exhibits no cogging or eddy current drag, since there is no relative movement between the magnets and the iron flux return ring. Because of this, the iron components need not be laminated, which reduces the cost of these parts. The efficiency of an ironless armature motor is maximized by utilizing the largest possible diameter, since the number of poles is increased and torque radius is increased. By increasing the number of poles, the resolution of the tachometer signal from the commutation signal is also increased. Hence, the ironless armature motor is ideal for the reaction wheel drive, by being both power and weight efficient. In typical applications, the ironless armature motor is more massive than a comparable conventional brushless DC motor, because the magnet gap is extremely large to accommodate a thin section armature inserted into the gap with clearance on both sides. This enlarged gap requires large magnets and heavier low reluctance iron components to compensate for the increase in magnetic gap. In the reaction wheel application, however, the added weight is where it would be required anyway to fulfill the flywheel inertia requirements.

5.4.2 Motor Selection

The unique combination of lowest power consumption and lowest weight makes the ironless armature motor the obvious choice. This unlikely result occurs once in a lifetime in tradeoff analyses, so it would be a shame to not take advantage of this configuration. The ironless armature motor is not new in the reaction wheel arena. European manufacturers of spaceflight reaction wheels have been using ironless armature motors in their designs for many years.

Initial estimates predicted a higher cost for procurement of the ironless armature motor, but this was offset by the drastic weight savings over conventional motors. The weight savings was on the order of a pound, which can translate to several thousand dollars in launch costs on even the most economical launch vehicles. However, actual quotes to manufacture production quantities of flight quality motors were much higher than expected, in the $8K - $12K range, resulting in an impossible price tag for a low-cost reaction wheel. The high cost was primarily due to the fabrication complexity of the armature, due to the hand labor for winding and the numerous spaceflight quality solder connections required.

Rather than discard the ironless motor design, a possible solution was presented to MacBar Mechanisms to reduce the recurring costs. Most commercial ironless motors have a printed circuit armature in a disk configuration. If it were possible to manufacture the armature windings on a flexible printed circuit and laminate it to a fiberglass epoxy ring, the recurring costs would be competitive with conventional motors, and the reliability would also be enhanced. MacBar agreed that it could be done, but that they did not have enough experience with flexible printed circuits to take on the job. Other commercial printed circuit motor manufacturers did not want to bother with the unconventional configuration for a short-order design.

A make/buy decision was made at ITHACO to design and build the ironless armature motor in-house. MacBar Mechanisms was solicited to perform the electrical and magnetic design of the motor on a consulting basis, and the mechanical packaging of the armature and the fabrication was performed at ITHACO.

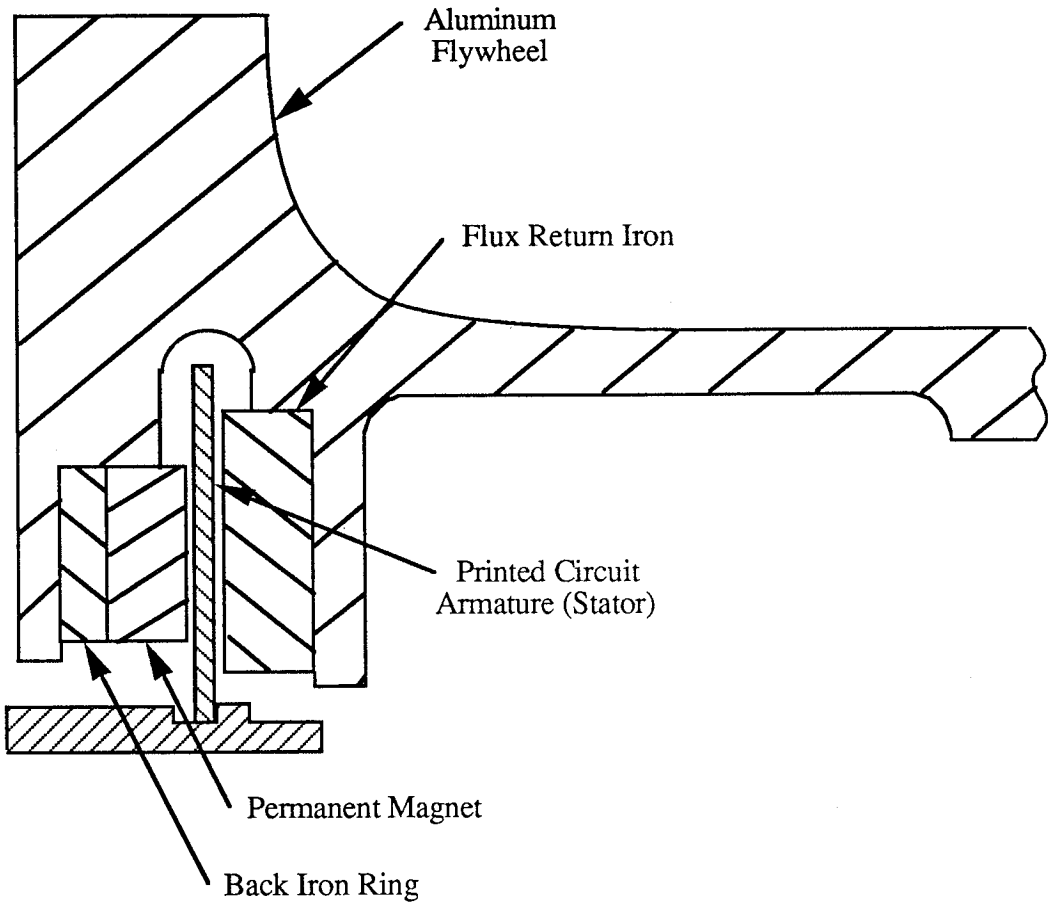

Figure 5-20: The Ironless Armature Brushless DC Motor is an optimum drive for momentum/ reaction wheels due to its unique combination of high efficiency and high inertia/weight

5.5 Tachometer

A tachometer signal is required for speed and direction of rotation feedback from the reaction wheel. Attitude control systems can use either an analog tachometer voltage proportional to speed, or a digital tachometer of a square wave with a frequency proportional to speed. The analog tachometer can be easily derived from the digital type of tachometer, so the logical type of tachometer is the digital type. The incorporation of a digital tachometer with an analog tachometer circuit as an option also lets the customer select the preferred tachometer signal for his system. In addition, a discrete digital signal is required to commutate the brushless DC motor.

Digital tachometer signals are commonly generated by magnetic pickups, eddy current probes, hall generators, and optical switches.

Magnetic pickups are rugged, reliable, passive devices, used commonly in momentum wheel applications operating at a biased speed. However, the amplitude of the signal generated from these devices is proportional to speed, so the signal degrades as the speed is reduced. This is not compatible with a reaction wheel application requiring bi-directional operation through zero speed.

Signals derived from eddy current probes are insensitive to the speed of the flywheel, but require a complex, unreliable oscillator circuit to stimulate the eddy current effect. The accuracy of the eddy current systems is low and the power consumption is high relative to other devices. A machined gear in the flywheel is required to stimulate the eddy current probe, which increases manufacturing costs.

Optical switches are also used commonly for reaction wheel tachometers, especially where high resolution and high accuracy is desired. Light from an LED is directed towards a phototransistor and interrupted by a shutter or a alternately reflecting/absorbing surface. The simplicity of this design ranks it very high, but the high power consumption required to illuminate the LED is too high for an ultra-low power consumption design.

Hall generators are commonly employed for commutation of brushless DC motor. The hall generators can be stimulated directly from the permanent magnets in the motor, so a separate gear or code wheel is not required. The phasing of the hall sensors signals when stimulated by the actual motor magnets is exactly correct for commutation, eliminating any alignment procedure required to clock a separate gear to the motor. The circuitry to bias the hall sensors is very simple, requiring only a constant current source. The sinusoidal output of the hall sensors when excited by the motor magnets can be easily processed into discrete commutation and digital tachometer signals with a simple comparator circuit.

5.5.1 Tachometer Selection

The hall generators were selected for the reaction wheel tachometer because of their low cost and the fact that their simplicity eliminated the need for many additional parts. They can be integrated directly into the armature assembly to minimize the packaging requirements for the commutation and tachometer components.

5.6 Motor Driver

5.6.1 Motor Driver Design Goals

Goals for the motor driver design echo those for the entire reaction wheel. These goals are summarized as follows:

Extremely low power consumption, high efficiency (less that 0.5 Watt at 1000 rpm)
Simple Reversing
Motor Drive Down Capability
Operation on 6 V Power Bus (0-2500 rpm Operation)
Adaptability to 28 V Power Bus (0-5100 rpm Operation)
Motor Control via Torque Command
Return of Stored Energy to the Power Bus
Low Cost

In order to fulfill the design goal for minimum power consumption, the motor driver had to be as power efficient as possible. The design specification of less than 1 Watt of power consumption at 1000 rpm leaves less than 0.5 Watt for the motor driver when the bearings and motor consume over 0.5 Watt under normal conditions. In order to fulfill a variety of applications, bi-directional torque and speed capability was required, and simple reversing of torque and speed was desired. For the sake of convenience at the attitude control system level, a motor torque control proportional to an analog torque command was desired, with torque linearity an asset, but not a rigid specification. Return of stored energy in the flywheel to the power bus was also a desirable option. The 6 volt bus on the XSAT satellite dictated that the motor driver be designed for this voltage, but because of market demands, it was deemed extremely desirable to be able to adapt the motor driver to operate with a 28 volt bus as an option.

5.6.2 Motor Characteristics

The electromagnetic requirements for the design of the ironless armature motor resulted in an unconventional design with the following basic parameters:

Motor Type:	3 phase, delta connected brushless DC
Winding Resistance:	0.1 Ω
Winding Inductance:	35 μHy
Position Sensors:	3 hall sensors
Back EMF:	0.00167 V/rpm
No. of Poles:	36

The 0.1 ohm winding resistance of the motor indicates that connecting the windings directly across the power bus would result in a 50 amp current. Consequently, the driver design must have instantaneous control of motor current at all times.

5.6.3 Driver Topology

A functional block diagram of the motor driver circuit is shown in Figure 5-21.

5.6.3.1 Power Bridge

The efficiency requirements mandated a directly switched pulse width modulated three-phase bridge. Due to the extremely low winding inductance, small discrete inductors were added in series with the bridge outputs. These inductors also serve to reduce RF emissions from the driver.

Because of the low 6 volt bus voltage, inefficiencies from diode forward drops and bipolar transistor base drive requirements could not be tolerated. Consequently, the three-phase bridge is constructed from power MOSFETS. In addition to reducing drive power requirements, diode drops from the bridge were eliminated, since, with proper gate drive, the MOSFETs act as synchronous rectifiers.

5.6.3.2 Commutation

In order to meet the power and performance requirements the commutation control circuitry is implemented from discrete CMOS digital and low power opamps and comparators.

For simplicity and low cost, a conventional "square wave drive" scheme was selected. This results in a textbook torque ripple of 15%, which has been judged not to be significant in the application, since the steady state torque is very low and the large number of poles results in a fairly high torque ripple frequency. Motor current control was chosen as an approximation of output torque control. This is compatible with typical momentum bias Attitude Control Systems.

Conventional BDC drivers operate in either "current mode" (two quadrant) or "voltage mode" (four quadrant). Current mode operation is simpler to implement and slightly more efficient than voltage mode, however, the following limitations prevented its use:

Motor Braking is difficult and unsafe, especially with a low resistance winding.
Bi-directional operation requires a "direction command".
The current mode driver will not return motor kinetic energy to the bus.
Use of the bridge MOSFETS as synchronous rectifiers is not straightforward, limiting efficiency potential.

Consequently, a 4-quadrant drive scheme was selected. This scheme allows simple monitoring and control of the bridge current under all conditions as well as seamless reversing and full four-quadrant torque controlled servomotor operation. When the motor is driven down, the bridge acts as a boost converter, and delivers the motor kinetic energy safely to the power bus instead of dissipating it in the bridge or the motor windings.

5.6.3.3 Pulse Width Modulation

A hysteresis - type "pulse width modulator (PWM)" provides coherent and instantaneous control of the motor winding current. The PWM operating frequency is essentially proportional to bus voltage. Components are selected so that the PWM nominal frequency is close to 20 KHz.

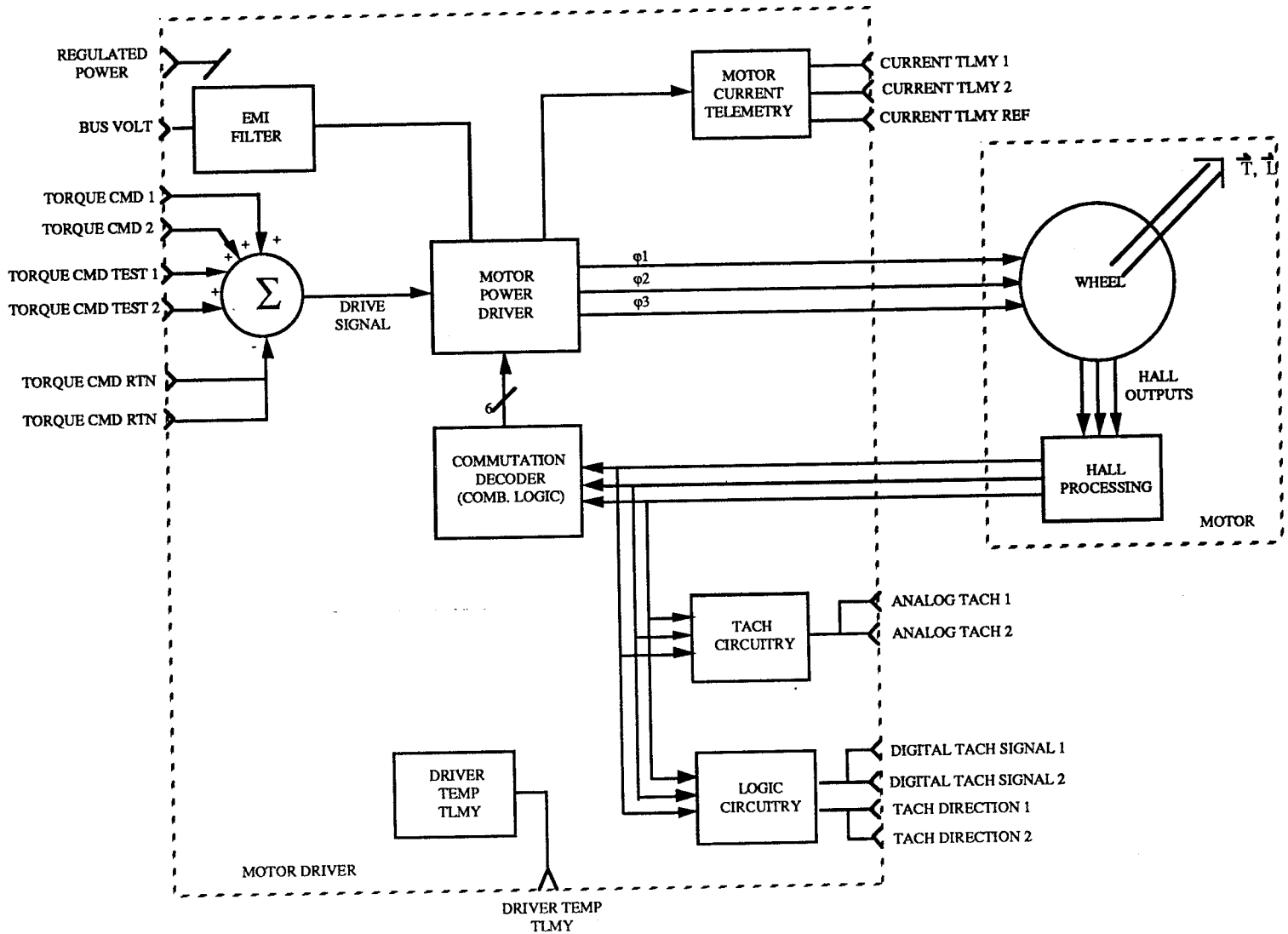

Figure 5-21: Motor Driver - Functional Block Diagram

5.6.3.4 Supplementary Features

5.6.3.4.1 Ballast Circuit

Many motor driver users cannot absorb the negative bus current obtained during motor drive down. The Ballast circuit is an optional current shunt that sinks all negative bus current generated by the motor driver to the power return.

5.6.3.4.2 Telemetries

The motor driver was designed for maximum versatility by offering a wide variety of telemetries.

5.6.3.4.2.1 Temperature Telemetry

One conditioned thermistor is located on the motor driver circuit board. No thermistor was designed into the reaction wheel itself in order to maintain modularity within the wheel housing, for the incorporation of a thermistor requires a solder operation at the top assembly which must be desoldered if the unit is ever disassembled. The configuration of any reaction wheel does not allow instrumentation of both bearings without dual connectors. The ITHACO Reaction Wheel configuration does allow for a thermistor to be added to the motor side of the wheel with minor impact. However, its value is questioned.

The primary function of locating a thermistor on the bearing is to monitor the health of the bearing. However, this can be monitored with more precision using the motor current telemetry. The temperature telemetry data is clouded by changes in ambient temperature, high thermal time constants, and low resolution. A thermistor within the wheel would be located directly on the bearing cartridge on the motor side. Due to the low thermal resistance between the bearing cartridge and the mounting surface, the resolution of the thermistor would be less than 0.25 volts per oz-in of increase in bearing drag torque. Temperature rise in the opposite bearing would be imperceptible since the bearings are practically decoupled from each other by the low thermal conductivity of the shaft. However, the same one oz-in of drag torque increase in either bearing would result in more than a 0.5 volt differential in the motor current telemetry while operating at a steady state speed of 2000 rpm.

The tradeoffs in utilizing the thermistor interface within the motor housing involve sacrificing redundancy on the +5 V going to the wheel assembly, and sacrificing the redundancy on the chassis ground connection to the wheel, as well as sacrificing the thermistor located on the motor driver card. As a result, the baseline design utilizes only the thermistor on the motor driver, with an option to relocate the thermistor within the reaction wheel housing with the described sacrifices.

5.6.3.4.2.2 Speed/Direction of Rotation Telemetry

Each hall sensor provides an 18 pulse per revolution digital signal for speed information. The relative phasing between any two hall sensors is used in a phase detector circuit to generate a rotor direction of rotation flag. Combining the edges from the three hall sensors with digital logic results in a 54 pulse per revolution digital tachometer signal. The same information is processed to deliver a complementary bipolar analog tachometer.

5.6.3.4.2.3 Motor Current Telemetry

An analog signal proportional to current in the motor windings is provided, since it contains the most significant data regarding the health of the motor, motor driver, and bearings. Small changes in bearing drag torque can be detected by monitoring the steady state motor current at a specific speed.

5.6.3.4.3 Commands

The user has access to four summed bipolar analog torque commands and a driver enable command.

5.6.4 Motor Driver Packaging

An effort was made to identify off the shelf motor controller and driver Hybrids and ICs which could be used in this driver. A market survey identified a Unitrode 3620/3622 which is a complete motor driver in a plastic power package. The vendor has been trying to successfully install this part in high reliability packaging. The part had the following limitations:

Quiescent Power Consumption was greater than the entire motor/driver power budget.
True 4 - quadrant control was not possible.
Potential efficiency using the bipolar technology was limited.
Operating voltages were not compatible with the 6 V bus.

Ideally, the entire motor driver should be enclosed within the motor. Because of the discrete circuitry, and space limitations within the motor, the motor driver was designed to be installed on a 6x6 circuit card compatible with ITHACO's modular packages. A portion of the circuitry was installed within the motor housing on a small round circuit card required for termination of the flexible printed circuit motor windings from the ironless armature motor. The constant current source to power the hall sensors and the comparators required for the discrete commutation signals are included on this circuit card.

The design of the printed circuits in the ironless armature motor allows the torque constant of the motor to be modified with simple jumper wires on the circuit board within the motor housing. By stringing the four motor windings in series, series-parallel, or parallel, three torque scale factors could be used, along with three back-emf constants. This allowed the versatility to use the same motor at different bus voltages, as the back-emf constant typically limits the speed of operation. The motor driver was designed to accommodate the three winding configurations along with multiple bus voltages by simply adjusting the motor current scale factor by component value substitution on the circuit card.

6.0 FINAL DESIGN DESCRIPTION

The Reaction Wheel consists of an aluminum flywheel with a thermal fitted stainless steel shaft suspended on ball bearings and driven by an ironless armature brushless DC motor. The housing structure is made up of two symmetrical aluminum plates which are separated by a cylindrical ring on the outside diameter and form a spider-web bridge to support the rotor. As is common with many flight proven reaction wheel assemblies, the housing is vented to space to minimize viscous drag torque from the flywheel due to windage. A cross section identifying the major components of the assembly is shown in Figure 6-1.

6.1 Ball Bearing Suspension System

The flywheel is suspended by a pair of non-separable, angular contact, spring preloaded ball bearings. The inner races of the bearings are clamped onto a stainless steel shaft by spanner nuts, and the outer races are slip fit into stainless steel cartridges. A wavy washer preload spring provides a light preload to remove the axial and radial play in the bearings, and accommodate the axial thermal expansion of the shaft and housing. The two bearing cartridges are identical, and are aligned with a similar slip fit with the aluminum housing. Assembly machining of the bore through the housing ensures precision alignment of the bearings, and also provides excellent momentum vector alignment. A sketch of the suspension system layout is shown in Figure 6-2.

The bearings are a standard R4 configuration purchased to ABEC 7 tolerances. The arrangement shown was chosen for its stability and low drag torque, since a complete suspension can be accomplished with two bearings by preloading the bearings with a preload spring. An alternate method of preloading with duplex pairs requires twice the bearing count, which doubles both the power and cost of the bearing units. The angular contact bearings employ one piece phenolic ball separators, which do not significantly contribute to wear, and can be impregnated with a small supply of lubricant.

6.2 Lubrication System

Since the Reaction Wheel Assembly is vented to space, a low vapor pressure oil is used to minimize lubricant depletion due to outgassing. The Pennzane X2000 is a synthetic hydrocarbon with an extremely low vapor pressure, which has demonstrated excellent boundary lubrication capability when used with Lead Napthanate as an extreme pressure additive.

The bearings selected for ITHACO's Reaction Wheel use conventional 52100 steel races, and steel balls coated with titanium carbide (TiC) applied by chemical vapor deposition. The insolubility of the TiC ball coating with the steel races eliminates the microwelding during sub-EHD operation. In addition, the TiC coating provides an 'emergency lubrication' scheme, providing extended lifetime throughout the entire operating speed range even after the lubricant supply is completely exhausted. An optional high capacity bearing using 440C stainless steel balls and races is available for applications which have severe random vibration requirements.

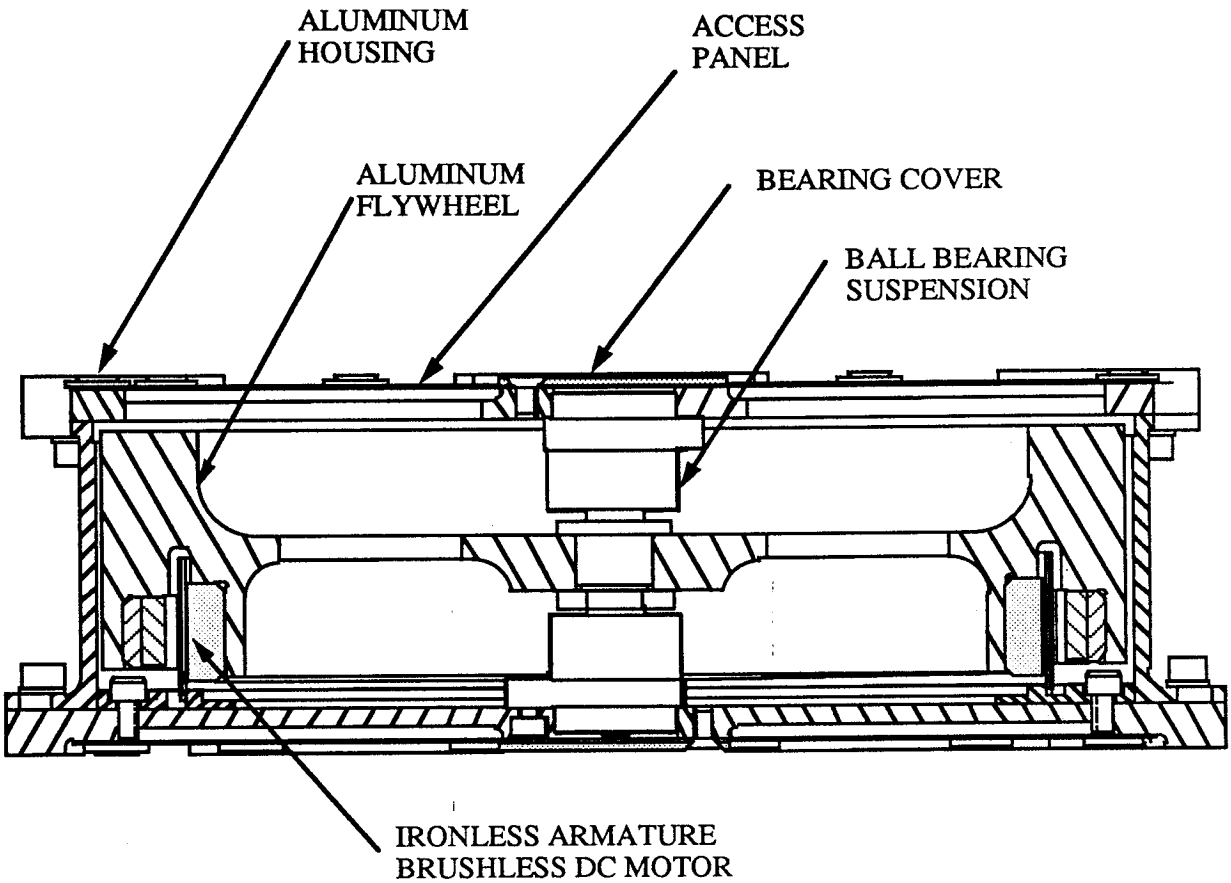

Figure 6-1: Reaction Wheel Assembly

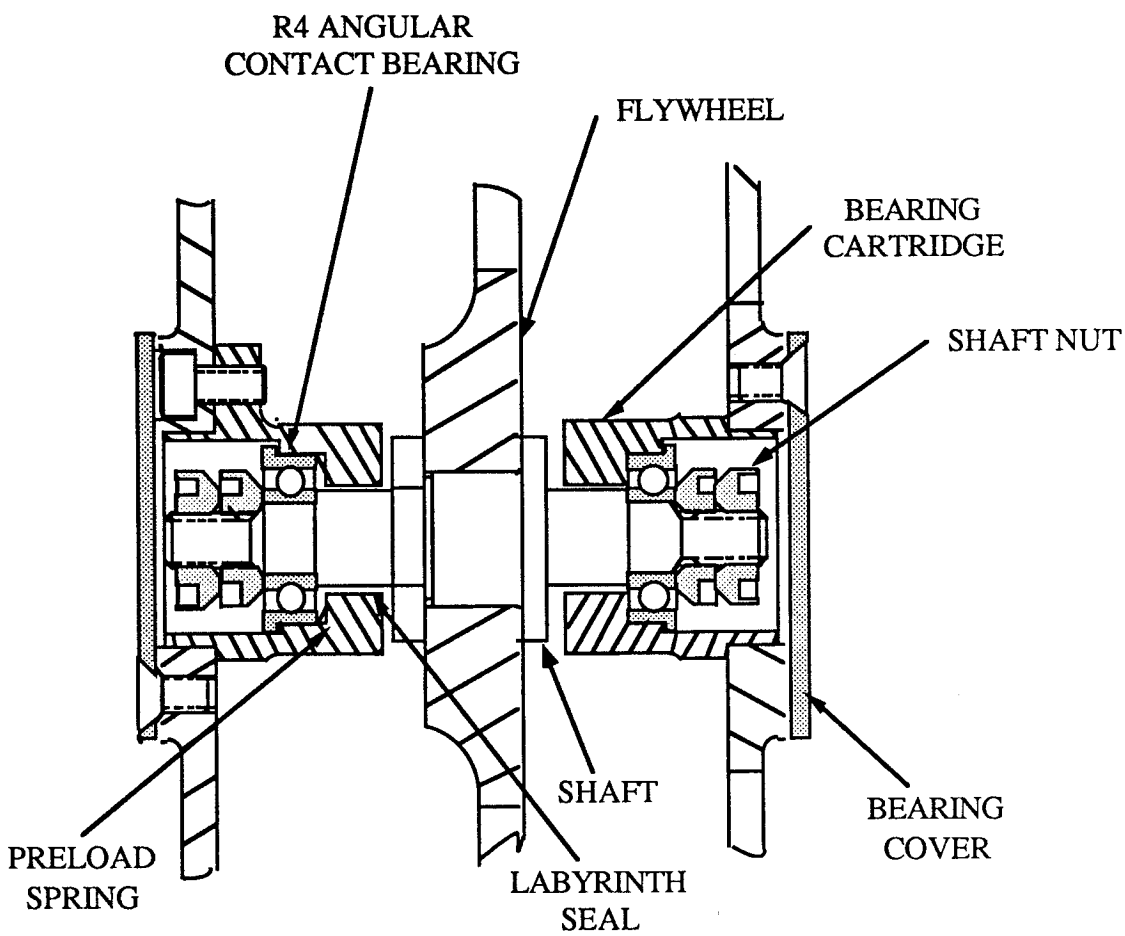

Figure 6-2: Reaction Wheel Suspension System

6.2 Lubrication System (Cont'd)

Several features are incorporated into the design of the lubrication system in order to minimize the loss of lubricant from the bearings. Close clearance labyrinth seals are used between the rotating shaft and the bearing cartridges to restrict the flow of molecules toward the vacuum, and the surfaces inside the bearing cartridges are coated with a thin film of the bearing oil to provide a sacrificial oil atmosphere inside the bearing cartridge volume. This film not only serves to provide the oil atmosphere, thereby reducing the net evaporation rate from the bearings, but it will also inhibit the surfaces from becoming a condenser that would rob molecules from the atmosphere surrounding the bearings. In addition, the one piece phenolic retainers are vacuum impregnated with bearing oil in order to serve as a small oil reservoir within the bearing volume. Another source of lubricant depletion from bearings is surface migration. In order to prevent this, a barrier film coating is placed at strategic locations near the bearings. No barrier film is used directly on the bearings, in order to avoid contamination of the bearing surfaces, which would cause non-wetting of that area resulting in a local area of high wear.

6.3 Motor

The Reaction Wheel motor is driven by a discretely commutated, ironless armature, brushless DC motor. Maximum inertia to weight ratio is realized with the large diameter motor components and the unique feature of the ironless armature motor which strategically places all of the mass of the iron and magnets on the rotor. Hall sensors integrated directly on the armature sense the alternating flux field from the permanent magnets to provide commutation information for the motor driver, as well as a high resolution tachometer signal for speed and direction of rotation information. The motor driver is conveniently packaged in a 6" x 6" x 1" card frame, for integrating into a modular attitude control system, or as a separate enclosed electronics box.

7.0 BREADBOARD UNIT MANUFACTURE

An engineering prototype of the reaction wheel was fabricated in order to validate the design decisions and assess the manufacturability of the hardware. The following sections address the problems encountered during the fabrication, and the resulting solutions.

7.1 Rotor Assembly Manufacture

The assembly of the rotor was basically a three part process. The first process is the thermal fitting of the shaft in the flywheel. This was successfully accomplished by heating the aluminum rotor to 200°F, and cooling the shaft in liquid Nitrogen. The shaft was then placed into the central bore in the flywheel and allowed to return to room temperature. A locking nut was then installed, torqued, and staked with epoxy.

The installation of the magnets onto the magnet ring was performed with a special geared fixture which aligns the magnets relative to each other. Structural epoxy was placed on the inside diameter of the magnet ring, and the magnets were installed in the respective locations. Aluminum spacers were installed between the magnets with structural epoxy. When the magnet ring was installed into the aluminum flywheel, a film of epoxy was applied to the bore diameter in the flywheel and the magnet ring was inserted. This process forced a small spot of excess epoxy to form in the motor gap, which was later detected during a test where the unit was being run at high speed with high drag torque bearings. The motor armature heated slightly and caused interference between the epoxy and the motor armature. The friction heating from the interference caused local expansion of the armature which increased the friction and the heating, resulting in a seizure of the motor, and destruction of the windings in that area. This process was modified for subsequent builds of the rotor by applying the epoxy to the outside diameter of the magnet ring, rather than the inside diameter of the bore, so that any excess epoxy is forced out the bottom of the rotor where it can be easily cleaned off. Additional inspection steps were also incorporated to ensure sufficient motor clearance. The rotor was sent to Schenck Trebel for precision balancing.

7.2 Stator Manufacture

The first motor stator was assembled from a fiberglass epoxy ring, an aluminum base ring, and three Kapton flexprints with a single zig-zag conductor for an equivalent of one turn per pole, per phase. The flexprints were bonded to the fiberglass epoxy ring with transfer film adhesive, and the assembled armature was bonded into the aluminum base ring with epoxy. Hall sensors were installed using transfer film adhesive, and all components were terminated on a piece of vector board attached to the inside diameter of the aluminum base ring.

This preliminary assembly was installed in the housing with the rotor and bearings, and integrated with the breadboard motor driver. The performance seemed to indicate the presence of a source of high drag torque increasing proportional to speed. Investigation revealed that the losses were caused by eddy currents in the motor windings themselves. The copper conductors were 0.1 inches wide, resulting in a large surface area for circulating eddy currents from the dynamic magnetic fields of the motor. This was corrected by striating the conductors into 8 parallel conductors. By terminating the eight conductors at four separate pads, the option was opened to adjust the motor torque scale factor and back emf constant by simply modifying the termination jumpers on the flexprints. The windings could be connected all in parallel, in series parallel, or all in series to result in three different motor designs.

7.2 Stator Manufacture (Cont'd)

The flexprints were redesigned and assembled onto a fiberglass epoxy armature support. In order to minimize the eddy current drag torque due to leakage flux from the motor magnets in the aluminum stator base ring, the material for the base ring was changed to fiberglass epoxy. The low electrical impedance of the motor windings results in very little heat dissipation in the windings, so the low thermal conductivity of the fiberglass epoxy was not considered to be detrimental. The striated flexprints effectively eliminated the eddy current drag torque.

7.3 Breadboard Unit Configuration

The only change required in the configuration of the engineering breadboard unit reaction wheel assembly was the fabrication of a new motor armature when excess epoxy in the motor gap caused interference and subsequent destruction of the flexprint motor windings. Various bearings have been alternately installed in the unit for engineering testing. Currently the unit consists of mechanical components dimensionally the same as flight hardware, a vector board within the wheel housing for termination of the motor winding flexprint assemblies and hall sensors, and a breadboard motor driver on vector board. The breadboard motor driver and the reaction wheel are interconnected with a 15 pin sub-miniature D connector pigtailed off of the termination vector board in the motor housing, and three pigtailed banana jacks from each node of the delta configured motor windings.

8.0 BREADBOARD UNIT TEST DATA

The development testing performed on the breadboard engineering unit consisted of a vibration modal survey of the structure, measurement of the external magnetic field, extensive testing of lubricants and bearings, and performance characterization.

8.1 Modal Survey

In order to verify the predicted dynamic characteristics of the reaction wheel structure a modal survey was performed on the breadboard engineering unit. The resonant frequencies and transmissibilities of the rotor assembly are critical in order to accurately predict the statistical bearing loads during random vibration exposure. A small analytical vibration facility at Cornell University was used for the testing.

Using a constant white noise spectrum on the order of 0.001 g^2/Hz from 10 to 1000 Hz, transfer functions were obtained in several hardware configurations. Response accelerometers were placed directly on the rim of the rotor. The axial response to an axial input is shown in Figure 8-1. A classic response of a single degree of freedom system is apparent, with a resonance at 89.13 Hz. This correlates very well with the predicted resonant frequency of 100 Hz. The measured transmissibility of 5.9 also corresponds to a predicted value of 5.6, based on the square root of the resonant frequency. The radial response to a radial input is shown in Figure 8-2. The radial resonance of 365.2 Hz also corresponds with the designed resonant frequency of 350 Hz, and the measured transmissibility of 10.5 shows some conservatism in the estimated value of 14. Figure 8-3 shows the axial response to a radial input, which shows the rocking mode resonance to appear at 129.6 Hz. This is very close to the predicted frequency of 122 Hz. Figure 8-4 shows the phasing of opposite ends of the rotor to verify the rocking mode is indeed in the neighborhood of 130 Hz, by highlighting the phase shift which occurs at that frequency.

The measurements taken were very close the the responses predicted by the structural math model. The successful results enable confident prediction of bearings loads and structural factors of safety, and form a baseline from which the effect of design iterations and modifications can be extrapolated.

8.2 Drag Torque Data

Drag torque measurements were performed throughout the development testing on the breadboard engineering unit. The drag torque is the best measurement of the health of the unit and a primary contributor to the performance of the hardware.

The drag torque is determined by measuring the rate of decay of the rotor speed. Using a computer or a stopwatch for data acquisition, the rotor speed vs. time is measured. From these data, the drag torque is determined from the following relationship:

$$\text{Drag Torque (oz-in)} = I \cdot (rpm_1 - rpm_2) \cdot 20.11/\Delta time$$

where: I = Flywheel Inertia (ft-lbf-sec^2)
rpm_1 = first speed reading
rpm_2 = second speed reading
$\Delta time$ = time between speed readings

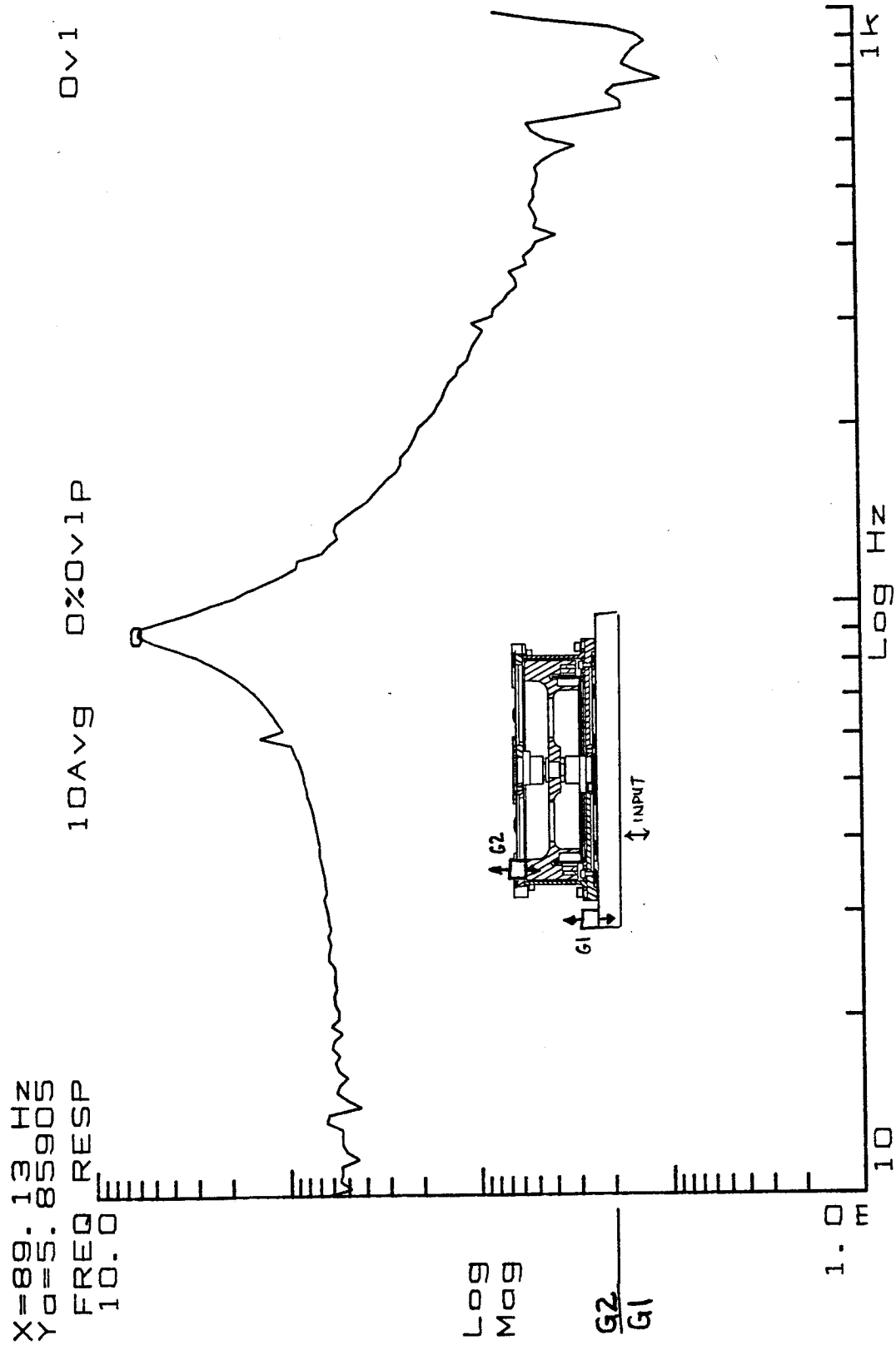

Figure 8-1: Random Vibration Transfer Function Axial Input - Axial Response

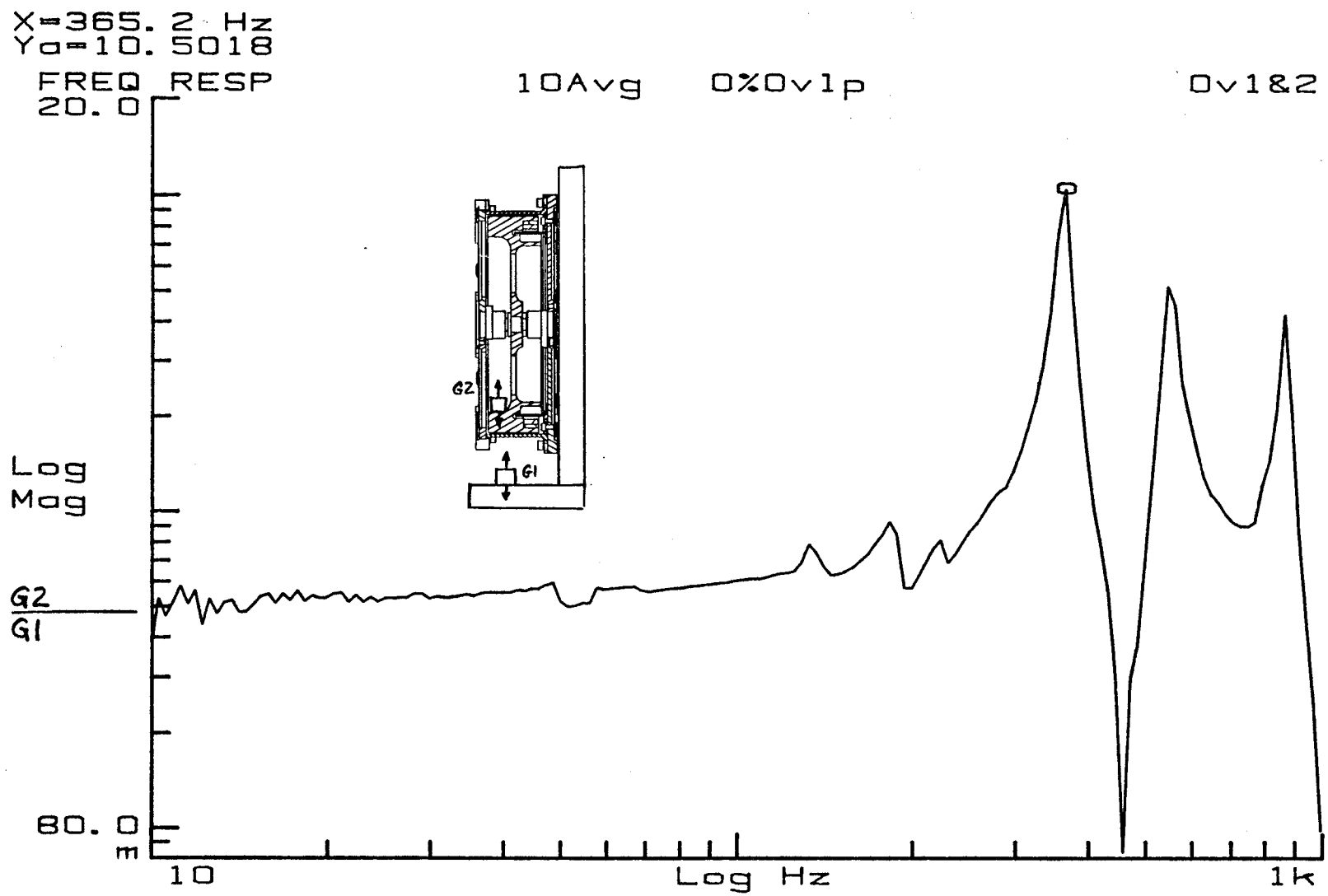

Figure 8-2: Random Vibration Transfer Function Radial Input - Radial Response

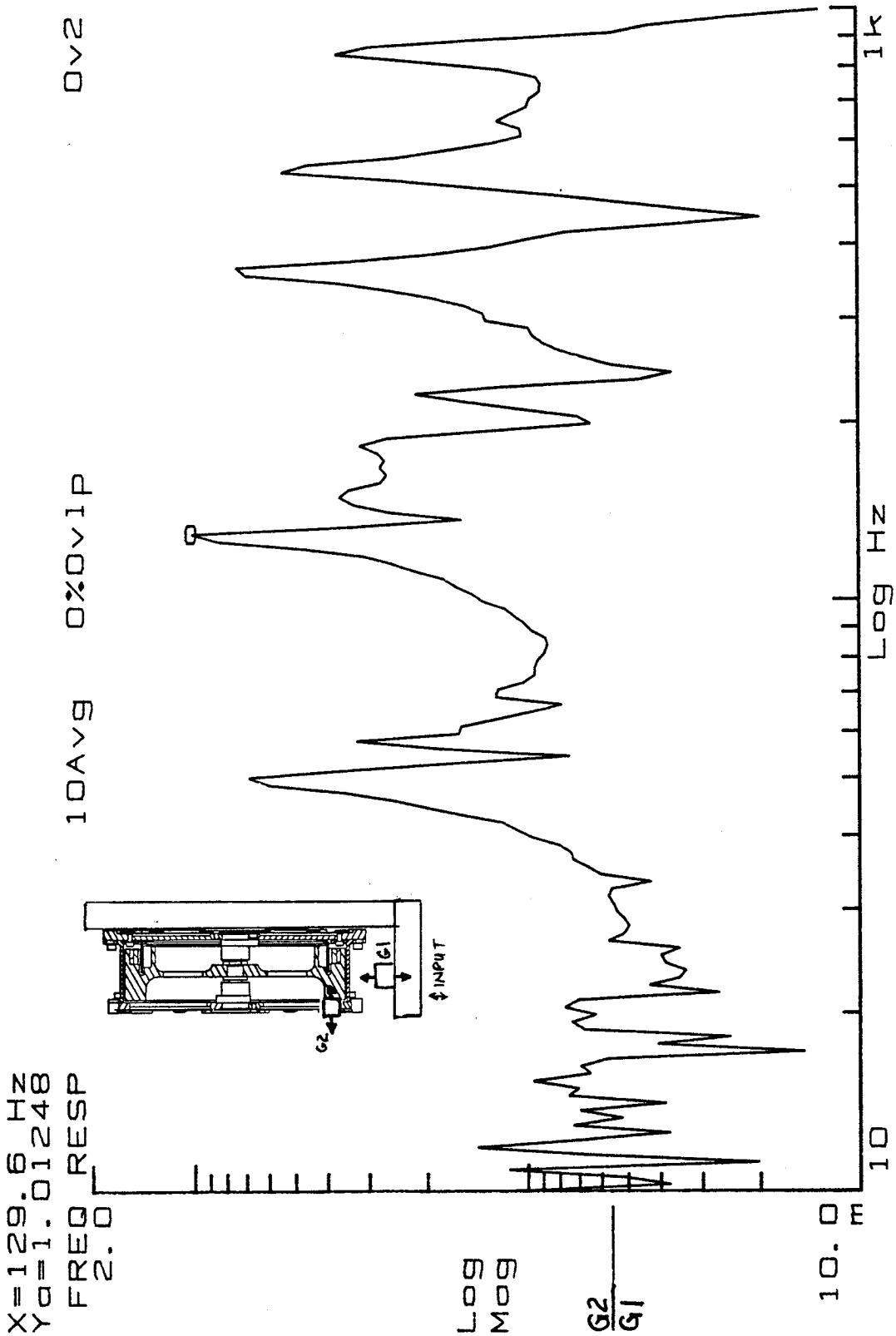

Figure 8-3: Random Vibration Transfer Function Radial Input - Axial Response

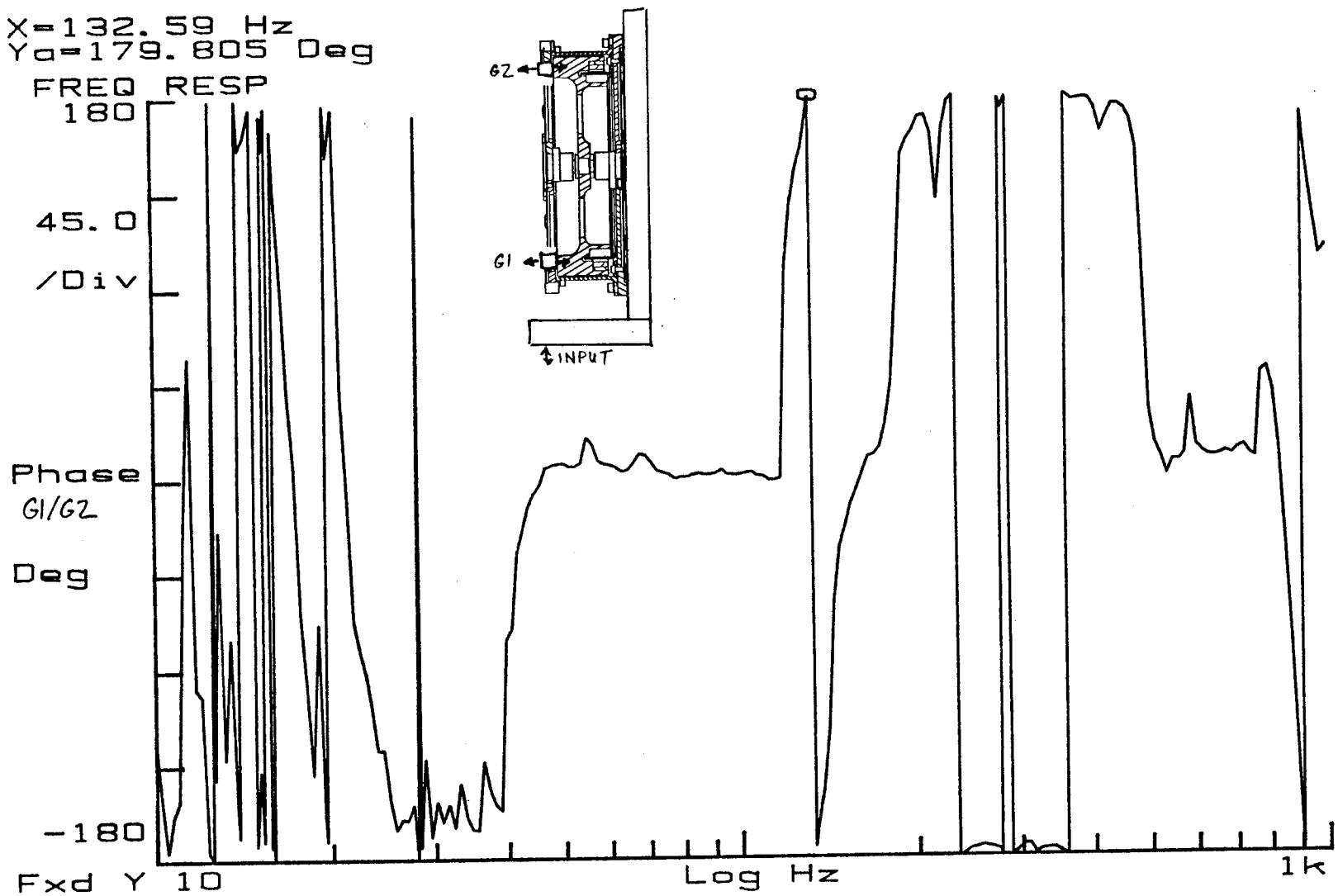

Figure 8-4: Sinusoidal Rotor Phasing Radial Input

8.2 Drag Torque Data (Cont'd)

Drag torque testing was performed in order to compare the performance of the two types of bearings used in the design, and to evaluate lubricants in a lubricant selection tradeoff. Some of the more relevant drag torque curves are presented.

Figure 8-5 shows a baseline drag torque curve taken in air with the MPB bearings with TiC coated balls. In order to quantify the proportion of the drag torque due to the viscosity of the lubricant the bearings were assembled with no lubricant. Figure 8-6 shows the drag torque in vacuum with no lubricant. A subsequent drag torque curve with a small amount of Bray 815Z lubricant in the bearings is shown in Figure 8-7. This shows that in the open conformance TiC coated bearings, the lubricant is not a significant contributor to drag torque, resulting in only a 15% increase in overall drag torque. A drag torque curve of the Barden high capacity bearings with the same quantity of Bray 815Z lubricant is shown in Figure 8-8. The close conformity of the high capacity bearings results in a significant drag torque increase over the standard MPB configuration bearings.

Extensive drag torque testing was performed during the tradeoff study between the Bray 815Z and the Pennzane™ X2000 lubricants. These data are presented in the lubricant tradeoff in Section 5.3 of this report.

8.3 Bearing EHD Film Testing

The design and analysis of long life bearing systems has been greatly influenced by elastohydrodynamic (EHD) theory. A rotation speed at which the asperities on the balls and races are separated by a thin film of high pressure lubricant has been referred to as the EHD liftoff speed. If a pair of lightly loaded bearings is operated above this speed, there is virtually no wear on the bearing surfaces. The bearing will then last as long as it is properly lubricated. In order to measure this critical speed, a simple test is performed where the electrical resistance is measured through the bearings. When the separation occurs, the resistance goes towards infinity. This type of measurement was made on both types of bearings used in the reaction wheel design and with the two lubricants in the final lubricant tradeoff analysis. The relationship of EHD liftoff speed vs. temperature was characterized for the two candidate lubricants, and these data are presented in Section 5.3.1 of this report.

Typical EHD liftoff charts obtained on the breadboard engineering unit with both types of bearings and the two candidate lubricants are shown in Figures 8-9 to 8-12.

8.4 External Magnetic Field Measurements

A test measuring the external magnetic field generated by the permanent magnets within the reaction wheel motor revealed a once per revolution alternating flux field which is attributed to the asymmetry of the strength of the individual motor magnets. The measurements were taken with a single axis magnetometer nulled to the earth's magnetic field. A once per revolution field was measured with a maximum value of .04 milligauss at a distance of one meter from the RWA. This is less than the .2 milligauss goal established in the RWA specification. The maximum field increases to .4 milligauss at a distance of 50 cm. Graphs of the data taken on the breadboard engineering unit are shown in Figure 8-13 and 8-14.

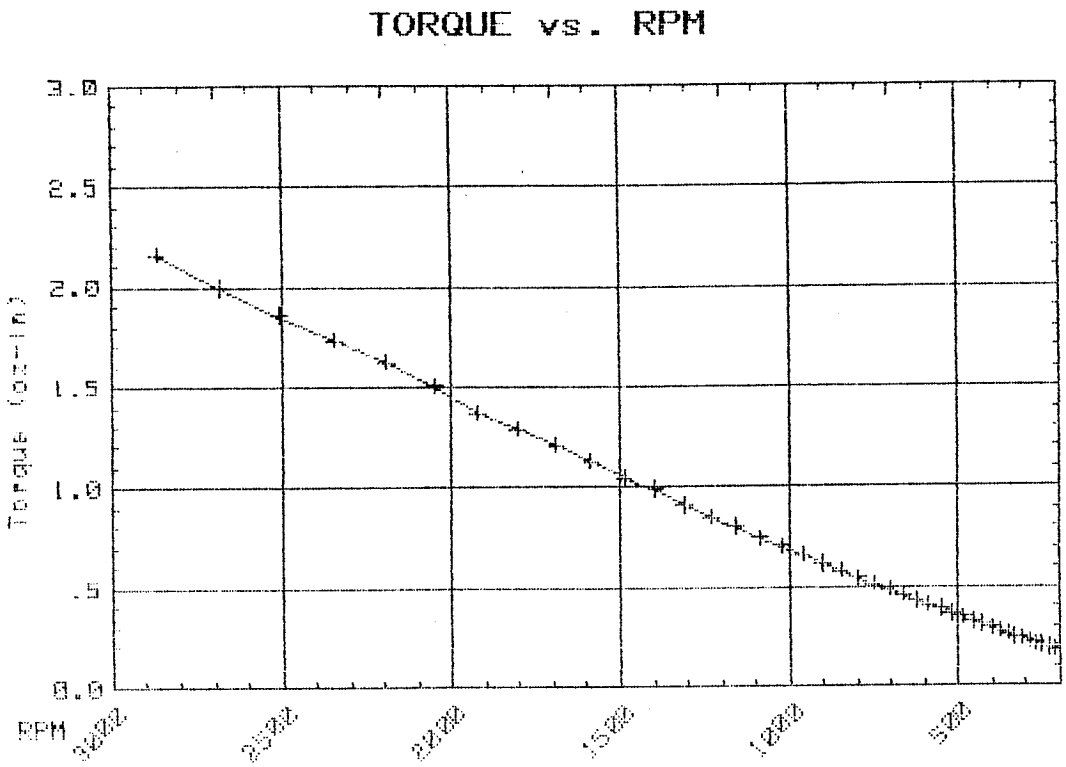

Figure 8-5: Drag Torque in Air - MPB Bearing

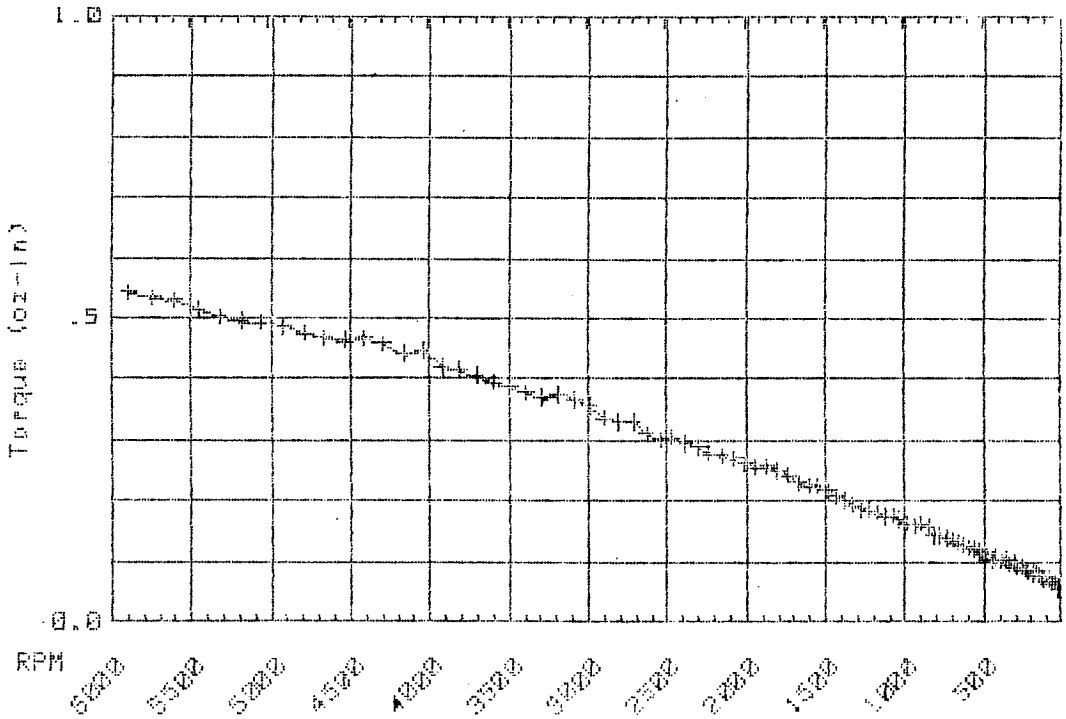

Figure 8-6: Drag Torque of Dry MPB Bearing in Vacuum

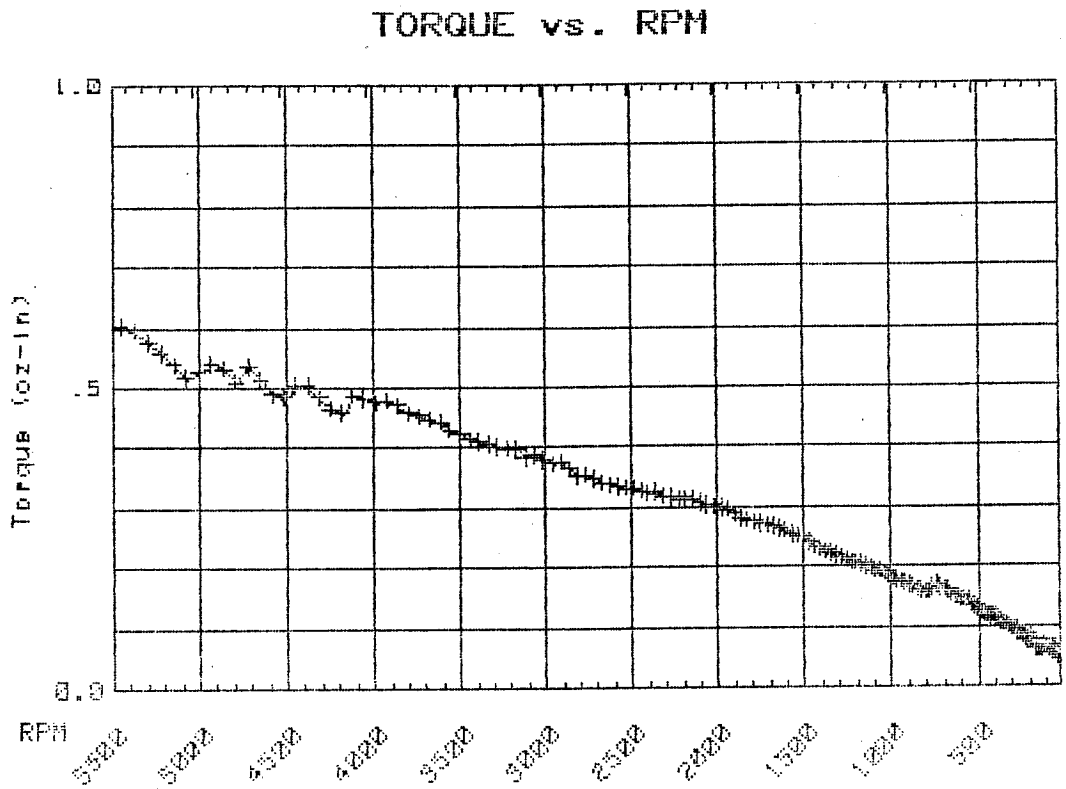

Figure 8-7: Drag Torque of TiC Bearings Lubricated With ≈15 mg of Bray 815Z in Vacuum

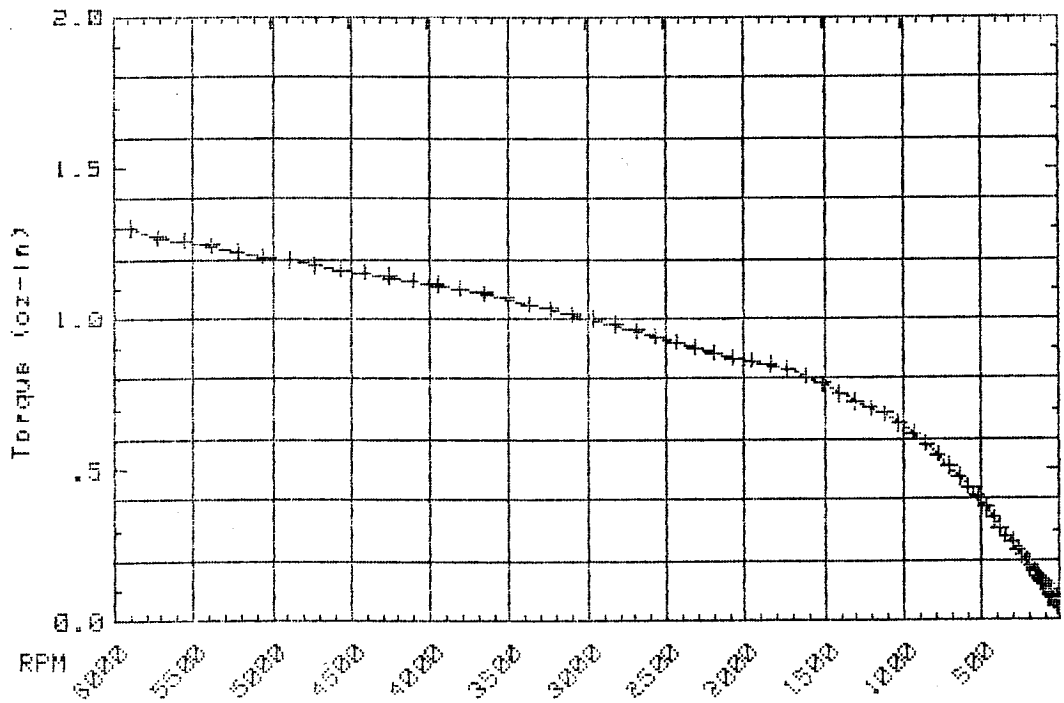

Figure 8-8: Drag Torque of Barden Bearings Lubricated With ≈20 mg of Bray 815Z in Vacuum

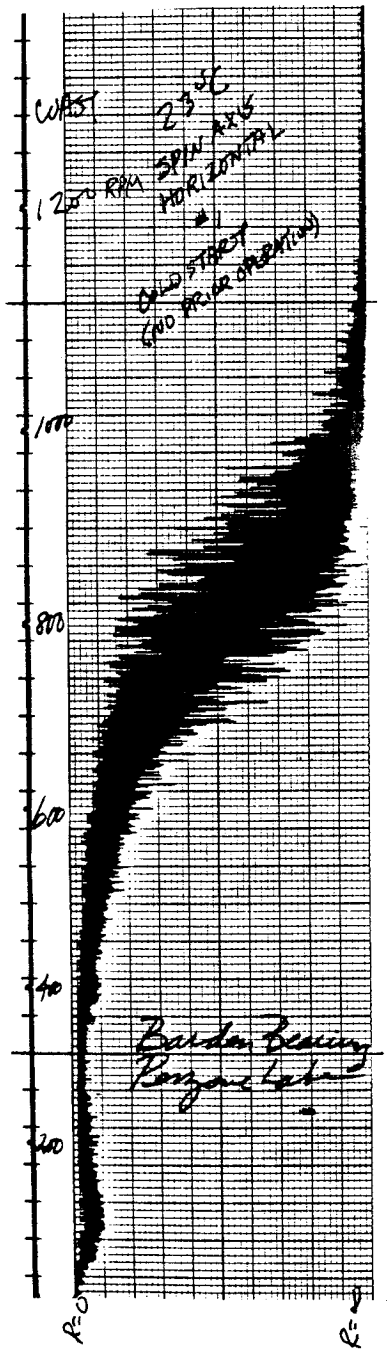

Figure 8-9: Bearing Resistor Vs. Speed
Barden SFR40H81 Bearing
Pennzane™ X2000 Lubricant

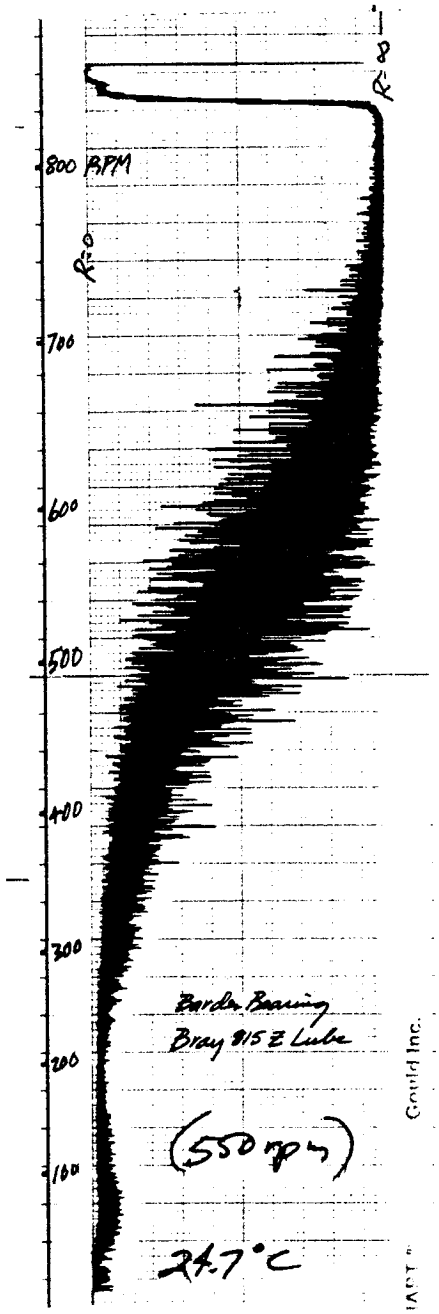

Figure 8-10: Bearing Resistor Vs. Speed
Barden SFR48X1 Bearing
Bray 8152 Lubricant

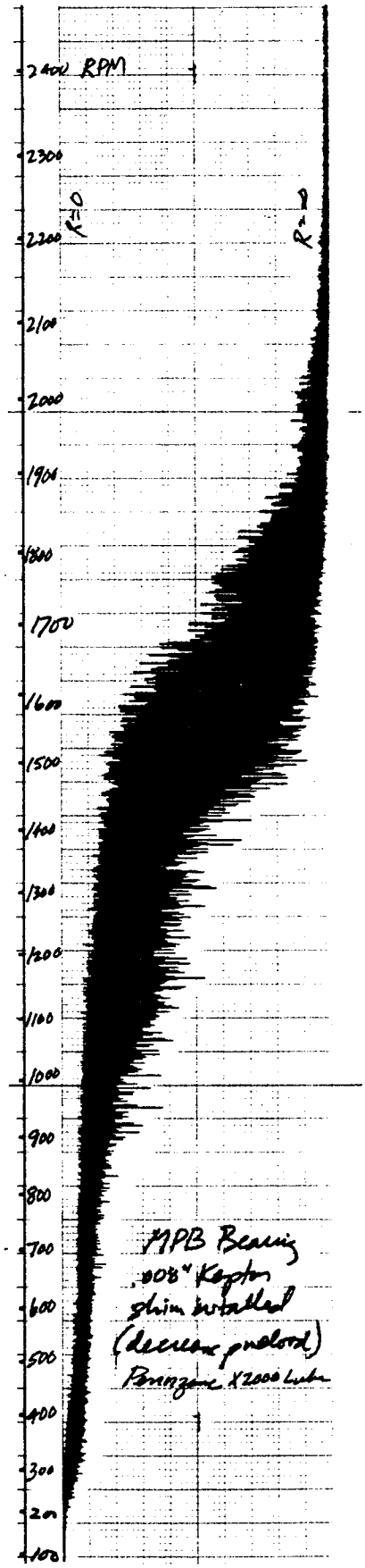

Figure 8-11: MPB CR4FM7 Bearing
Pennzane™ X2000 Lubricant

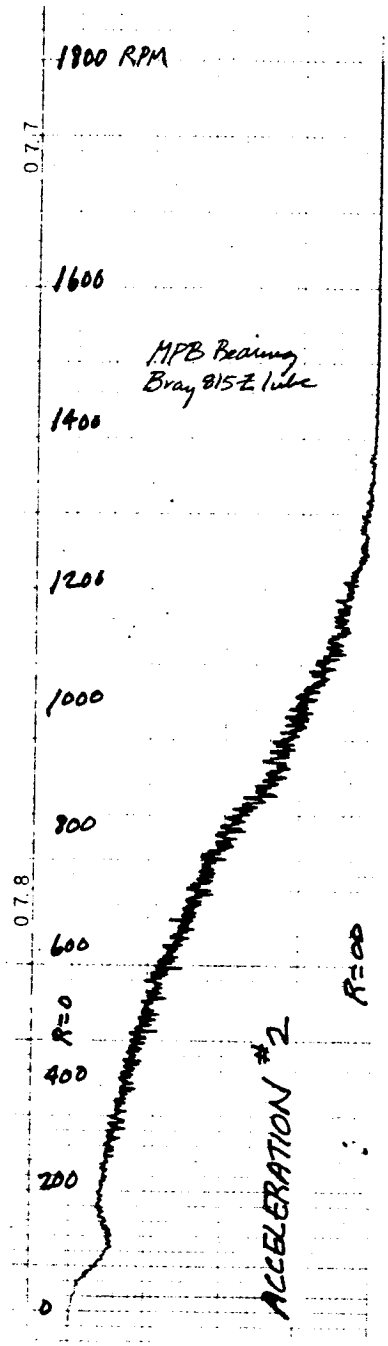

Figure 8-12: MPB CR4FM7 Bearing
Bray 8152 Lubricant

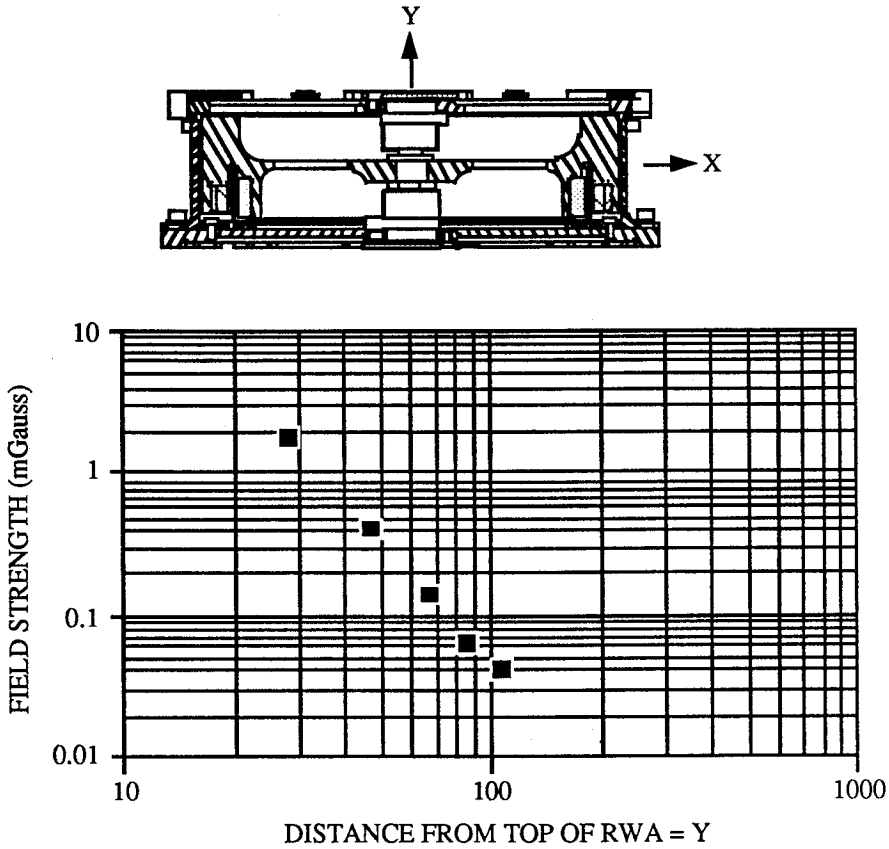

Figure 8-13: RWA External Magnetic Field (Axial)

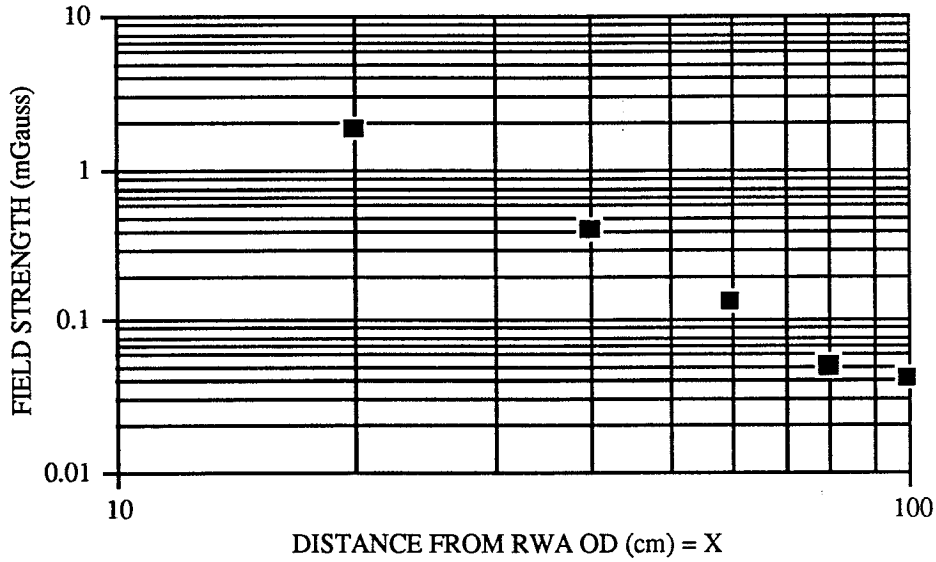

Figure 8-14: RWA External Magnetic Field (Radial)

8.5 Power Consumption Measurements

Power consumption tests on the breadboard engineering unit consisted of steady state power consumption measurements in vacuum, and peak power measurements. Figure 8-15 shows the measured steady state power consumption as a function of speed with the MPB bearings and the Barden high capacity bearings. The overall power consumption is the combined power from the bus and the +15 V, -15 V and +5 V secondary power supplies. The power consumption specification of less than 1 Watt total for the reaction wheel and motor driver was met with the MPB bearings, and nearly met with the Barden bearings. The overall efficiency increases with load and speed, typical of a low torque motor, as the quiescent power consumption of 0.5 Watt becomes a smaller percentage of the total load. The overall efficiency of the reaction wheel and motor driver approaches a phenomenal 90% at 6000 rpm. At lower speeds, the efficiency is more on the order of 60% to 70%.

The peak power consumption occurs when full torque is commanded. Figure 8-16 shows measurements taken of the power consumption from the bus during a full torque acceleration of the rotor.

8.6 Acceptance Test Plan

A test plan to be used in the acceptance testing of flight hardware was prepared which specified critical tests for the most effective screening of defects and unacceptable performance. The planned test sequence includes a thermal vacuum test which includes all performance testing, and an exposure to random vibration. Functional checks which acquire relative health check data are performed in air before and after the thermal vacuum test and random vibration. The following outline consists of summary descriptions of the testing and presents the suggested sequence.

8.6.1 Functional Test

A Functional Test is performed to verify healthy operation of the RWA prior to and following environmental exposures, and during initial checkout of the assembled RWA. This type of test can also be referred to as a 'health check', since it only verifies proper operation, but does not thoroughly check every performance requirement over the entire range of voltages or temperature.

A Functional Test is performed prior to conformal coating and close up of the RWA measuring run-up time, peak power, drag torque, tachometer phasing, and direction of rotation. The Functional Test can be performed on a lab bench in ambient conditions.

8.6.2 Performance Test

A Performance Test is completed to assure that the RWA meets the performance specifications throughout the range of input bus voltages and over a range of ambient temperatures. The RWA is not hermetically sealed, so on orbit the drag torque on the flywheel due to windage will be eliminated. In order to get an accurate measurement of the performance of the RWA, the tests need to be performed in a vacuum. This is accomplished by performing the tests in a thermal vacuum chamber. The critical performance parameters are measured in vacuum at room temperature and at high and low temperature extremes. This testing also constitutes an environmental exposure to thermal vacuum.

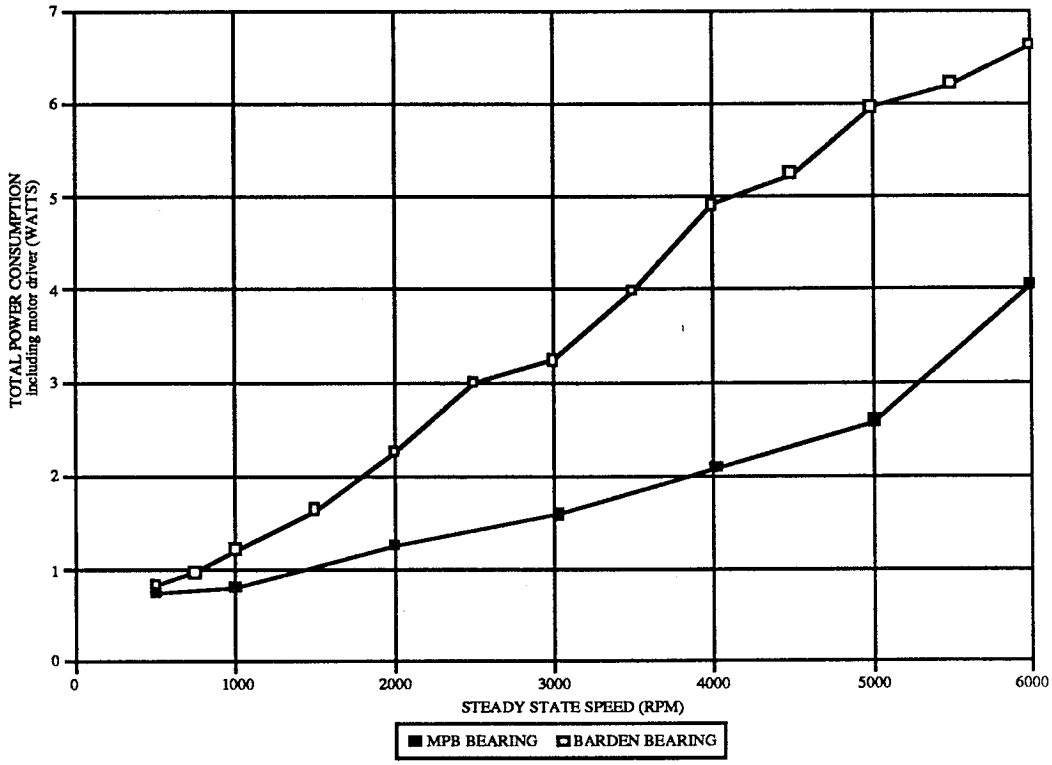

Figure 8-15: Steady State Power Vs. Speed

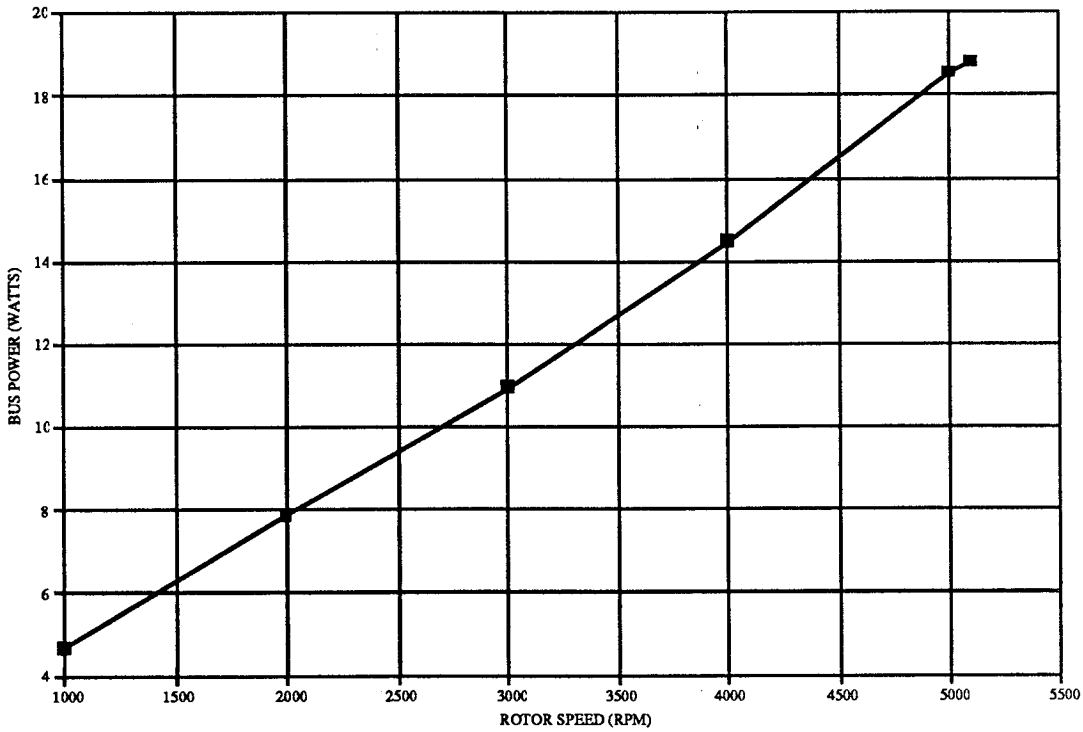

Figure 8-16: Peak Power Consumption Vs. Speed (5 oz-in Motor Torque)

8.6.2 Performance Test (Cont'd)

The performance test will include run-up time, peak power, steady state power, motor torque scale factor, and drag torque in both the CW and CCW directions . These tests are performed at the nominal bus voltage. At the low and high temperature extremes, the same tests are run at nominal bus voltage and the bus voltage extremes. The testing done at these extremes represents the worst case combined operating conditions.

8.6.3 Burn-In

Following the performance testing, an additional 3 cycles of thermal vacuum temperature cycling is performed to accumulate running time at the high and low temperature extremes. A room temperature performance test is performed at the end of the thermal vacuum temperature cycling.

8.6.4 Random Vibration

Random vibration exposure to the appropriate random vibration spectrum will be performed. A functional test is performed prior to and following the vibration exposure.

9.0 PHASE III STATUS

The SBIR successfully transitioned into Phase III development with a contract to deliver the first flight Reaction Wheel Assembly to the University of Bremen in Germany, which will fly on BREMSAT, a small microgravity experiment to be launched from a Get Away Special cannister on a space shuttle mission. Production on this unit is nearing completion. A contract has also been awarded to deliver a Reaction Wheel Assembly and two SCANWHEELs for the Air Force STEP (Space Test Experiment Platform) mission, with follow on contracts imminent for this series of small satellites. ITHACO has also internally funded a life test of the Reaction Wheel Assembly which is currently accumulating operating time.

The design of a larger version of the reaction wheel is underway, under a contract with Space Industries, Inc., for an attitude control system for the Wake Shield Facility, which is a free flying spacecraft delivered to orbit by the Space Shuttle and retrieved on a single mission. This hardware to be delivered on this program includes a 5 ft-lbf-sec SCANWHEEL operating at 2000 rpm and a supplementary 15 ft-lbf-sec reaction wheel operating at 6000 rpm.

Potential spacecraft which have baselined the reaction wheel or SCANWHEEL include APEX, SeaStar and SeaWiffs with Orbital Sciences Corporation, and IRIDIUM with Motorola. These missions generally fall into the category of a new breed of small, low cost satellites requiring low cost, short lead time, proven attitude control systems. The Modular Attitude Determination and Control System (MADACS) developed by ITHACO utilizing the SCANWHEEL and optional supplementary reaction wheels has been found to satisfy the cost, power consumption, and weight requirements for these types of missions.

10.0 CONCLUSION

The development effort did not encounter any insurmountable obstacles which would preclude the low-cost manufacture of a low-power consumption Reaction Wheel Assembly. Simplistic and reliable techniques were employed to result in a rugged, yet efficient, design. Processes are in place to manufacture the reaction wheel in large or small quantities, and with options for various levels of traceability and documentation. An interface description of the final design available for off-the-shelf delivery of the reaction wheel is included as Appendix A.

11.0 REFERENCES

(1) Peter Conley and John J. Bohner, *Experience With Synthetic Fluorinated Fluid Lubricants*, Hughes Aircraft Company, Space & Communications Group, El Segundo, CA

(2) Bryan H. Baxter and Barry P. Hall, *The Use of Perfluoroether Lubricants in Unprotected Space Environments*, European Space Tribology Laboratory, Risley England

(3) W. Tsusaki, *Test Report on B/C Actuator Life Test With Pennzane Lubricant,* TRW Space & Technology Group, June 7,1989

(4) David J Carre', *The Performance of Perfluoropolyalkylether Oils under Boundary Lubrication Conditions*, The Aerospace Corporation, El Segundo, CA

(5) ITHACO Report 94028, EHD Liftoff Speed vs. Temperature Test Data

(6) Dushman, *Scientific Foundations of Vacuum Technique*, Wiley

APPENDIX A

ITHACO REPORT 93945, REV. A

Report 93945
Revision A
March 14, 1991

RW4A28V

REACTION WHEEL ASSEMBLY

INTERFACE DESCRIPTION

Prepared by

ITHACO, Inc.
735 W. Clinton St.
P.O. Box 6437
Ithaca, NY 14851-6437

Rev.	Description	Approval / Date
A	Revision A to Report 93945 incorporates the following changes: Section 3.4: Second sentence was "Most hardware as designed will tolerate approximately 10^4 Rad (Si). Sections 3.6, 3.7: "Class 100 K" was "Class 10K" "Class 100 K" was "class 10 K" Section 3.7; item 2: Added "but above -50°C." Section 4.1.1.3: Was "The scale factor of motor torque vs. command voltage is projected to be nominally 0.005 N-m/V (0.71 oz-in/V). The actual Motor Torque Scale Factor will be measured in test." Section 4.1.1.8: "scale factor" was "projected scale factor" Figure 4-3: Corrected pin designations. Table 4-1: J9-7 voltage range was: "-5 to +5 V" J2-20, J2-21 were: "SPARE" J8-8 Impedance was "100 KΩ" "Digital Tach 1/2" was "Digital Tach" "Analog Tach 1/2" was "Analog Tach" "Tach Direction 1/2" was "Tach Direction" J2-3 min/max volt was "0.0/35.0 V" J3-10 was "5 V/Optional Thermistor" "Test Only" was "Box Level Test Setup" Section 4.3.3, Paragraph 7: Last two sentences were "The MD bridge and the input filter remains connected to the 28 V power bus regardless of the state of the bus power command. ITHACO recommends fusing the MD bus power for redundant applications." Last paragraph was "MD 28 V bus power can be directly switched by the user if desired. Under these conditions, maximum inrush current is approximately 16.5 A provided power bus risetime is less than 4 V/μs." Section 4.3.4, Paragraph 3: First sentence was "The Torque Command input has a single pole at approximately 70 Hz." Section 4.3.6: Added section headings 4.3.6.1, 4.3.6.2, 4.3.6.3.	

Rev.	Description	Approval / Date
A	(Cont'd)	
	Section 4.3.6.2: Last sentence added.	
	Section 4.3.6.3: Added first sentence.	
	Section 4.3.6.4, 4.3.6.5: Added.	
	Section 4.5: Typical data added. (Also Figure 4-4).	

TABLE OF CONTENTS

1.0 SCOPE 1

2.0 REFERENCE DOCUMENTS AND DEFINITIONS 1

2.1 ITHACO Drawings 1
2.2 ITHACO Documents 1
2.3 Definitions and Abbreviations 1

3.0 HARDWARE ENVIRONMENTAL CAPABILITIES 2

3.1 Thermal 2
3.1.1 Temperature Range 2
3.2 Vibration 2
3.2.1 Vibration Dynamics (FOR REFERENCE ONLY) 2
3.3 Electromagnetic Compatibility 2
3.3.1 Regulated Power EMC Requirements 4
3.3.2 Power Bus Requirements 4
3.3.3 External Magnetic Field 4
3.4 Charged Particle Radiation 6
3.5 Operating Lifetime 6
3.5.1 Bearing Lifetime 6
3.5.2 Radiation Damage 6
3.6 Handling Precautions 6
3.7 Hardware Storage Requirements 6

4.0 REACTION WHEEL ASSEMBLY 7

4.1 RW Functional Description 7
4.1.1 RW Specifications 7
4.1.2 RW Component Interfaces 9
4.2 RWA Mechanical 9
4.2.1 Outline Drawings 9
4.2.2 Mounting Requirements 9
4.2.3 Mass Properties 9
4.2.4 Torque Output Vector/Momentum Vector Alignment 9
4.2.5 Direction of Rotation 11
4.3 MD-Electronic 11
4.3.1 Functional Description 11
4.3.2 Pinout Definitions 11
4.3.3 Power Interface & Grounding 11
4.3.4 Torque Control Interface 15
4.3.5 Signal Interface 16
4.3.6 Telemetry Interface 16
4.4 RW Electronic 16
4.4.1 Functional Description 16
4.4.2 Pinout Definitions 16
4.4.3 User Interface 18
4.5 Power Profile 18
4.5.1 Power Consumption 18
4.5.2 Power Dissipation 18

1.0 SCOPE

The component hardware described herein consists of one Reaction Wheel and an electronics box consisting of one motor driver card.

This document contains descriptions of component capabilities, interconnection requirements, and user interfaces.

2.0 REFERENCE DOCUMENTS AND DEFINITIONS

2.1 ITHACO Drawings

D43378	RWA Mechanical Outline Drawing
C33328	Electronics Box Mechanical Outline Drawing

2.2 ITHACO Documents

RQPS 64.7	ESD Operating Procedure, SSD Manufacturing

2.3 Definitions and Abbreviations

CCW	Counterclockwise
CW	Clockwise
MD	Motor Driver
Motor Torque	Motor torque is the torque generated in the armature of the RW motor.
N	Newton
Reaction Torque	Reaction torque is the torque applied to the spacecraft mounting surface. This is equal to the RW motor torque minus the drag torque.
RW	Reaction Wheel
RWA	Reaction Wheel Assembly
TBC	To Be Confirmed
TBD	To Be Determined

3.0 HARDWARE ENVIRONMENTAL CAPABILITIES

This section outlines the environmental capabilities and requirements of the ITHACO supplied hardware.

3.1 Thermal

All supplied components utilize conduction as the primary mode of heat rejection. Aluminum mounting interfaces are flat within 2 mm/m (.002 inch/inch), have surface finishes better than 62 microinches, and are finished with alondine per MIL-C-5541. Similar interfaces are required on the mating surfaces of the spacecraft in order to sufficiently preserve the conduction scheme.

3.1.1 Temperature Range

All components will tolerate an operating baseplate temperature range of -20 to +50°C and operate within spec.

Non-operating temperature range for all hardware is -50 to +85°C.

3.2 Vibration

All components are compatible with random vibration environment shown in Figure 3-1.

3.2.1 Vibration Dynamics (FOR REFERENCE ONLY)

The standard 6" x 6" ITHACO card frames have demonstrated resonant frequencies greater than 200 Hz. The flywheel in the Reaction Wheel is suspended on a set of flexures which results in three vibration modes. The first mode occurs in the axial direction at 100 Hz, with a Q of 6. The second mode is a rocking resonance of the flywheel at 122 Hz. The third mode is a radial translation mode at 350 Hz and a Q of 10.

3.3 Electromagnetic Compatibility

There are no EMC requirements on the ITHACO components. In general, good Engineering practices, such as ground plane construction and on-board power filtering, will be used. In addition, most components contain low frequency analog and digital circuitry which do not generate substantial emissions.

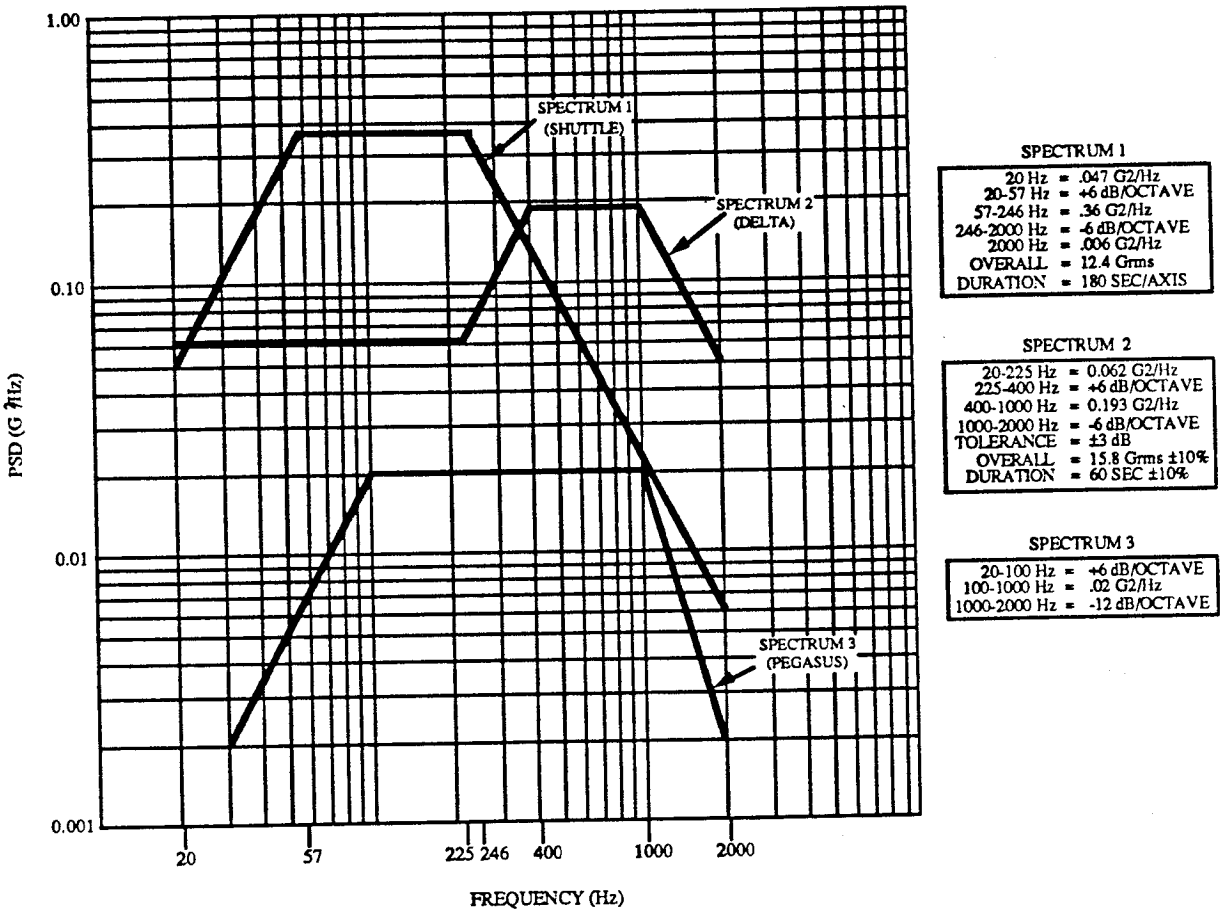

FIGURE 3-1
RANDOM VIBRATION SPECTRUM

3.3.1 Regulated Power EMC Requirements

The components require regulated voltages of +5 V ± 5% and ±15 V± 5%. The ITHACO components are designed to tolerate:

Ripple:

+5 V Supply:	50 mV p-p Max,	0-10 MHz
±15 V Supply:	100 mV p-p Max,	0-10 MHz

Transients:

+5 V Supply:	±5 V Max,	10 usec max duration
±15 V Supply:	±15 V Max,	10 usec max duration

Source Impedance:

0.1 to 1 Ω at DC, rising to 50 Ω at 2 MHz.

Emissions of the components onto the regulated power lines are limited by local R-C and L-C decoupling as appropriate.

3.3.2 Power Bus Requirements

The Motor Driver draws power directly from the spacecraft unregulated bus. Requirements are as follows:

Voltage:	28 ± 6 V
Transients:	±28 V, 10 μsec max
Ripple Voltage:	1 V RMS Max, 30 Hz - 400 MHz

3.3.3 External Magnetic Field

The external magnetic field produced by the permanant magnets in the brushless DC motor exhibits a once per revolution alternating flux field which is attributed to the asymmetry of the strength of the individual motor magnets. Figure 3-2 shows nominal measurements of the field strengh amplitude taken in line with the RWA rotation axis. Figure 3-3 shows nominal measurements of the field strength amplitude taken radially from the RWA rotation axis.

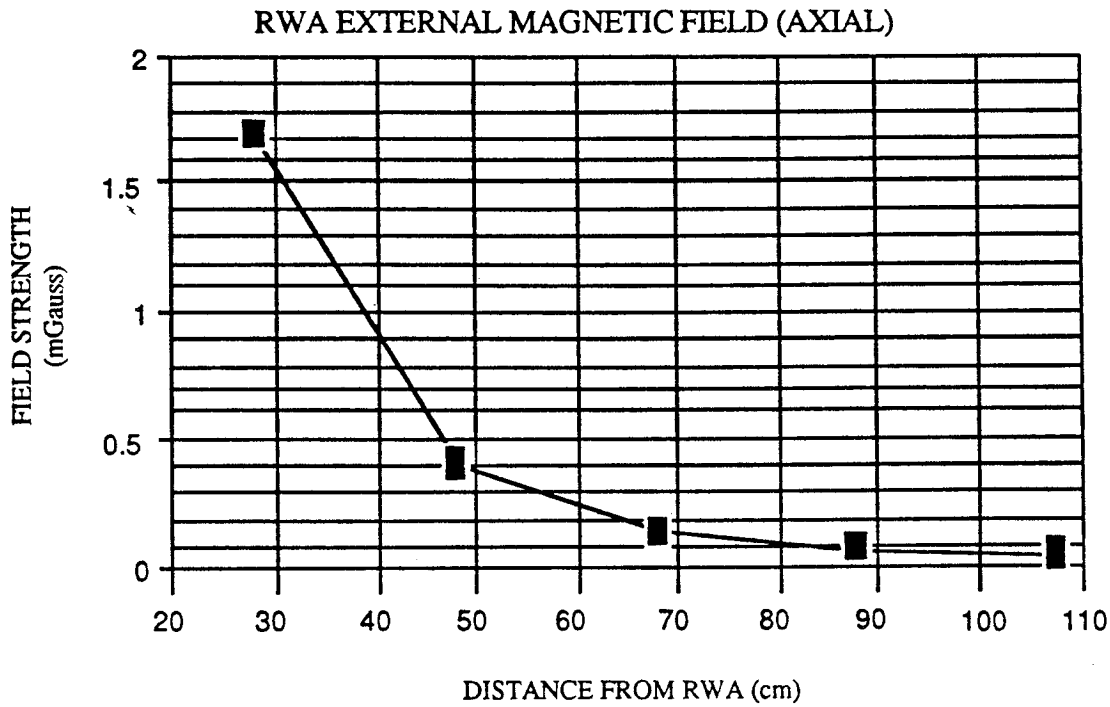

FIGURE 3-2

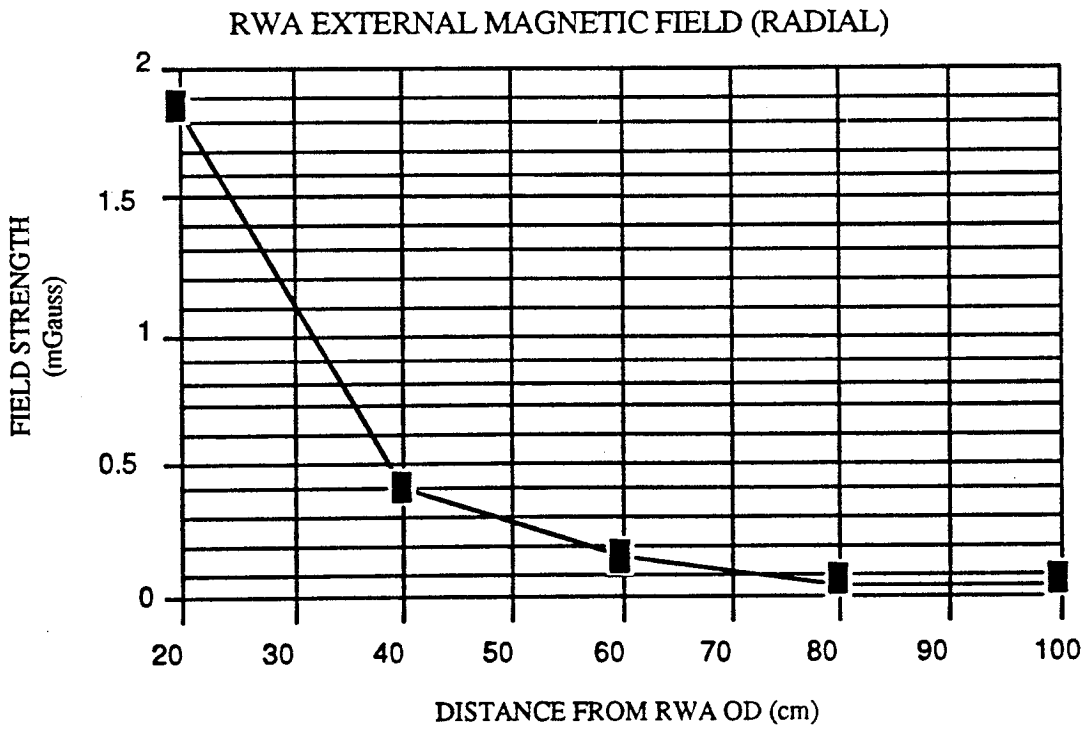

FIGURE 3-3

3.4 Charged Particle Radiation

There are no requirements for radiation tolerance.

3.5 Operating Lifetime

3.5.1 Bearing Lifetime

The bearing lubrication system in the Reaction Wheel is the only life limiting mechanical item in the components. The lubricant quantity is compatible with an expected operating lifetime of 3 years.

3.5.2 Radiation Damage

Electronics lifetime is governed by the charged particle radiation environment and the inherent hardness of the semiconductors. The components will tolerate approximately 10^4 Rad(Si).

3.6 Handling Precautions

The following precautions should be observed when handling the hardware:

1. When unpacked from their shipping cartons, the RWA should be maintained in a Class 100 K Clean area. Any disassembly of the RWA which exposes the bearings should only be performed in a Class 100 Clean area.

2. All hardware is ESD sensitive and should be handled per the guidelines of ITHACO RQPS 64.7.

3. The RWA should be securely attached to a workbench or suitable structure prior to being operated at any speed.

3.7 Hardware Storage Requirements

Optional conditions for long-term storage of the RW and SW are as follows:

1. Spin Axis: Horizontal
2. Ambient Temperature: As low as practical but above -50°C
3. Cleanliness: Unit packaged. Store in Class 100 K clean area.

4.0 REACTION WHEEL ASSEMBLY

4.1 RW Functional Description

The RWA will provide reaction torque to the spacecraft mounting surface and storage of angular momentum. The RWA will consist of two separate units; an RW and an MD. An interface cable, not supplied by ITHACO, will be required to interconnect the two units.

4.1.1 RW Specifications

4.1.1.1 Torque Capability

When operated in a vacuum, the RWA will be capable of providing a minimum reaction torque of 20 mN-m (2.8 oz-in) in the speed range from 0 to 4000 RPM and a minimum reaction torque of 15 mN-m (2.1 oz-in) in the speed range from 4000 to 5100 RPM.

Figure 4-1 shows the relationship between nominal drag torque and wheel speed. Maximum breakaway torque is 0.0015 N-m (0.21 oz-in). Maximum stall torque is 0.0005 N-m (0.071 oz-in).

4.1.1.2 Torque Command

Motor torque is commanded by a bipolar analog voltage.

The user should note that the reaction torque is equal to the motor torque minus the drag torque.

4.1.1.3 Motor Torque Scale Factor

The scale factor of motor torque vs. command voltage is nominally 0.005 N-m/V (0.71 oz-in/V). The actual Motor Torque Scale Factor will be measured in test.

4.1.1.4 Motor Torque Ripple

The torque ripple during steady state operation within the specified speed range is projected to be less than 1.0 mN-m (0.14 oz-in) peak. Fundamental torque ripple frequency is at the motor commutation frequency of 54 times the wheel rotation rate.

4.1.1.5 Operating Speed Range

The RWA will be capable of operating in the CW or CCW between 0 and at least ±5100 RPM while in a vacuum. When operating in air at atmospheric pressure, the RWA will be capable of operating between 0 and at least ±3000 RPM. Maximum RPM as a function of bus voltage is given by the following expression:

$$RPM_{max} = (298\ RPM/V)\ V_{BUS}$$

Care must be taken to prevent speeds in excess of 7000 RPM at high bus voltages.

NOMINAL RWA/SWA DRAG TORQUE IN VACUUM

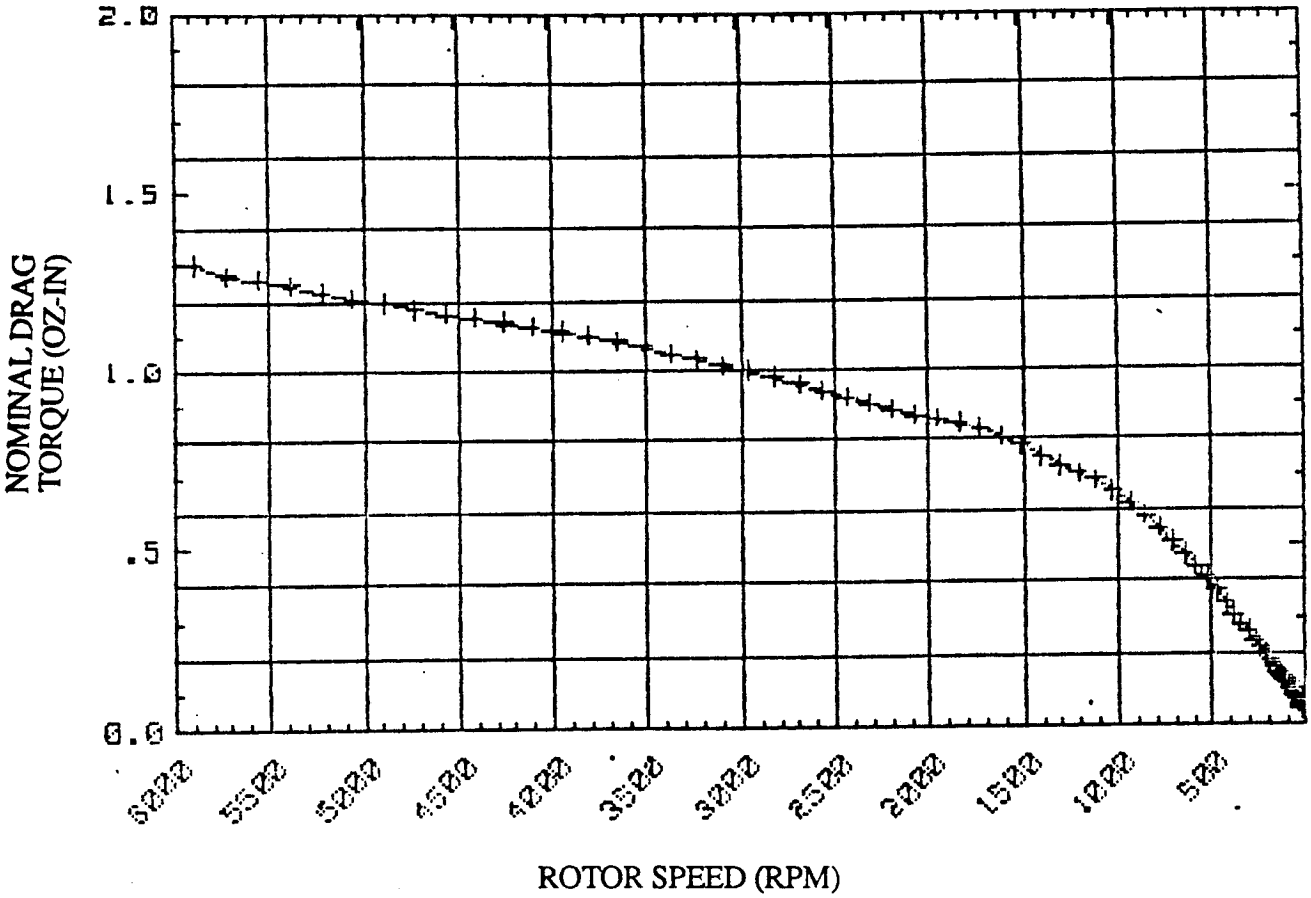

FIGURE 4-1

4.1.1.6 Momentum Storage Capacity

The RWA will be capable of storing a minimum of 4.0 N-m-s (3 ft-lb-sec) of angular momentum at 5100 RPM.

4.1.1.7 Digital Tachometer

A tachometer will provide 54 square wave pulses per revolution to indicate wheel speed.

4.1.1.8 Analog Tachometer

A secondary tachometer will provide an analog signal proportional to absolute speed with a scale factor of 1000 RPM/Volt.

4.1.2 RW Component Interfaces

4.1.2.1 MD-RW Interface Cable

Figure 4-2 identifies the cabling requirements for the interface between the motor and the MD. Due to the switchmode driver waveforms and the significant influence of wiring resistance on RW efficiency, it is recommended that the cabling be less than 2 m (79 in) in length. Due to the critical nature of this interconnect, it is imperative that the designated shielding be used.

4.2 RWA Mechanical

4.2.1 Outline Drawings

The outline for the RW is defined by Drawing D43378. The MD is included in the Electronics Outline Drawing C33328. See Appendix A for outline drawings.

4.2.2 Mounting Requirements

The RW may be mounted from either of the two identical mounting surfaces shown on the outline drawing as Datums A and B. Six equally spaced holes on the specified diameter provide mounting provision for #8 screws or bolts.

4.2.3 Mass Properties

The mass of the RW is projected to be 2.5 Kg (5.5 lbm). The mass of the MD is projected to be less than 0.8 Kg (1.7 lbm).

4.2.4 Torque Output Vector/Momentum Vector Alignment

The Spin axis, Torque Output Vector, and Momentum Vector axes will be perpendicular to either of the wheel mounting surfaces within ±15 arcminutes.

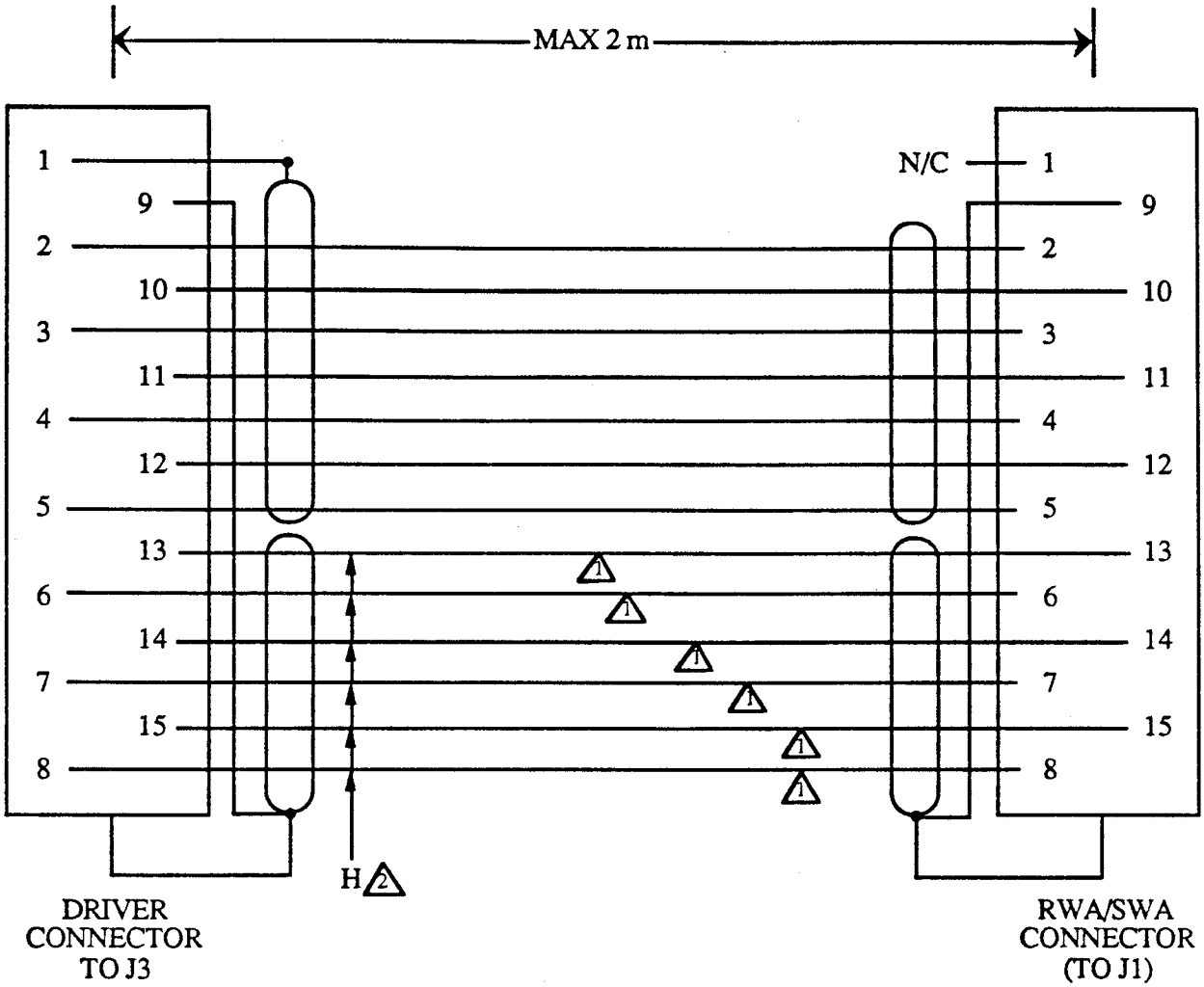

1 Recommended Wire Gauge 20 AWG

2 Twisted Hex

Connectors to be Female Non-Magnetic Subminiature D Shell

FIGURE 4-2
MOTOR DRIVER - SW/RW INTERFACE CABLE

4.2.5 Direction of Rotation

Relative to the NON-connector side of the RW, a CW torque will result on the flywheel when a positive torque command is applied. This will result in a CCW reaction torque on the spacecraft. If started from zero RPM, the application of CW motor torque will cause the flywheel to rotate in the CW direction, resulting in a logic "1" from the direction telemetry. If the flywheel is rotating in the CCW direction, a logic "0" will result. The analog tach polarity is positive when the flywheel rotates in the CW direction.

4.3 MD-Electronic

4.3.1 Functional Description

Refer to Figure 4-3 for a Functional Block Diagram of the MD. The MD interfaces the Brushless DC motor in the reaction wheel to the Power Bus. The MD/RW combination has true DC servo capability and can provide instantaneous torque in either direction. In addition, the wheel can operate in either direction of rotation, and near zero speed without the need for intentional direction switching.

4.3.2 Pinout Definitions

Each MD contains the following connectors:

Designation	Function	No. of Pins	Connector Type
J2	Test/Telemetry	25	Male Subminiature D Shell
J3	Motor Interface	15	Male Subminiature D Shell
J8	Power Interface	15	Male Subminiature D Shell
J9	Command/Signals	9	Male Subminiature D Shell

Table 4-1 describes the motor driver pinouts.

4.3.3 Power Interface & Grounding

MD power interface is to the J8 connector. Refer to Table 4-1 for detailed information.

MD power requirements are as follows:

Voltage	Type	Max Current	Max Turn on Surge
+15 V	Regulated	15 mA	300 mA
-15 V	Regulated	15 mA	300 mA
+5 V	Regulated	25 mA	300 mA
+28 ± 6 V	Unregulated or regulated	1.5 A	**Input filter always tied to bus**

The returns of the regulated voltages are connected internally to the power bus return.

The MD contains no internal power switching for the ±15 V and +5 V power. This power must be switched by the user.

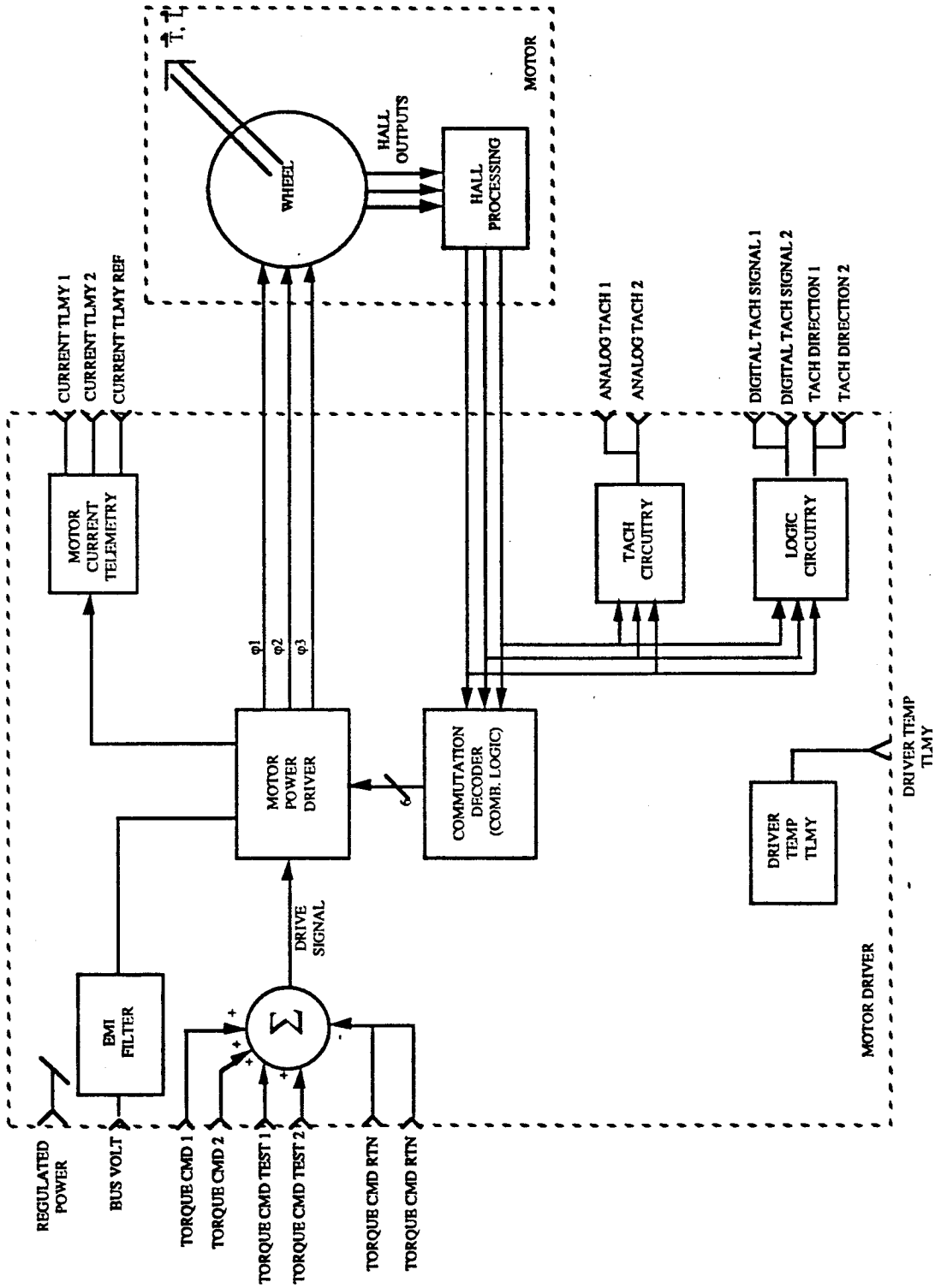

FIGURE 4-3
MOTOR DRIVER - FUNCTIONAL BLOCK DIAGRAM

TABLE 4-1: MOTOR DRIVER - PINOUTS

Connector	Pin	Name	Destination	Comments	Input/ Output	Impedance	Min Volt	Max Volt	I/O Type
J8	1	Chassis							
J8	2	Power Bus +	Power Bus +	Note 1	Input	N/A	-1.00	35.00	Power
J8	3	Power Bus Return	Power Bus Return	Note 1	Input	N/A	N/A	N/A	Power
J8	4	Neg 15V Input	Neg 15V Input	Note 1	Input	N/A	-15.75	1.00	Power
J8	5	Power Return	Power Return	Note 1	Input	N/A			
J8	6	Pos 15 V Input	Pos 15 V Input	Note 1	Input	N/A	-1.00	15.75	Power
J8	7	5 V Input	5 V Input	Note 1	Input	N/A	-1.00	5.25	Power
J8	8	Bus Power Command	User Interface	Active High	Input	50 KΩ	0V	5V	CMOS
J8	9	Chassis							
J8	10	Power Bus +	Power Bus +	Note 1	Input	N/A	-1.00	35.00	Power
J8	11	Power Bus Return	Power Bus Return	Note 1	Input	N/A	N/A	N/A	Power
J8	12	Neg 15V Input	Neg 15V Input	Note 1	Input	N/A	-15.75	1.00	Power
J8	13	Power Return	Power Return	Note 1	Input	N/A			
J8	14	Pos 15 V Input	Pos 15 V Input	Note 1	Input	N/A	-1.00	15.75	Power
J8	15	5 V Input	5 V Input	Note 1	Input	N/A			
J9	1	Chassis							
J9	2	Torque Command 2	User Interface	Protected to ±15V, 0.005n-m/V Note 2	Input	50KΩ min	-5.00	5.00	Analog
J9	3	Torque Command 1	User Interface	Protected to ±15V, 0.005n-M/V Note 2	Input	50KΩ	-5.00	5.00	Analog
J9	5	Torque Cmd Reference	User Interface	For input ground isolation, Note 1	Input	50kΩ min	-5.00	5.00	Analog
J9	6	Digital Tach 1	User Interface	54 pulses per revolution	Output	5KΩ max	0.00	5.00	CMOS
J9	7	Analog Tach 1	User Interface	1000 RPM/V	Output	5KΩ	-10.00	10.00	Analog
J9	8	Tach Direction 1	User Interface	1=TBD, 0=TBD	Output	5KΩ max	0.00	5.00	CMOS
J9	9	Signal Reference	User Interface						
J2	1	Chassis							
J2	2	Analog Tach 2	User Interface	1000 RPM/V	Output	5KΩ	-10.0	10.0	CMOS
J2	3	Torque CMD Test 1	Opt User Interface/Test	0.005n-M/V, Note 2	Input	50KΩ	-15 V	15 V	Analog
J2	4	Torque CMD Test 2	Opt User Interface/Test	0.005n-M/V, Note 2	Input	50KΩ	-15.00	15.00	Analog
J2	5	Torque CMD Reference	Opt User Interface/Test	For input isolation, Note 1	Input	50KΩ Min	-15.00	15.00	Analog

Note 1: Connector pins bearing identical names are redundant and are connected together within the card.
Note 2: Torque command voltages are summed by the motor as follows:
Total Torque Command = (J9-2) + (J9-3) + (J2-3) + (J2-4) - (J9-5).
Unused Torque Command inputs must be tied to J9-5 or J2-5.

TABLE 4-1 (CONT'D): MOTOR DRIVER - PINOUTS

Connector	Pin	Name	Destination	Comments	Input/ Output	Impedance	Min Volt	Max Volt	I/O Type
J2	6	Current Telemetry 2	User Interface	0.4 A/V (RW), 0.2 A/V (SW)	Output	5KΩ Max	-15.00	15.00	Analog
J2	7	Current Telemetry 1	User Interface	0.4 A/V (RW), 0.2 A/V (SW)	Output	5KΩ Max	-15.00	15.00	Analog
J2	8	Sig RTN							
J2	9	Sig RTN							
J2	10	Digital Tach 2	User Interface	54 pulses per revolution	Output	5KΩ max	0.00	5.00	CMOS
J2	11	Current TLM Reference	User Interface	For TLMY ground isolation	Output	5KΩ Max	-15.00	15.00	Analog
J2	12	Driver Phase 3 Test	Test Only	Switchmode driver outputs	Output	100KΩ	0.00	35.00	Analog
J2	13	Driver Phase 2 Test	Test Only	Switchmode driver outputs	Output	100KΩ	0.00	35.00	Analog
J2	14	Tach Direction 2	User Interface	1=TBD, 0=TBD	Output	5KΩ max	0.00	5.00	CMOS
J2	15-19	Spare		Open					
J2	20-21	Sig RTN							
J2	22	Spare		Open					
J2	23	Temp TLM	User Interface	Biased Thermistor TLMY	Output	5KΩ Max	0.00	5.00	Analog
J2	24	Temp TLM Return	User Interface	Biased Thermistor TLMY	Output	5KΩ Max	0.00	5.00	Analog
J2	25	Driver Phase 1 Test	Test Only	Switchmode driver outputs	Output	100KΩ	0.00	35.00	Analog
J3	1	Chassis	Motor	NOT USER INTERFACE					
J3	2	Tach 1	Motor	NOT USER INTERFACE	Input	15K	0.00	5.00	CMOS
J3	3	Tach 2	Motor	NOT USER INTERFACE	Input	15 K	0.00	5.00	CMOS
J3	4	Tach 3	Motor	NOT USER INTERFACE	Input	15 K	0.00	5.00	CMOS
J3	5	Sig Rtn	Motor	NOT USER INTERFACE	Output	N/A	0.00	5.00	Analog
J3	6	Motor Winding A	Motor	NOT USER INTERFACE	Output	N/A	-1.00	35.00	Power
J3	7	Motor Winding B	Motor	NOT USER INTERFACE	Output	N/A	-1.00	35.00	Power
J3	8	Motor Winding C	Motor	NOT USER INTERFACE	Output	N/A	-1.00	35.00	Power
J3	9	Chassis	Motor	NOT USER INTERFACE					
J3	10	5 V	Motor Hall Sensors	NOT USER INTERFACE	Output	N/A	4.75	5.25	Power
J3	11	5V	Motor Hall Sensors	NOT USER INTERFACE	Output	N/A	4.75	5.25	Power
J3	12	Sig Rtn	Motor	NOT USER INTERFACE	Output				
J3	13	Motor Winding A	Motor	NOT USER INTERFACE	Output	N/A	-1.00	35.00	Power
J3	14	Motor Winding B	Motor	NOT USER INTERFACE	Output	N/A	-1.00	35.00	Power
J3	15	Motor Winding C	Motor	NOT USER INTERFACE	Output	N/A	-1.00	35.00	Power

4.3.3 Power Interface & Grounding (Cont'd)

Power can be applied in any sequence without overstressing the MD. For an orderly power up, the 5 V should be applied last. For an orderly shutdown, remove the 5 V first.

This driver configuration will not return energy to the bus. If the commanded torque requires a motor speed reduction, kinetic energy stored in the motor is dissipated by a ballast transistor in the driver card frame.

The MD can be effectively disconnected from the 28 V power bus with the bus power command on J8-8. This CMOS level input simply disables the drive signals to the MD bridge, so that the driver draws no current from the 28 V bus regardless of torque command or power status. The MD power circuitry remains connected to the 28 V power bus regardless of the state of the bus power command. ITHACO recommends fusing the MD bus power for redundant applications. The motor driver will not operate unless the bus power command is tied to +5 V.

MD 28 V bus power can be directly switched by the user if desired. Under these conditions, maximum inrush current is approximately 16.5 A. This inrush estimate excludes the current into a 0.1 μf capacitor connected between the +28 V and 28 V return terminals.

CAUTION:

All signal returns in the MD are tied internally to the power bus return. In order to maintain isolation for the analog inputs and outputs, the Torque Command inputs and the Current Telemetry outputs are implemented using differential amplifiers. Further detail is given in Sections 4.3.4 and 4.3.5.

4.3.4 Torque Control Interface

MD control interface is to the J9 connector. Refer to Table 4-1 for detailed information.

The Wheel Torque Command input is implemented with a multiple input differential amplifier. The differential amplifier allows communication between ground systems with less than 5 V difference. The differential amplifier sums the 4 Torque Command and Torque Test inputs on J9 and J2. All Torque Command inputs must have the same reference. For true differential operation of the input amplifier, unused torque command inputs must be tied to the Torque Command reference pins J9-5 or J2-5.

The user should be aware that the Torque Command does not account for motor bearing drag.

The transfer function between the wheel torque output and torque command input has a single pole at approximately 1000 Hz.

4.3.5 Signal Interface

The MD produces the following output signals on the J9 connector:

Digital Tach
Tach Direction
Analog Tach

Interface details are provided in Table 4-1. All signals are referenced to the power supply returns.

Due to the 4.64 KΩ nominal output impedance of the Digital Telemetries, ITHACO recommends that the user use a line receiver with hysteresis and no internal pullup resistors such as the CD40106 hex Schmitt buffer.

4.3.6 Telemetry Interface

4.3.6.1 Telemetry Connector

MD telemetry interface is to the J2 connector. Refer to Table 4-1 for detailed information.

The MD produces an analog tach telemetry, an MD temperature telemetry, a motor current telemetry, digital tach telemetry and motor direction telemetry. Details of these signals and their scale factors are provided in Table 4-1.

4.3.6.2 Motor Current Telemetry

The motor current telemetry has a differential output amplifier to permit easy communication between ground systems. All other telemetry outputs are referenced to the power bus return. Current telemetry outputs are buffered so that a short circuit on one telemetry will not affect the other telemetry.

4.3.6.3 Driver Temperature Telemetry

Driver temeprature telmeetry is provided by a biased thermistor. Table 4-2 shows the temperature telemetry output voltage as a function of temperature.

4.3.6.4 Motor Driver Analog Tach

The motor driver provides two isolated bipolar analog tach telemetries scaled to 1000 rpm/V. The polarity of the tach voltage indicates tach direction. Maximum DC output voltage is ±10 V. The tach telemetry transfer function has a two-pole filter with a corner frequency of 5 Hz. Ripple voltage at 100 rpm or higher is less than 5 mV. Ripple voltage at any speed will not exceed 15 mV. The analog tach outputs are buffered so that a short circuit on one tach output will not affect the other tach output.

4.3.6.5 Digital Tach Telemetry

The motor driver provides two buffered digital tach telemetries and two buffered motor direction telemetries. The digital tach telemetry produces 54, approximately square, pulses per motor revolution. Both tach and direction outputs are 5 V CMOS compatible signals.

TABLE 4-2

Temperature (°C)	Temp TLMY Min (V)	Temp TLMY Nom (V)	Temp TLMY Max (V)
-30	4.48	4.82	5.16
-25	4.43	4.77	5.10
-20	4.37	4.70	5.03
-15	4.30	4.62	4.95
-10	4.21	4.53	4.84
-5	4.10	4.41	4.72
0	3.98	4.28	4.58
5	3.83	4.12	4.41
10	3.67	3.95	4.23
15	3.50	3.76	4.02
20	3.30	3.55	3.80
25	3.10	3.34	3.57
30	2.89	3.11	3.33
35	2.67	2.88	3.08
40	2.46	2.64	2.83
45	2.24	2.41	2.58
50	2.04	2.19	2.34
55	1.84	1.98	2.12
60	1.66	1.78	1.91
65	1.48	1.60	1.71
70	1.33	1.43	1.53
75	1.18	1.27	1.36
80	1.05	1.13	1.21
85	0.93	1.00	1.08
90	0.83	0.89	0.95
95	0.74	0.79	0.85
100	0.65	0.70	0.75

4.4 RW Electronic

4.4.1 Functional Description

The RW contains a Brushless DC motor with hall sensors and hall sensor pre-amplification.

4.4.2 Pinout Definitions

Each RW contains the following connector:

Designation	Function	No. of Pins	Connector Type
J1	Motor Interface	15	Male Subminiature D Shell

4.4.3 User Interface

There is no direct electronic user interface to the RW. All electronic RWA user interface is via the MD.

4.5 Power Profile

4.5.1 Power Consumption

The power consumption for the RW and MD at 5100 RPM and maximum commanded motor torque will be less than 30 W (20.0 W typical) at 23°C.

The power consumption for the RW and MD at 5100 RPM steady state operation will be less than 7 W (6.5 W typical) at 23°C.

4.5.2 Power Dissipation

Typical measured RW dissipations are:

Speed	Reaction Torque	Driver Dissipation	Wheel Dissipation
5100 RPM	0	1.0 W	5.0 W
5100 RPM	Max (increase speed)	10.5 W	6.0 W
5100 RPM	Max (decrease speed)	30.0 W	6.0 W

Figure 4-4 shows typical RWA power consumption as a function of steady state speed.

TYPICAL RWA/DRIVER STEADY STATE POWER CONSUMPTION IN VACUUM

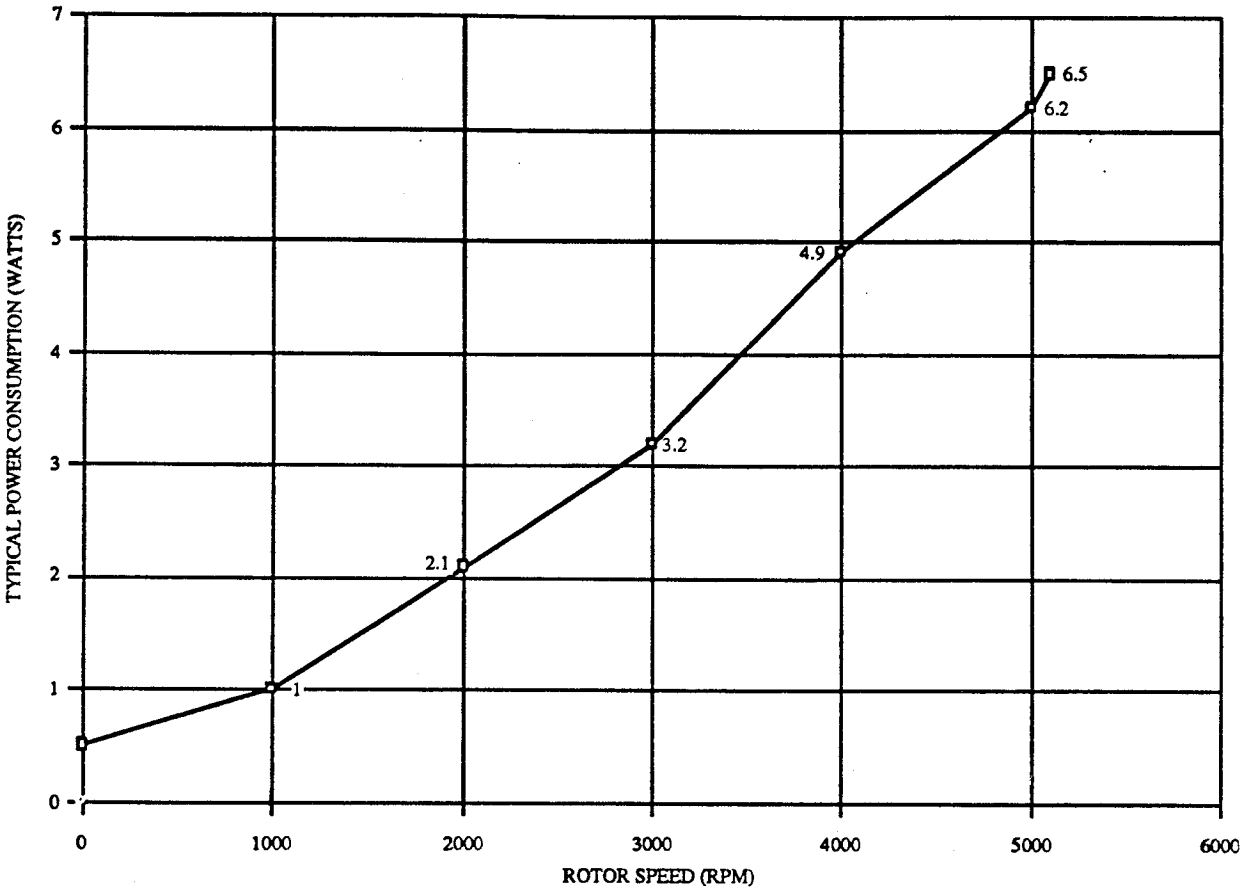

FIGURE 4-4

APPENDIX A

OUTLINE DRAWINGS

FOLDOUT FRAME

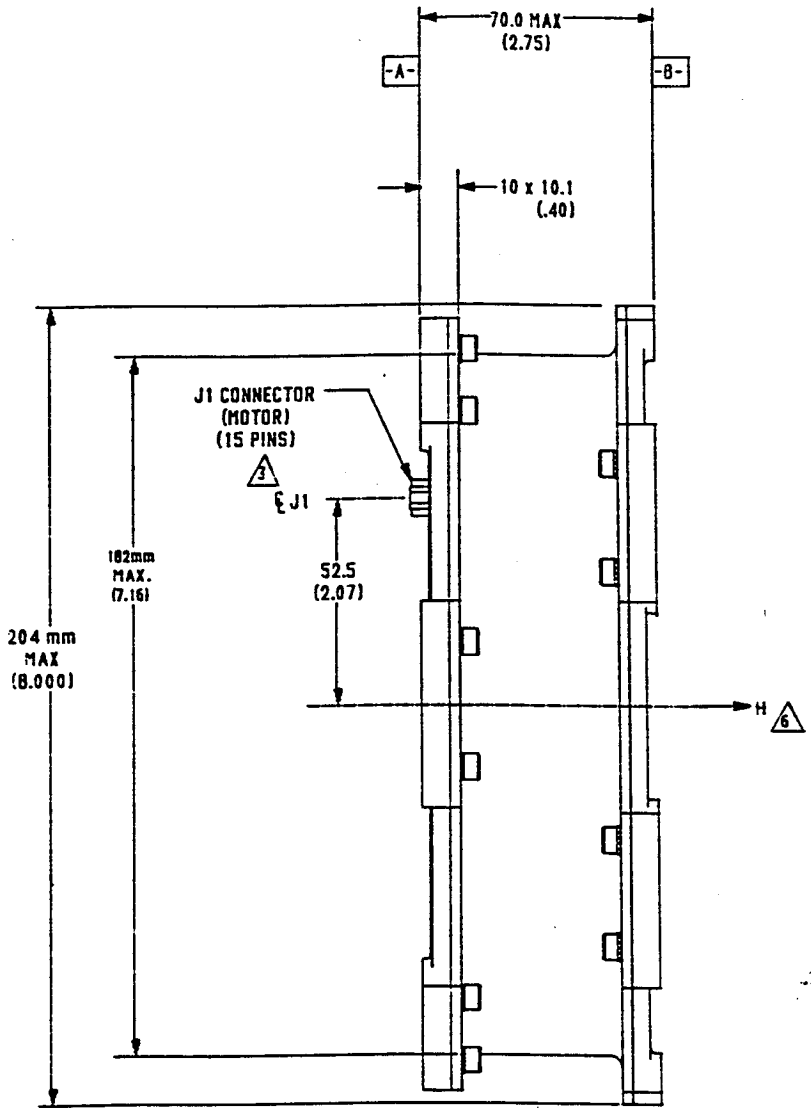

C-2

REVISIONS	D	43378
SYM	DESCRIPTION	DATE	APP

2

FOLDOUT FRAME

Report 93945
Revision A
March 14, 1991
Appendix A-1

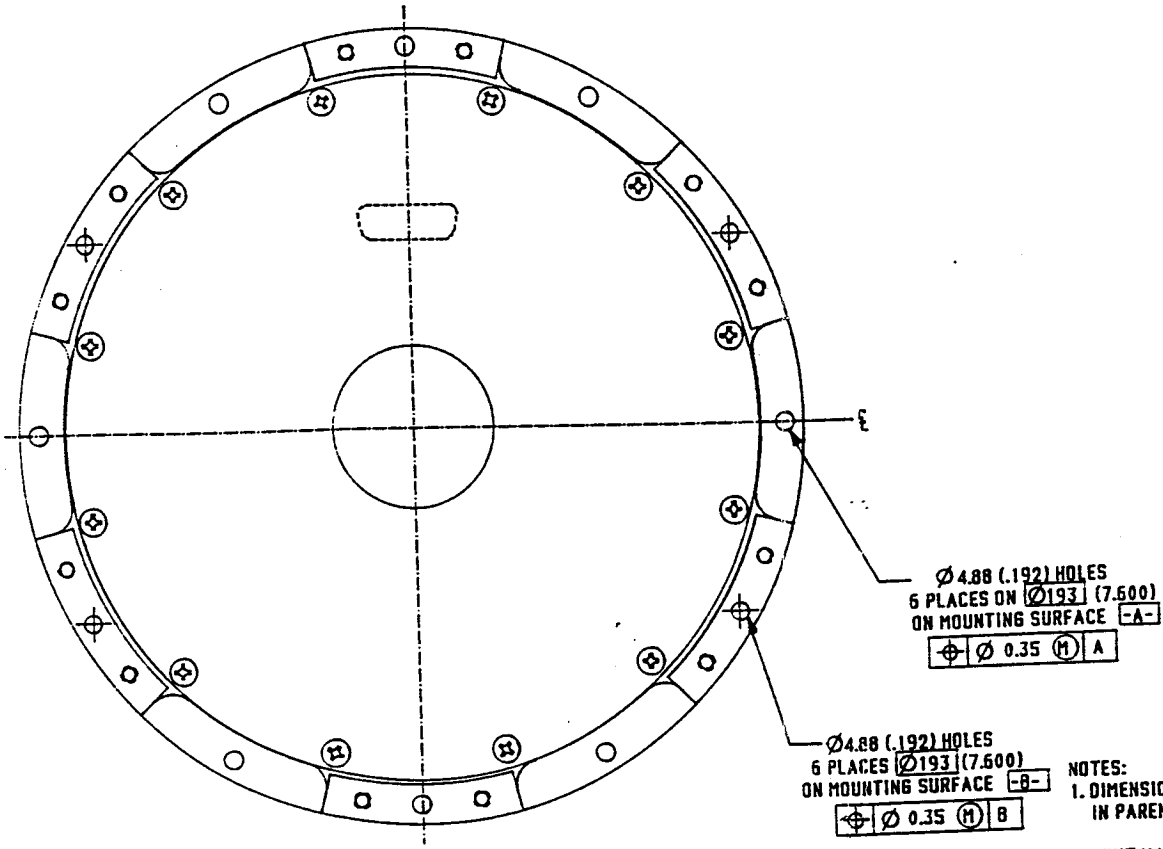

NOTES:

1. DIMENSIONS ARE IN mm. INCHES ARE INCLUDED IN PARENTHESIS FOR REFERENCE.
2. UNIT MAY BE MOUNTED FROM EITHER SURFACE -A- OR SURFACE -B-.
3. CONNECTOR: 15 PIN MALE SUBMINIATURE D (MECHANICAL INTERFACE COMPATIBLE WITH M24308/3-2 AND MIL-C-24308/3)
4. TOLERANCE: XX.X = ±2 mm
   X.XX = ±0.2 mm
5. WEIGHT: 2.5 KG (5.5 LBS) MAX.
6. ARROW DEFINES MOMENTUM AND TORQUE VECTOR ORIENTATION.

WHERE USED			UNLESS OTHERWISE SPECIFIED DIMENSIONS ARE IN INCHES	OUTLINE REACTION WHEEL	ITHA INC ITHACA, NE
DRAWING	IDENTIFICATION NO.	MODEL/PROG	LINEAR: .XX ± .02 .XXX ± .010 ANGULAR: ± 0.5°	FMF: JOB NO.	
		STEP	APPROVALS	DRAWN BY: W. THURSTON DATE: 9-26-90	CODE IDENT. NO.
			CHK LCT 9-26-90 MFG	DO NOT SCALE PRINT. REPRODUCTIONS OF THIS DRAWING MAY NOT BE TO SCALE.	D 43
			DFTG LCT 9-26-90 R&QA TR 9-27-90		
			ENG 133 9-26-90 [illegible]		

FOLDOUT FRAME

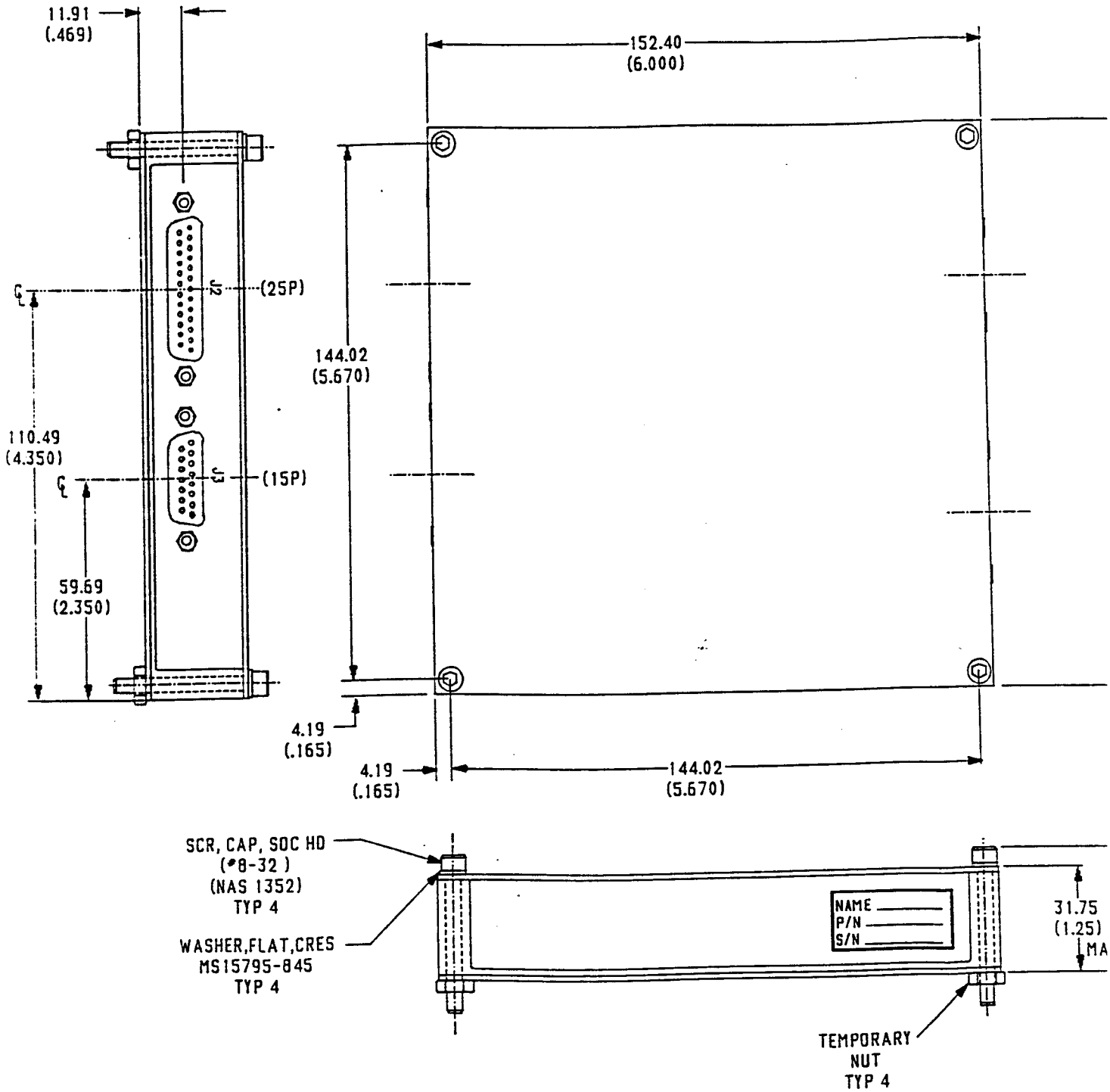

FILE: C:DRAWINGS --033257--REV9-26-90

FOLDOUT 1

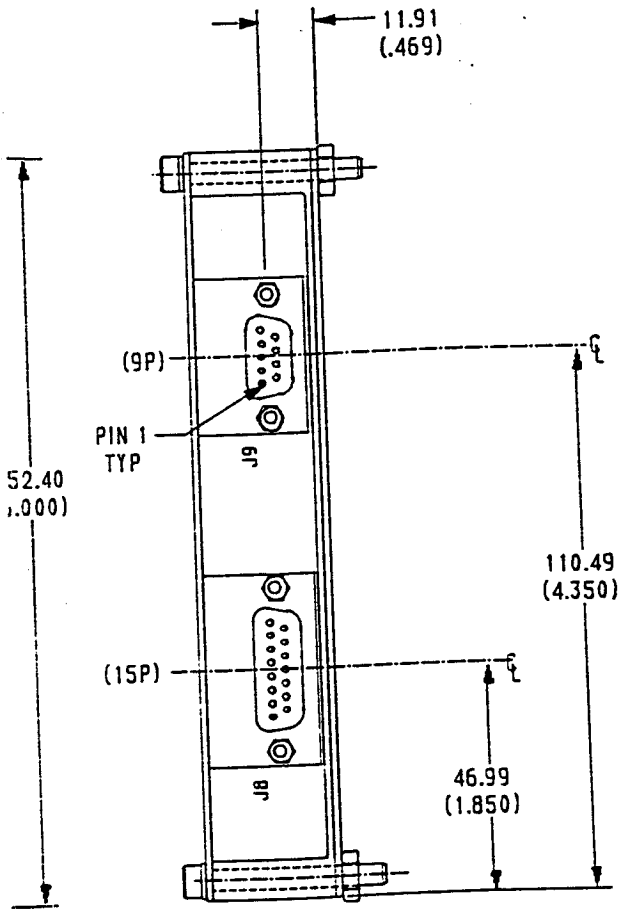

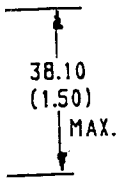

NOTES
1. DIMENSION ARE IN MM., DIMENSIONS INSIDE ( ) ARE INCHES.
2. WEIGHT: 0.8 KG (1.7 LBS.) MAX.
3. CONNECTORS:
   J2 IS CANNON DBMA-25P-NMB-K56 OR EQUIV.
   J3 AND J8 ARE CANNON DAMA-15P-NMB-K56 OR EQUIV.
   J9 IS CANNON DEMA-9P-NMB-K56 OR EQUIV.

OUTLINE
MOTOR DRIVER
ELECTRONICS